Novel Formulations of Photocurable Multi-arm Polycaprolactone

A thesis submitted in fulfilment of the requirements for the award of the degree of Doctor of Philosophy

Boyang Liu

Supervised by

Professor Frederik Claeyssens

Department of Materials Science and Engineering

Faculty of Engineering

University of Sheffield

September 2023

This thesis is dedicated to my beloved maternal grandmother and paternal grandfather.

Acknowledgment

First of all, I would like to express my greatest gratitude to my family. Their unconditional support and inifinite love are the cornerstone for my study.

I would like to pay highest respect to my supervisor Prof Frederik Claeyssens who is always enthusiastic to help with brilliant ideas and happy to provide guidance, and also for making PhD much more enjoyable than I thought. Also, I would like to thank my co-supervisors Prof Cornelia Rodenburg and Dr Nicola Green who are always happy to help and provide professional advice with profound expertise, and my assessors Prof Gwendolen Reilly and Prof Ipsita Roy who provided helpful advice during progress monitoring. Specially, to Vanessa, who is our great lab manager, I would like to pay my gratitude due to her outstanding management and spirit of responsibility, without which our research work would never be carried out smoothly. Also, I would like to thank Dr Chris Holland and Dr Shanshan Lyu for sharing characterisation equipment and their expertise selflessly.

Moreover, my appreciation to all lab buddies: to Enes, who is always keen to discuss problems in experiments; to Mina, for always being cheerful, helpful, and considerate in the lab; Louis, Denata, and Meghna, I do appreciate the huge amount of cell work that you did on my samples, and the experience of biological experiments you shared; Rachel, Caitlin, Nihan, Nam, Jonathan, Sara, and Sarah, thank you very much for bringing positive vibes and really helpful advices. Also, to Fer, Betul, Cristina, and Jose, who guided me a lot during the beginning of my PhD study. Particularly, many thanks to the postdocs in Kroto: Colin, who is considered as the almighty troubleshooter, for being my lab mentor providing essential trainings and for the endless encouragement; Caroline, Nik, and Vicki, who helped organise wonderful academic seminars and always kept an eye on the good practice in our lab.

Besides, I would like to thank Dr Yiliang Li, Yifan Zhang, and Le Wu for accompanying during vacations, particularly during the tough time with COVID-19, without which this PhD journey would not be accomplished.

Abstract

Polycaprolactone (PCL) is an excellent FDA-approved biomaterial but still has potential for further functionalisation to obtain broadened range of applications. In this work, I synthesised a novel form of PCL – 4-arm PCL and performed methacrylation (PCL-M) and acrylation (PCL-A) on it. Characterisations of basic properties, which were chemical structures and molecular weights, were performed. By using PCL-M as a matrix, two series of composites were formulated. One was reinforced by commercial linear PCL, of which the curing performance, mechanical properties, crystallinity, microstructures, biocompatibility, degradability, and shape-memory effect were characterised. Another formulation was using hydroxyapatites (HAp) as reinforcements. HAp-reinforced PCL-M composites were fabricated as films, dog-bone-shaped samples, and 3D scaffolds. Mechanical properties test, wettability test, extrusion-based additive manufacturing, scanning electron microscopy (SEM) imaging of microstructures, 2D and 3D cell culture, and accelerated degradation were performed. For PCL-A, an alternative synthesis method, Steglich Esterification, was applied to obtain this compound. PCL-A synthesised *via* conventional way and Steglich Esterification were compared. Mechanical properties of cured PCL-A were characterised. I also deployed two light-based additive manufacturing systems, which were single-photon microstereolithography and two-photon laser direct writing (DLW), to fabricate 3D structures from PCL-A. Particularly, the ability of PCL being structured into ultra-fine geometries *via* two-photon polymerisation (2PP) without photoinitiator was confirmed. Additionally, PCL-A's capability of surfactant-free emulsion templating, biocompatibility, and degradability were explored.

Table of contents

1. Literature Review

1.1. Polycaprolactone

Polycaprolactone (PCL) is synthetic material approved by FDA for biomedical purposes [1]. This material is normally synthesised *via* ring-opening reaction of ε-caprolactone with the presence of stannous octoate as the catalyst. The most common PCL products that can be found in the market have linear chemical structures with a wide range of molecular weights. Linear PCL products normally possess semi-crystalline microstructures, of which the crystallinity is approximately 60%, with a melting temperature (T_m) of 60°C and a glass transition temperature (T_g) of -60°C [2]. This semi-crystalline structure offers relatively good mechanical properties below T_m due to the highly ordered structure of molecules which limit the mobility of molecules and bring promising applications under heavy loads, such as dental filling materials.[3] For example, there is a commercially available polycaprolactone-based dental materials product, Resilion, which is used for root canal filling.[4] Due to its excellent biocompatibility, PCL has been widely explored on it potential for tissue engineering.[5, 6] In Yoshimoto *et al.*'s study, a porous material fabricated by electrospinning PCL nanofibers was reported for bone tissue engineering.[5] Promising results, such as multilayers of cells covering on the scaffold and mineralisation, were observed after 4 weeks of cell culture.[5] However, PCL is generally not considered as a hydrophilic material resulting in possibly poorer cell adhesion than other hydrophilic polymers, such as poly(vinyl alcohol) (PVA) and poly(ethylene glycol) (PEG), which are able to fabricate hydrogel.[7] Additionally, the crystallinity not only brings strong mechanical properties but also poor degradability.[8, 9] Though PCL is considered as a degradable material due to abundant ester bonds in its molecular structure where hydrolysis could happen,

such degradation process always starts from the amorphous region rather than the crystallised one, because the former one is poorly ordered so that water molecules could more easily penetrate inside these less dense structures and the degradation products could have more space to move out [8, 9]. Also, the water penetration is dependent on the hydrophilicity of the materials, i.e., the more hydrophilic the faster the water penetration, and PCL is reported to be a hydrophobic material with a water contact angle of 112° [10], so water ingress is slow to more hydrophilic biodegradable polymers, such as poly(glycolic acid) (PGA) [11]. PCL's relatively low hydrophilicity comes from a less ratio of polar functional groups, such as -(C=O)- and -O-, on a single repeating unit (Figure 1), resulting in a lower overall polarity thus lower ability of attracting water molecules.

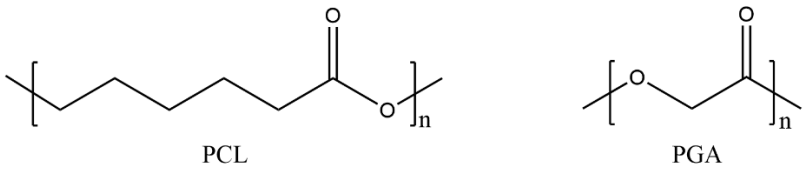

Figure 1. Chemical structures of PCL and PGA.

Thus, as a 60% crystallised material, the degradation rate of PCL is relatively low, which could last up to 4 years [12]. Additionally, the mechanical properties of linear PCL mostly rely on the entanglement and crystallinity of molecules, of which the degrees are dependent on its molecular weight and temperature. However, linear PCL is commonly used above its T_g, the movability of PCL molecules would be allowed to slide away from each other under stress, a permanent deformation would occur on the material so that its performance might be critically affected. Particularly, when it is applied as an implant in human body, the temperature (approximately 36 – 37 °C) is close to its T_m, along with the long-term stress applied to it,

deformation such as creep is highly likely to happen to cause a secondary damage, however, without being noticed. Accordingly, PCL is an excellent material for biological applications but still to be further improved for better performance.

1.2. Multi-arm Polycaprolactone

To overcome the natural defects of linear PCL, research work to turn this material into a thermoset with chemically crosslinked structures has been proposed and conducted in previous years [13-15].

To obtain a polymer material with a highly crosslinked structure, star-shaped multi-arm pre-polymers with curable functional end groups have been developed. These pre-polymers play a role of being a 'core' or 'pre-crosslinked' structure. And when one end of a pre-polymer's arm is covalently bonded to another one, a thermoset material with chemically crosslinked structure can be built up along with the accumulation of such behaviour. Compared to materials constructed from linear molecules, crosslinked star-shaped molecules usually have higher thermal stability as the molecules have already been 'locked' in a network once formed and the structural integrity can be maintained before reaching their thermal degrading temperature, which is normally over 300°C.[16] As such, polymer materials with these structures could be more suitable for applications for heavy loads, high temperatures, and scenarios requiring rapid-curing rate such as dental filling materials and biomedical adhesives [17-19]. Indeed, a large number of acrylic based resins are used as dental resins which are typically hard, but can be brittle [20]. Previously, biomaterial researchers have started work on multi-arm polycaprolactone (multi-arm PCL) and due to PCL's biocompatibility and relatively straightforward synthesis. A three-arm PCL, PCL triol, has been explored for bio-applications, such as tissue engineering and drug delivery [21]. However, similar to the linear PCL products, the mechanical properties

of these multi-arm PCLs mostly rely on molecular entanglement and crystallinity of which the degree is affected by the arm lengths, but generally the crystallinity of multi-arm PCL is lower than that of linear PCL due to large steric effects [22]. And yet, the molecular entanglement and crystallinity of polymer are influenced by temperature as well. Higher temperature usually leads to higher mobility of the molecules so that the molecule chains could be easily untangled under external stress and the distance between crystallised chains gets increased to break the intermolecular hydrogen bonds that build up crystallinity. Thus, the mechanical properties of PCL triols would become significantly poor when temperature is high, particularly beyond its melting point where the molecules are de-crystallised.

To overcome such disadvantages, a few approaches could be worthy to conduct. One of them would be chemical crosslinking, which forms strong covalent bonds between these multi-arm molecules, and has become a preferable solution [13, 23]. To achieve this, the multi-arm PCLs have to be further functionalised with curable groups at the end of their arms [13, 23]. Another possible way is to fabricate composites. Work reported by Doganci *et al* showed that by blending star-shaped PCL with linear poly(lactic acid) (PLA), the PLA matrix had improved mechanical properties and transformed from a brittle material to a ductile one [24]. The results of this work also showed that the star-shaped PCL/PLA blend also brought larger ultimate tensile strain values and the materials were more elastic than linear PLA [24].This work used star-shaped PCL as a reinforcement, but it provides an inspiration for enhancing the mechanical properties of multi-arm PCL as a matrix by blending linear polymer inside. By combining the two approaches mentioned above, it would be intriguing to fabricate composites with a photo-curable star-shaped PCL as the matrix and linear polymer materials as reinforcement, which is further discussed in Section 1.4.

1.3. Functionalisation

1.3.1. Methacrylation vs Acrylation

The major methods of functionalisation for photocuring are methacrylation and acrylation, of which the products are usually referred to as methacrylate and acrylate, respectively. The only difference of chemical structures between these two types of functionalisation is the methyl group (-CH_3, red segment in Figure 2) attached to the -C=C bond on the methacrylate group but hydrogen instead at the same position on acrylate group.

Figure 2. Chemical structures of methacrylate (left) and acrylate (right).

However, a mere change on the chemical structure could bring vital impact on the physical and chemical properties. The -C=O structure shows strong electron withdrawing effect on the (meth)acrylate group which makes the -C=C end highly active. However, the -CH_3 group of methacrylate group, which is usually considered as an electron donor, is able to compensate the electron withdrawn effect. Moreover, since the -CH_3 substitution on -C=C is rotatable along the -C-C- axis between them, one of the -C-H bonds from -CH_3, which are all σ bonds, is able to locate within the same plane with the π bond of -C=C, so that there is a hyperconjugation formed in between. Summing up these two effects that this -CH_3 brings, the entire methacrylate group is stabilised and shows higher stability than acrylate. As a result, the methacrylate products normally show less reactivity than the acrylate ones do, so that the former one is

suitable for longer storage, which is preferable for mass production, and the latter one is suitable for scenarios requiring high activity such as two-photon polymerisation, which could be more customisable. Moreover, the additional -CH_3 brings more hydrophobicity to methacrylate products. For example, methyl methacrylate has a lower solubility in water (1.6 g/100 ml) compared to methyl acrylate (6 g/100 ml) [25, 26].

The way of methacrylation performed on PCL is straightforward, which is to use methacrylic anhydride (MAA) in an organic solvent, which is usually dichloromethane (DCM), to react with the -OH end groups so that methacrylate groups can be introduced on to PCL molecules with methacrylic acid generated as a by-product. To increase the conversion of this reaction, an organic alkali triethylamine (Et_3N) is usually added in the reaction solution to absorb the generated acid and help push the reaction to the product side. The reaction mechanism is shown in Scheme 1 below.

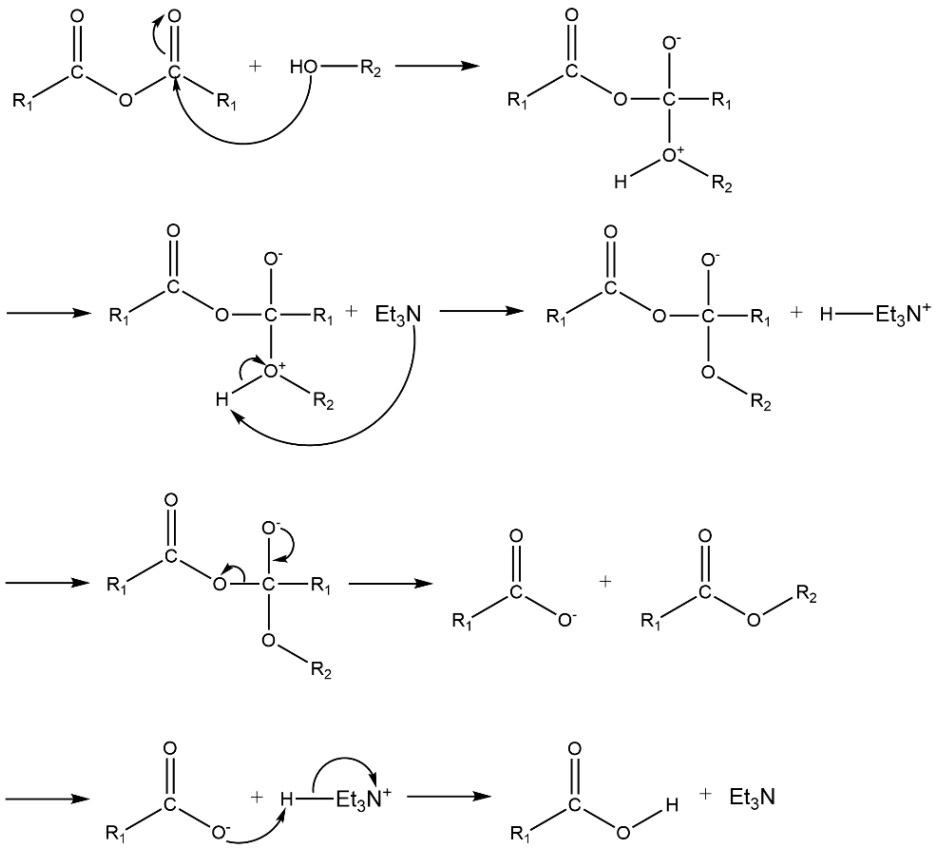

Scheme 1. Mechanism of methacrylation between anhydride and alcohol with the presence of Et_3N.

Methacrylation of a three-arm PCL monomer is reported by Field *et al*. to be both a molar-ratio-dependent and time-dependent reaction [13]. The conversion rate showed a linear increasing trend along with increasing added amount of MAA+Et_3N (from 0.5 molar eq. to 2 molar eq.) [13]. When the 2 molar eq. ratio was used, the conversion rate could reach ~50% after 20 hours of reaction [13]. However, the conversion did not show significant growth from 40 hours to 96 hours, which was from 63% to 77%, after which the degree of methacrylation could maximally reach 80% [13]. However, in Dikici *et al*.'s work, a methacrylation functionalisation was performed on a 4-arm PCL for 68 hours, but the degree of methacrylation reached near 100% [15].

For acrylation, a similar reaction route is commonly used. In this reaction, acryloyl chloride (AC) is the key reagent, which shows high reactivity with -OH, thus the acrylate groups can be introduced from AC to the substrate. The by-product of this reaction is HCl, which is usually removed by Et_3N mixed in the solution. Due to the high activity of AC, the conversion rate can easily reach 70% to 80% after an overnight reaction. However, several studies reported that the final product showed a yellow colour which was difficult to be purified. The yellowish impurity is considered to be a complex compound produced from a side reaction between AC and Et_3N and shows potential cytotoxicity. Thus, optimisations should be carried out for acrylation for biomaterial. An alternative way to perform *via* Steglich Esterification is further discussed in Section 1.6.

Additionally, arylates can be used in a wide range of biomedical applications due to their good biocompatibility, tunable physicochemical properties, excellent photo-curablility, and low price, such as hydrogels for tissue engineering and dental materials [27-29]. However, risks have also been found, such as allergy when acrylates are used [30]. To overcome such issues, particularly *in vivo*, surface treatment, such as plasma treatment and coating, could be a solution to avoid direct contact with cells.

1.3.2. Photo-curing

There are multiple approaches to trigger the curing process of pre-polymer with -C=C bonds, such as redox reaction, heat absorption, adding crosslinking agents such as multifunctional amine or thiol compounds, and light absorption, among which the light absorption method shows efficiency, tunability, and low energy cost features indicating its promising application prospects, such as coating, printing, and additive manufacturing.

Polymerisation triggered by light absorption is referred to as photopolymerisation. This reaction usually happens on unsaturated -C=C bonds, which can react with the radicals generated by the photoinitiation process. To reduce the quenching of the reaction, the radicals during the propagation stage of the reaction need to be stabilised (see next paragraph). This is typically done *via* conjugation, in the case of styrene with a benzene group and in the case of (meth)acrylate with a C=O group. In the case of methacrylate compared to acrylates the double bond is further stabilised by the pendant methyl group, as previously discussed. This conjugation allows for the propagation reaction to proceed in ambient atmosphere without complete quenching (by oxygen for example), since the free carbon radical occurring in the propagation reaction is stabilised *via* conjugation with the π-orbitals.

In this work, free-radical photopolymerisation is employed as it is relatively easy to initiate compared to the ionic method and the process can be immediately ceased once the light source is withdrawn, which is preferable for light-based additive manufacturing where photo-sensitive resin can be selectively cured within the local region. The basic mechanism of free-radical photopolymerisation, which is shown by the chemical reactions, is that in reaction (1) the photosensitive pre-polymers' -C=C bonds themselves or photoinitiator molecules (PI) absorb energy from light hν, which is usually visible light to UV (wavelength 700 to 200 nm) [31], being excited to free radicals with unpaired electrons R·[32], this is called the intiation stage of the addition reaction. Then the R· activates photosensitive monomer or macromer M, and the polymer chain grows through this continuous radical forming, as shown in reaction (2) and (3) [32], this is called the propagation stage. The termination of the free-radical photopolymerisation reaction can be either combination of two radicals (4) or disproportionation between two radicals (5) [32], and this is called the termination stage.

$$PI \xrightarrow{h\nu} PI^* \rightarrow R\cdot \quad (1)$$

$$R\cdot + M \rightarrow RM\cdot \quad (2)$$

$$RM\cdot + M_{n-1} \rightarrow RM_n\cdot \quad (3)$$

$$RM_n\cdot + \cdot M_mR \rightarrow RM_{n+m}R \quad (4)$$

$$RM_n\cdot + RM_m\cdot \rightarrow RM_n + RM'_m \quad (5)$$

Nevertheless, it should be noted that, if there is only one -C=C group on a single pre-polymer molecule, the result of polymerisation would possibly be polymers with long linear chains rather than chemically crosslinked network, which normally requires two or more -C=C bonds on one molecule. Hence, the degree of functionalisation is vital for curing multi-arm PCL into a thermoset material.

Specifically, a phenomenon of ceasing polymerisation process caused by the presence of oxygen, which is referred to as oxygen inhibition or quenching, has been a challenge for curing acrylate products [33, 34]. Briefly, oxygen can attack the free radicals and a peroxide free radical would be formed during the chain propagation and the chain reaction is stopped leaving abundant unreacted -C=C on the surface or even inside the cured material [33, 35]. This leads to a lower crosslinking density thus poor mechanical properties and tacky surfaces [35, 36]. These residual -C=C groups could be left still or further oxidised to -COOH so that the surface would show acidity in water environment, which could affect the cell culture. Thus, if acrylate products are to be applied as biomaterials, oxygen inhibition has to be prevented as much as possible or a surface treatment has to be performed to create a more biocompatible environment. To perform such optimisations, Norrish Type (II) photoinitiator (further discussed in Section 1.3.3) or higher light intensity can be used, which could help generate more radicals under the

same time of light exposure and they could promote polymer chain propagation rather than be terminated by oxygen [37]. Another potential route to achieve this is curing under inert gas environment [35, 38], which is less preferable since 100% inert gas environment is difficult to achieve particularly when a complex sample is moulded, and that oxygen, as a non-polar molecule, is more likely to be dissolved in organic compounds which generally show low polarity, which means that the dissolved oxygen is difficult to remove thoroughly. Interestingly, oxygen quenching can give some advantages for stereolithography-based printing, and this is exploited in Continuous Liquid Interface Production (CLIP) technology commercialised by the company carbon3D. The technology, published in Science, uses a gas permeable membrane as a platform for projection stereolithography [39]. This creates a dead zone near the window used to project the image into the resin, where photopolymerisation does not occurs. This means that we can change the layer-by-layer manufacturing that is slow to a continuous photocuring process that can be done at speeds of 100's of millimetres per hour. This decreases the print time from hours to minutes.

There are also other approaches to improve the curing performance from oxygen inhibition, such as applying 'thiol-ene' click chemistry or adding trivalent phosphites or phosphines [40-43]. A 'thiol-ene' click chemistry was used for photo-curing a 3-arm PCL acrylate poly-high-internal-phase-emulsion (polyHIPE) by Johnson *et al* [40] and Dikici *et al*. utilised the same method to fabricate PCL-M polyHIPEs [43]. Adding trivalent phosphites or phophines such as triethyl phosphite would significantly reduce the oxygen inhibition during photocuring acrylates, however, this series of reagents commonly lack stability under normal storage conditions [41].

Having a large amount of remnant acrylate groups on the surface because of quenching can on the other hand also be used to funtionalise the surface with cell-adhesive molecules. For example a rather easy method to post-functionalise these materials was reported by Zhou *et al*.,

which was to immerse the photocured objects into amine solutions so that the residual -C=C can react with -NH_2 to obtain an optimised surface [36]. This work showed high conversion rate on the surface *via* an immersion process that only took 10 minutes [36]. Furthermore, diverse surface modifications could be expected from this method by selecting different types of amine compounds [36].

1.3.3. Photoinitiators

To trigger free-radical polymerisation, photoinitiators are a series of compounds that can absorb energy from light and generate reactive species (free radicals) causing chain extending reactions among pre-polymers. According to the mechanisms, photoinitiators can be categorised into two types:

Table 1. Types of photoinitiators.

Type Names	Typical Compounds
Norrish Type I (Cleaving)	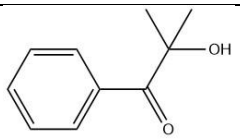 2-Hydroxy-2-methylpropiophenone
Norrish Type II (Hydrogen-abstracting)	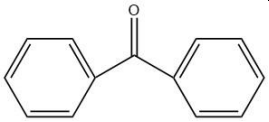 Benzophenone

The Norrish Type I photoinitiator is cleaved to directly produce the radicals, while a type II photointiator extracts a hydrogen from a donor, which is typically an amine. This creates the amine-based radical to initiate the reaction. This means that the Type I photoinitiator is incorporated into the growing polymer chain, while the Norrish Type II is not. Additionally, using Norrish Type II photoinitiator, which is usually deployed with hydrogen donors such as amines and thiols, could potentially reduce oxygen inhibition [35]. Also, Huang *et al*. reported a Type II photoinitiator modified by bis(trimethylsilyl)amino showed strong reduction of oxygen inhibition while curing acrylates under near UV [44].

A special type of photoinitiation is based on multi-photon absorption. In practice, usually two-photon absorption is achieved. In this process the photointiator absorbs 2 photons of half the absorption wavelength almost instantaneously *via* use of ultra-high intensity light sources, for example, for a photoinitiator than normally absorbs 400 nm light, an intense femtosecond light source of 800 nm is used. In this non-linear absorption behaviour, the absorption cross-section depends on the square of the intensity. This is opposed to normal 1-photon light absorption where the absorption cross-section depends linearly on the intensity. This means in practice, that for a Gaussian beam shape, when focused with a microscope objective, the photopolymerisation in the focal spot of the beam can be much more precisely controlled than single photon polymerisation. 2 photon polymerisation (2PP) thus allows for printing of high resolution structures, up to ~100 nm and polymerisation within the photocurable polymer [45] (2PP is discussed in more detail in Section 1.5.1.3). Importantly, 2PP requires typically specialised PIs as this unique type of polymerisation demands both a high efficiency of light absorption and a mechanism to retain an absorbed photon in a virtual state for long enough to achieve 2PA. But traditional commercial photoinitiators usually possess a low 2PA cross-section, which has to be exposed to a higher energy laser or for a longer time to trigger 2PA [46]. Yet higher power or longer exposure time could bring damage to the cured area [46]. Thus,

suitable selection of PI is the key factor for building 3D scaffold by 2PP. There is a large amount of research in 2PP photoinitiators [47], of which the chemical structures usually contain extended π-system connecting electron donor(s) (D) and(or) electron acceptor(s) (A). Among them, the complex A-π-D-π-A structure has shown (Figure 3) to increase the 2PP cross-section thus 2PP absorption [47].

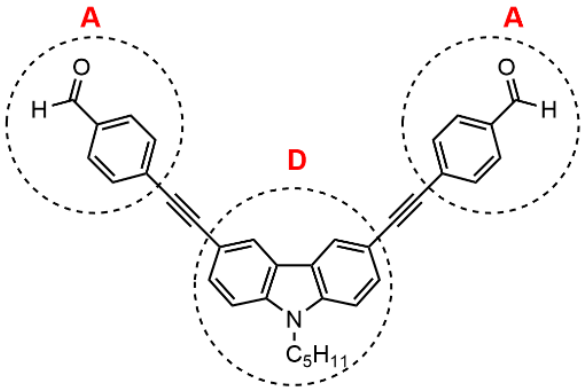

Figure 3. A typical 2PP photoinitiator with A-π-D-π-A structure synthesised by Xing *et al.* [46].

Moreover, in the Norrish type I PIs, the radicals eventually become part of polymer chains. As a result, if photocurable materials are to be utilised as biomaterials, the biosafety of PI directly influences the biocompatibility of tissue engineering scaffolds manufactured by light-based 3D printing. Thus, the PI should be cautiously selected, and various research has been done on the PIs applied in photocurable biomaterials [48]. This incorporation of the photointiator into the polymer chain is avoided in Norrish type II photoinitiation, where the synergist amine is incorporated into the polymer chain, providing an opportunity to produce inherently biocompatible materials easier *via* careful selection of the amine. A commonly used 2PP photoinitiator for biomaterials is a sodium salt that has benzylidene cycloketone structures

developed by Ovsianikov *et al*. (Figure 4), which is hydrophilic and can be used in combination with hydrogels and presents biocompatibility [49].

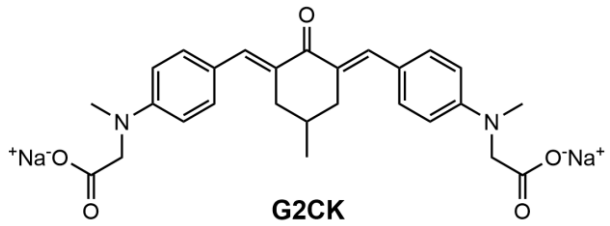

Figure 4. A hydrophilic and biocompatible 2PP photoinitiator (G2CK) developed by Ovsianikov *et al* [49].

Moreover, riboflavin (vitamin B2), which is a natural molecule and an essential nutrition in the human body, could be selected as a biocompatible photoinitiator for 2PP [50, 51]. Since it shows hydrophilic character, riboflavin has become an excellent choice for biomedical hydrogel structuring *via* 2PP [52]. Cross-linking of proteins such as silk was achieved with riboflavin as a photoinitiator by Brif *et al*., where the tyrosine groups in the protein were the hydrogen donors and cross-linked during UV-irradiation [53]. However, as a Norrish Type II photoinitiator, riboflavin has to be used with co-initiators as electron donors, which are normally amines [50, 52]. That brings another challenge that the co-initiator has to be biocompatible if the material is to be used for biological issues, and it has to be water soluble as well when hydrogels are to be fabricated [50]. For example, L-arginine, also as a common naturally occurring amino acid, was selected as the co-initiator by Kim *et al* for photocuring and obtained excellent curing performance [54].

In addition, it has been reviewed that it might be possible but extremely challenging to achieve 2PP without photoinitiator to avoid biocompatibility risk [51]. The energy of laser used has to be

above the 2PP threshold and below the charring threshold [51]. According to the previously mentioned work of Thompson *et al*., increasing the concentration of photocurable groups can lower the threshold of 2PP thus increase the possibility of 2PP without photoinitiator to maintain biocompatibility [55]. Apart from these methods, using molecules with lower 2PA threshold would be another direction for 2PP without photoinitiators. For instance, as discussed in Section 1.3.1, acrylates generally show higher reactivity than methacrylates, hence, photoinitiator-free 2PP structuring would be more likely to happen.

1.4. Polymer Matrix Composites

Composites are a series of solid materials composed of two or more distinct components, among which the advantages of one component are able to compensate for properties that other components lack of, so that the composites usually show superior performance compared to the single components under complex working conditions [56, 57].

Among natural tissues, composites can be widely found. For examples, wood is a composite of long cellulose fibres as the inclusions in a matrix of hemicellulose, and lignin. The hemicellulose and lignin help construct cell walls, connect cell walls and enhance the rigidity of the wood against degradation, respectively [58]. Also bone is a typical biological composite consisting of collagen providing elasticity and toughness, and hydroxyapatite providing strength, in particular when compressed [59]. Soft tissues, e.g., skin and blood vessels are composites consisting of collagen to provide toughness and strength when stretched, while elastin provides the elasticity [60, 61].

According to the composition of reinforcements or inclusions in typical industrial polymer based composites, they can be categorised as organic or inorganic reinforcements. Inorganic reinforcements have been applied to fabricate polymer-based composites for decades due to

their distinguished properties that polymers normally do not possess, such as glass or carbon fibre with ultra-high Young's Modulus and ultimate tensile strength (UTS), and calcium carbonate which extensively used for strengthening the material and also reducing the cost [62]. As for biomaterials, the reinforcements should be selected with caution to avoid cytotoxicity. These inorganic reinforcements would normally enhance the biocompatibility by creating rougher surface and introducing bioactive surfaces, which allow for protein adhesion, which then enables improved cell attachment and adhesion *via* integrin binding to these adhered proteins[63]. Hydroxyapatite (HAp) particles, which are natural ingredient in bone tissues as the inclusion that allows for compressive strength in load bearing bone, has become one of the most common inorganic materials for biological applications [64]. For example, back in 1997, Huan *et al*. reported that the introduction of HAp increased the mechanical properties of a polyethylene matrix, improved its stability in aqueous environment as a permanent implant, and promoted cellular activities such as attachment, proliferation, and differentiation [65]. As a ceramic, HAp is also capable of being manufactured into biomedical implants or cell scaffolds from an HAp powder *via* additive manufacturing by laser sintering [66, 67]. However, this technique consumes high energy due to the high melting point of HAp (1650 °C) [68], and pure HA material normally shows brittle feature as common ceramics do. Sintered HA is not overly suitable to be applied under complex load-bearing conditions. Therefore, being added to a polymeric matrix as a reinforcement would make the most of HAp's mechanical properties but also avoid the disadvantage brought by its high melting point and brittleness [69].

Moreover, HAp particles would also provide additional surface roughness and allow for protein adhesion [70, 71], so that the surface of composites could be more suitable for cell attachment. For light-based additive manufacturing, HAp and photocurable resin is a promising combination, which could encapsule HAp particulates and strengthen the structure simply after photocuring,

which is a more low-cost and efficient process compared to direct laser sintering and thermal extrusion-based additive manufacturing (see more information on additive manufacturing techniques in Section 1.5.1). Moreover, adding some inorganic particulates could normally increase the viscosity of liquid [72], and even make it as a paste so that it can maintain its configuration after extrusion so that a structural integrity can be maintained.

Organic reinforcements normally show better compatibility due to their similar carbon-based chemical structures. Currently, the most common organic reinforcements are other polymer materials with different properties, such as nylon-fibre-reinforced plastics, which normally have ultra-high molecular weights. However, if organic reinforcements with moderate molecular weights are used, due to the similarity with the polymeric matrix, the compatibility of this type of reinforcements in polymer would be increased and the distribution of organic reinforcements could reach molecular level, of which the phase separation might not be as clear as those doped with inorganic reinforcements, and the organic reinforcements might be able to merge into the matrix with higher homogeneity so that they can easily form composites with micro- or nano-domains, or even interpenetrating networks (IPNs) easily. Work on star-shaped PCL/PLA composites conducted by Doganci discovered that the mechanical properties of PLA matrix were significantly changed [24]. The microstructures under SEM showed immiscibility of star-shaped PCL and linear PLA [24]. However, the phase separation was observed in micro-scale (Figure 5) [24].

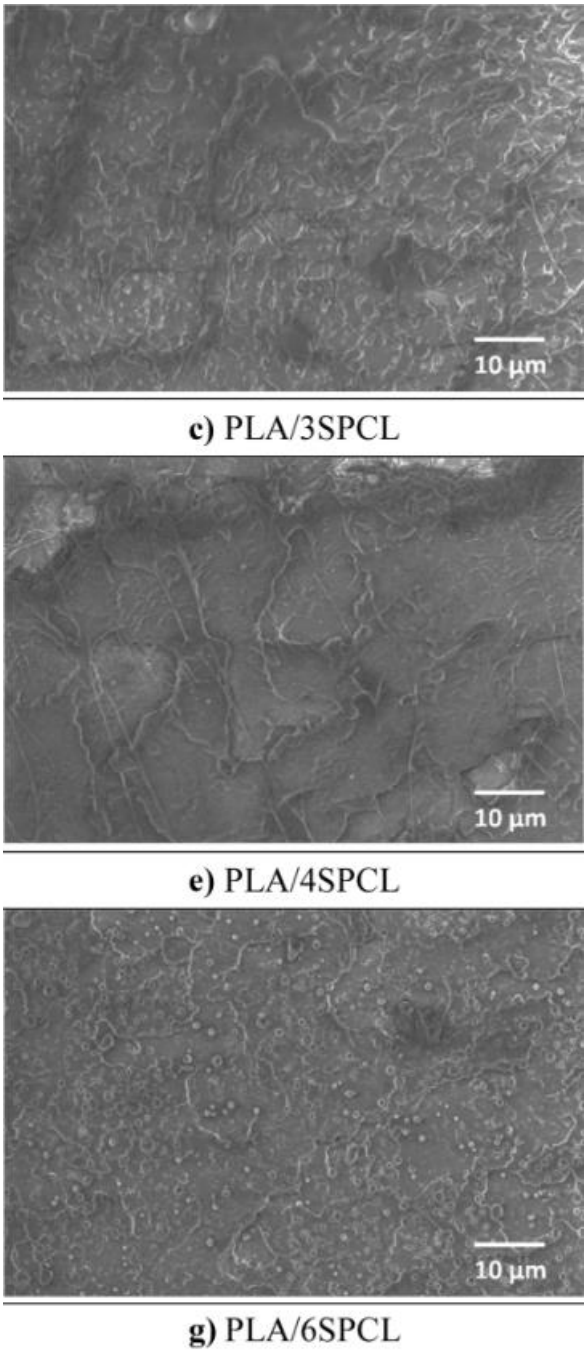

Figure 5. Linear PLA reinforced by star-shaped PCL (3SPCL: 3arm stars-haped PCL, 4SPCL: 4-arm star-shaped PCL, 6SPCL: 6-arm star-shaped PCL, figure adapted from Doganchi's work [24], copyright: Springer Nature).

This kind of distribution would not only compensate the defects from both matrix and reinforcements, but also could potentially give the material additional properties, such as tuned

physico-chemical properties, shape-memory properties, and self-healing properties. For example, a polycaprolactone diacrylate/poly(lactic acid) (PCL-DA/PLA) shape-memory semi-IPN was reported by Michaela *et al*. in 2020 [73]. In this work, linear poly(lactic acid) was encapsulated within a chemically crosslinked polycaprolactone diacrylate network, which not only increased Young's modulus, but also shape memory effect due to the penetrating PLA's molecular-level distribution into the PCL network preventing it from being permanently damaged during deformation [73]. Additionally, Mohsen *et al*. fabricated a series of semi-IPNs which demonstrated thermal-responsive self-healing properties, of which the self-healing behaviour was benefited from the linear polymer's intermolecular interaction [74]. The basic mechanism of this thermal-responsive semi-IPN is that when the 'wound' is compressed together, the linear molecules would form physical entanglement across the interface of the 'wound' when the temperature is above the linear component's melting point, subsequently, when the material is cooled down below the melting point, the entangled linear molecules are to be solidified across the interface and the 'wound' is 'healed'. To our knowledge, a photocurable PCL reinforced by linear PCL composite has never been formulated, and due to the similarity of their chemical structures, it would be intriguing to explore the miscibility of these two components, improvement of mechanical properties of photocurable PCL matrix, and the change of degradation rate.

1.5. Fabrication Methods

1.5.1. Additive Manufacturing

1.5.1.1. Extrusion-based Additive Manufacturing

Additive manufacturing, or commercially referred to as '3D printing', is a cutting-edge manufacturing technology that allows objects to be constructed layer-by-layer. In polymer manufacturing, compared to conventional methods for manufacturing 3D objects such as injection moulding, additive manufacturing, of which the basic concept is to use digital slices of the 3D object to construct this object from thin layers and fabricate it layer-by-layer, enables structural construction with far more complexity and customisability.

One of the additive manufacturing methods is extrusion-based, which allows the printing ink to be extruded and solidified onto a substrate. The solidifying process can be carried out *via* cooling and photo-curing, which applies to both thermoplastic and thermoset materials respectively. For the thermoplastic ones, the printing material is to be heated above its melting point and extruded out as a fluid, then cooled down on a substrate below its melting point so that one layer of object is constructed. For the thermoset ink, which is usually photo-curable, it is to be extruded onto a substrate and cured by a UV light source, rather than cooling, so that one layer is finished and another one is to be built on top. Following that, another layer is to be laid onto its previous one until the entire printing programme is finished. Generally, extrusion-based additive manufacturing could generally offer resolution up to 100 μm [75], which is fine enough to deal with most scenarios requiring relatively large objects. However, as for manufacturing cell scaffolds for tissue engineering, extrusion-based additive manufacturing might not be capable of building micro- or nano-scale structures to mimic the micro-environment for cells. Though fused filament fabrication (FFF), which is to melt thermoplastic material and extrude it layer by layer to build the demanded structure, could reach 50 and 2.5

μm resolution respectively, these two methods have either complexity of set-up along with high energy cost or uncontrollable pores in the fabricated structures [75].

When fabricating fine structures, small diameter nozzles are used. However, the 'inks' used for extrusion would possibly clog the nozzle and the manufacturing performance is influenced. Furthermore, a composite 'ink' doped with powdery reinforcements may make the situation even worse since the fine particulates on one hand will increase the viscosity of the liquid, on the other hand they may form large aggregations and jam the nozzle. As a result, the printability of extrusion-based additive manufacturing is limited.

Regardless of the natural defects, this technique is able to fabricate meso-scale porous materials. Dikici *et al*. reported scaffolds for tissue engineering were successfully fabricated by using high-internal-phase-emulsion (HIPE) made from a 4-arm PCL methacrylate *via* an extrusion-based 3D printer (BioBots 2, now Allevi 2) [15]. In Figure 6, meso-scale pores can be observed, where the large ones were the windows between the lines and the micro-scale ones were generated from the emulsion-templating.

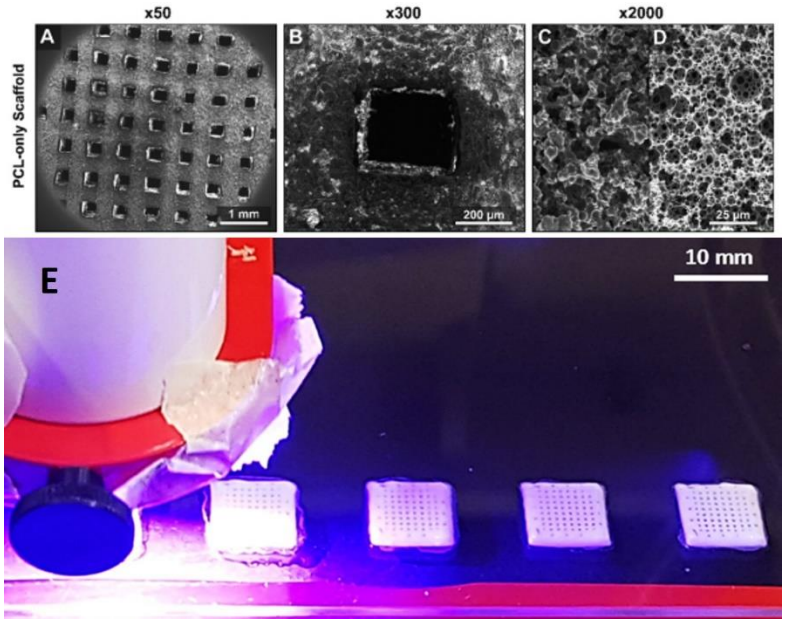

Figure 6. Meso-sacle porous PCL-M polyHIPE scaffolds manufactured *via* extrusion-based 3D printing, where A, B, C, and D are SEM images the meso-scale porous structure of 3D printed PCL polyHIPE, among which A and B show the large pores created by 3D printing with ~ 300 x 300 µm pore size , and C and D show the small pores with ~ 20 microns (diameter) pore size. Figures adapted from Dikici *et al*.'s work [15], copyright: American Chemical Society.

Leachable porogen can be a promising method for fabricating the ink and create meso-scale porous material as well. Liu *et al*. and Menshutina *et al*. used chitosan and alginate, respectively, as porogen dopants in the 'ink' and scaffolds with meso-scale porous structures were successfully fabricated [76, 77]. These additives could also increase and tune the viscosity thus help maintain the configuration after extrusion. So, this would also be a promising way to fabricate 3D objects with high structural integrity.

It is to be noticed that the ink could spread on the printing substrate, leading to thicker dots and lines than the designed parameters, which lower the resolution. Because of this, shear thinning

inks are typically used in the 3D extrusion process [78, 79]. These inks have high viscosity when static (low-shear situation). While being subjected to shear, their viscosity reduces. For polymers, the effect of shear-thinning could a result of the disentanglement of polymer chains upon shear [80]. Therefore, adjusting a polymer's entanglement would be key to obtain a preferable ink for extrusion. Particularly, for small molecule inks which normally have low entanglement, adding dopants, e.g., silica [81], could introduce extra intermolecular interactions, such as hydrogen bonds, so that the ink would have increased shear-thinning effect and better printing performance. On the other hand, when shear-thinning inks are used, they are able to stay still in the container without being extruded out until the compression breaches its threshold, which consequently would lead to a delay of extrusion, as shown in Figure 7, and defects on structures built at the beginning. Also, when changing layers, the monitoring programme would temporarily cut off delivering compression to the ink and to prevent over-extrusion. But this would bring defects to other layer or even ruin the entire additive manufacturing process. However, the length of delay varies along with the different recipes of ink, which means it is difficult to implement this in the monitoring programme from the manufacturer, and thus becomes time-intensive for researchers to optimise parameters. As a result, extrusion-based additive manufacturing is competent to carry out large-scale 3D construction work but has limited advantages in the manufacture of fine structures.

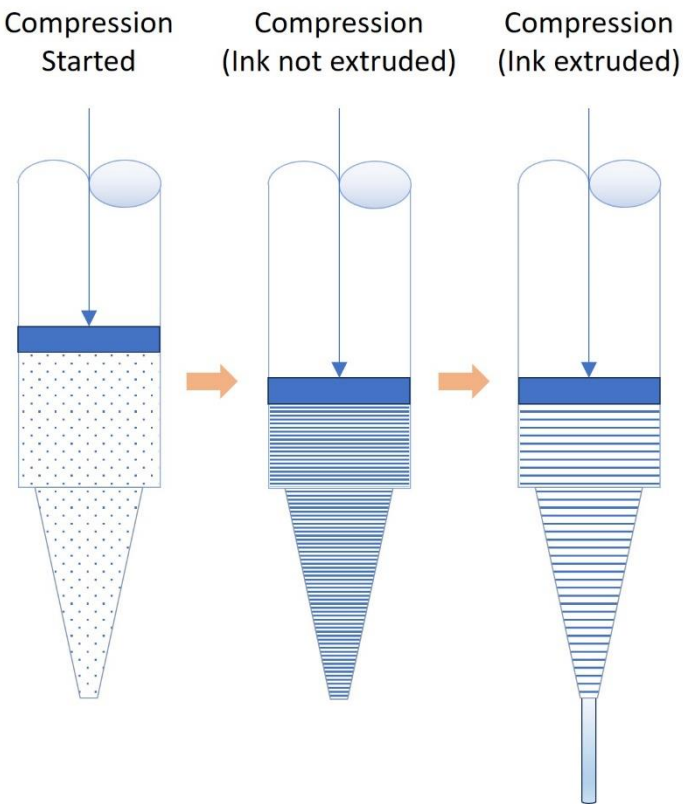

Figure 7. Delay of extrusion after compression being applied.

1.5.1.2. Vat photopolymerisation Single-photon Lithography

Vat photopolymersation typically uses a light source to cure a photocurable resin in a spatially controlled manner [82]. A few different techniques classified in vat photopolymerisation are stereolithography and digital light printing. Stereolithography typically scans a focussed light beam to scan through the photocurable resin to build the layer, while digital light printing projects a whole 2D image *via* a digital mask (e.g., micromirror array) to construct a layer. Additionally, LCD screens are becoming increasingly popular as light sources for cheap LCD-based vat photopolymerisation techniques.

Vat photopolymerisation could provide much higher resolution, which could easily reach a few microns [83], than extrusion-based additive manufacturing, which has been regarded as a

candidate for building fine structures. Particularly, in biomedical engineering field, such fine structures are preferable and often used to mimic the environment of living cells [84].

Before building up complex 3D structures, they are usually designed by using computer-aided design (CAD) software with well-defined dimensions [85]. Subsequently, the designed structure is to be 'sliced' into frames, of which the amount of slicing is dependent on the building resolution needed [85]. However, the time duration for printing would generally increase linearly along with the number of slices defined. Thus, a few trials of print set-ups should be carried out to find the optimum slicing number with the best resolution. The patterns sliced from the imported structure can be loaded to the printer's memory to scan the laser through the resin in stereolithography, while switching the laser on/off for the cured or non-cured sections. For digital light printing the sliced images get consecutively loaded onto a digital micromirror device (DMD) and projected through the printing platform or onto an LCD screen used as the printing platform [13, 86, 87]. The difference between the DMD and masking device is that the light selectively reflects from the pattern on DMD to the resin through the transparent build platform [87]. A new projection stereolithography-based printing technique is computer axial lithography, where tomographic sections of a 3D object are illuminated onto a rotating tank holding a photocurable resin [88]. This technique is likely the fastest stereolithography-based technique, because an entire 3D object is built in a single rotation of the resin tank [88]. Deploying maskless projection system or programmable DMD has become the standard in digital light projection [89]. Recently cheaper LCD-based systems are available that mimic the resolution for DMD-based systems. For a printing ink to work well, typical ink formulations include a photoabsorber to increase the printing accuracy by reducing the scatter. This was already highlighted in 2009 by Choi *et al*. who used Tinuvin 327 as a photoabsorber to produce sub-micrometer resolution scaffolds *via* DMD based projection stereolithography [90]. For fabricating biomaterials, it is necessary to avoid bringing extra risk of cytotoxicity into the product. Hence,

two common light absorbers, β-carotene and tartrazine, could be excellent candidates used in 3D printing biomaterials [91, 92]. These two compounds both show wide UV-vis absorbance range, which enables them to be eligible for most light-based additive manufacturing scenarios. Previously, Ozsoz *et al*. conducted an optimisation on 3D printing of polyHIPE *via* projection-based additive manufacturing by adding β-carotene, and the resolution of structures was significantly improved [91].

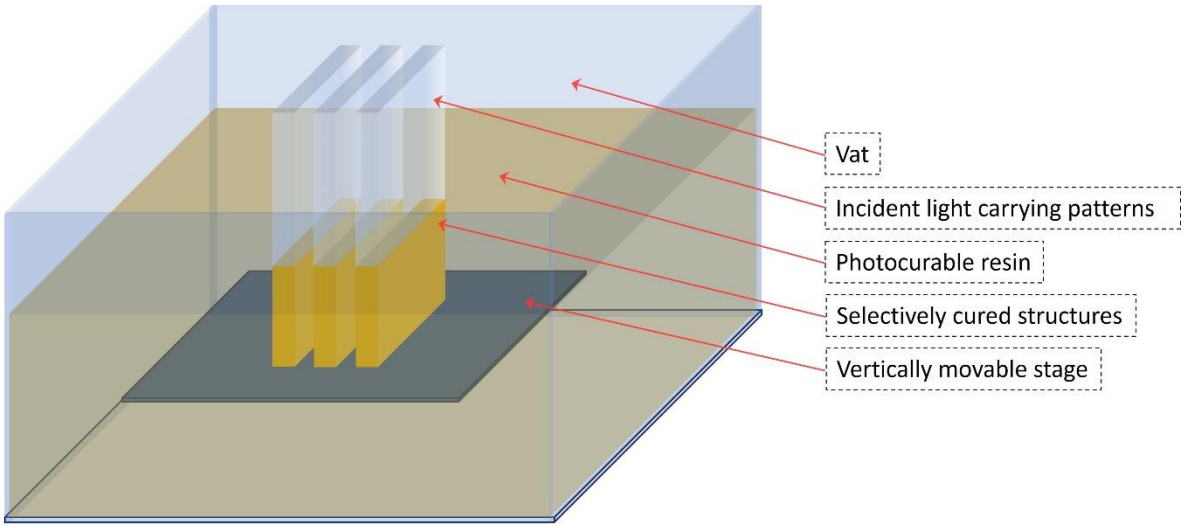

Figure 8. Schematic of stereolithography, where a polymer structure can be selectively cured on a vertically moving stage by being exposed to the incident light carrying specific patterns. The incident light could either come from above the vat and cure the top surface of the resin, or come from below the vat and pass through a transparent bottom and cure the bottom of resin.

1.5.1.3. Two-photon Direct Laser Writing

A cutting-edge method of light-based additive manufacturing is multi-photon direct laser writing (DLW), which is based on photopolymerisation triggered by multi-photon absorption,

of which two-photon absorption (2PA, Figure 9) is typically used. This phenomenon was originally described theoretically by Göppert-Mayer during 1930s and experimentally confirmed for the first time performed in *via* the use of a maser, microwave sources intense enough to achieve 2PA, in 1961 [93, 94]. It is a process that a photosensitive molecule, which is the photocurable monomer or the photoinitiator, absorbs two photons almost simultaneously and transits to an excited state to trigger following reactions.

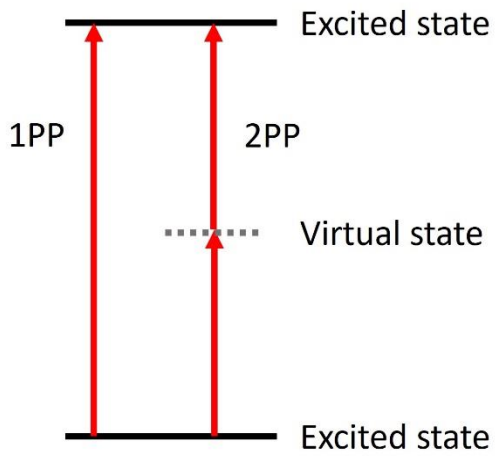

Figure 9. Single- (left) and two-photon (right) absorption.

Since 2PA is a non-linear photon absorption process and its probability is proportional to the square of the light's intensity [95], laser is the optimum light source for 2PA. Furthermore, the light intensity decreases rapidly from the focal point. So theoretically, 2PA only happens at the focal point of the laser (Figure 10), which brings opportunity for ultra-high resolution additive manufacturing, and the additive manufacturing method based on 2PA is called two-photon polymerisation (2PP). The resolution of 2PP can be sub-micron or even sub-100 nm [83], which can hardly be reached by 1PP due to its linear absorption and scattering features.

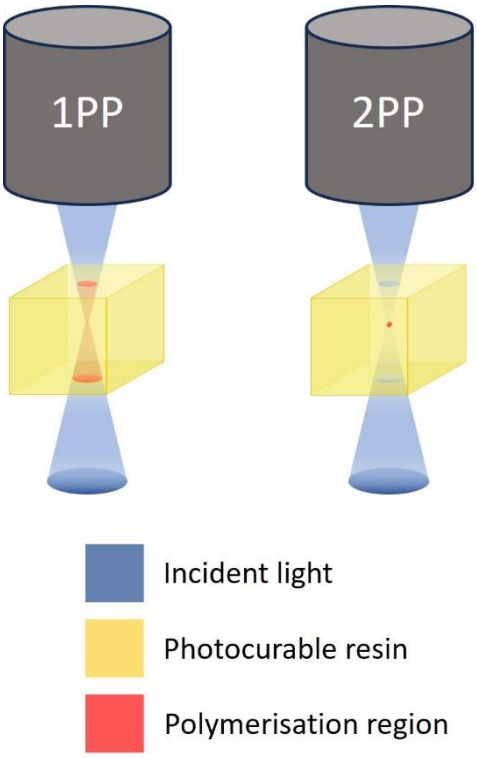

Figure 10. Difference of photo-polymerisation regions of 1PP (left) and 2PP (right).

For biomaterials, micro- and sub-microscale structures are always required to mimic the micro-environment that the cells are living in. With the help of ultra-high resolution manufacturing that 2PP can achieve, such requirements can be fulfilled with well-defined parameters and complex structures. In 2018, Samand *et al.* reported poly(glycerol sebacate) methacrylate (PGS-M) scaffolds fabricated *via* 2PP for tissue engineering, where ~70 μm chambers were built and muscular cells were successfully cultured [96]. 2PP can also be applied to other complex biomedical devices which require micro- and nanoscale features such as biochips, microfluidics, drug delivery systems [97].

However, the light intensity required by 2PP should be high enough to trigger the excitation, but the accumulation of such high energy would also burn the polymer at the focal point.

Therefore, femtosecond (10^{-15} second) laser is commonly used as the light source. The result of using a femtosecond laser to fabricate ultra-fine structures is that objects built by 2PP usually takes a considerably long time. As such, pre-polymers with higher photosensitivity, such as acrylate rather than methacrylate, would be preferable substrates for 2PP with a reduced light exposure time. Researchers have developed several approaches to improve the fabrication efficiency such as to deploy multi-spot laser (or multi-focus) systems, [98] and research groups are actively building a 2PP version of computer axial lithography (CAL). These methods would significantly increase the efficiency of 2PP DLW. However, due to the ultra-high resolution, the proximity effect between parallel laser beams would be inevitable, which could lead to poorly constructed objects [98].

1.5.2. Emulsion Templating

Another commonly used approach used for fabricating porous material is 'emulsion-templating', by which two immiscible phases are mixed into a status where one of the phases is suspended as small droplets as the porogen internal phase in another one which carries a curable ingredient as external phase. And when the external phase is cured, a porous structure can be formed up after the internal phase is removed (Figure 11). This approach brings high customisability to the critical features of porous materials, such as adjusting porosity and pore sizes simply by changing the amount of internal phase and mixing speed of the lab-based stirrer mixing the emulsion [99]. The amount of added porogen is the major factor of affecting porosity. Normally, the ratio between the volume of porogen and the entire mixture is considered as the porosity. When the internal phase reaches 74% or beyond, a high-internal-phase-emulsion (HIPE) can be formed, and the solid porous material cured from HIPE is referred for as polyHIPE [100]. A broad range of applications have been discovered based on this polymeric

porous material. Due to the ultra-large surface area feature, these materials can be used as gas storage and enzyme immobilisation [101, 102]. Also, when it is used in air, which is a poor thermal conductor, the micro-scale chambers filled with air make polyHIPE become an excellent heat insulator [103, 104]. Additionally, the extremely complicated internal structure of polyHIPE is capable of attenuating the propagation of sound inside so that it shows a great sound insulation performance [104, 105]. But most importantly, the micro-porous structures of polyHIPEs are becoming popular in bioengineering fields such as tissue engineering, due to that the microenvironment polyHIPEs can provide is capable of mimicking the natural living environment of cells [106].

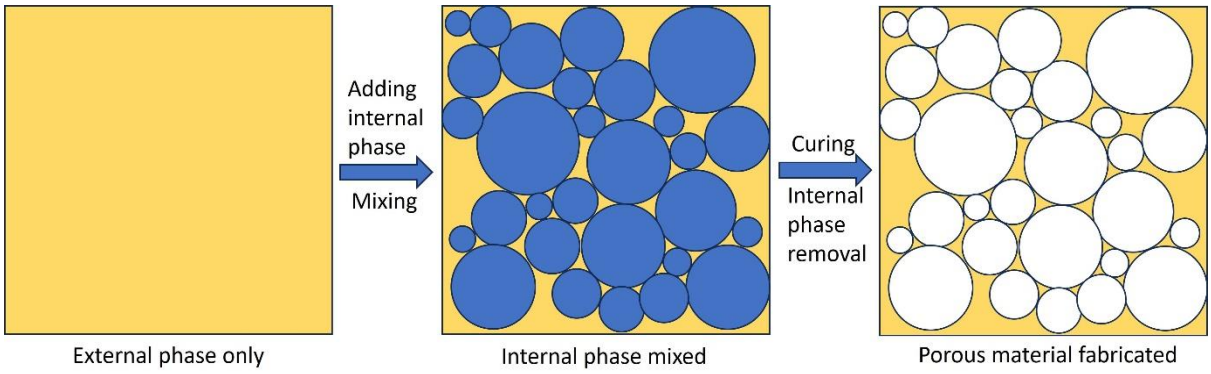

Figure 11. Schematic of fabrication of porous materials *via* emulsion templating.

Due to the immiscibility of the mixed phases, the instability of the mixture is usually inevitable, which would lead to a significant phase separation. Hence, surfactants are usually used to stabilise the emulsions to prevent phase separation.

Surfactants are a series of amphiphilic chemicals that have both polar and non-polar chemical structures on both sides of a single molecule, so that they can play a role of decreasing interfacial tension between the immiscible phases and stabilise the emulsion.

However, for biomedical applications specifically, the usage of surfactant actually introduces additional ingredients into the materials which could bring a risk of cytotoxicity and affect the porous material's own biological performance. Therefore, minimising the usage of surfactant and using surfactant-free methods have become trends of fabricating porous materials for biological applications. This concept requires that either the porogen internal phase or the curable external phase is able to stabilise emulsified structure on their own. Researchers have developed methods to fabricate surfactant-free emulsion-templated porous materials. A commonly used method is to utilise nanoparticles, to produce pickering polyHIPEs. In this method the nanoparticles line the droplet interface and stabilise the emulsion [107, 108]. Another interesting route to surfactant-free polyHIPEs is the use of macromolecules. For example, Furmidge *et al*. successfully fabricated polycaprolactone methacrylate (PCL-M) and poly(glycerol sebacate) methacrylate (PGS-M) polyHIPE materials without surfactant but using gelatine as a stabiliser in the internal phase [109]. Due to the strong intermolecular interactions among these large molecules, the internal phase is able to maintain its configuration under specific temperatures so that the phase separation from interfacial tension is not powerful enough to break the structure of the internal phase. Another possible approach is to synthesise amphiphilic curable molecules so that the external phase carrying these molecules is able to form a stabilised emulsion without surfactant.

According to a phenomenon described in Johnson *et al*.'s work of synthesising a 3-arm polycaprolactone acrylate, a thick cream-like emulsion was formed at the water oil (dichloromethane) interface during the washing process [40]. However, such phenomenon has never been reported by work done on the synthesis of 3-arm or 4-arm polycaprolactone methacrylate [13, 15]. According to estimated values of polarities of acrylate and methacrylate end groups on PCL by ChemDraw 19.0 and presented as log P (Figure 12), acrylate end shows a lower log P value than methacrylate does.

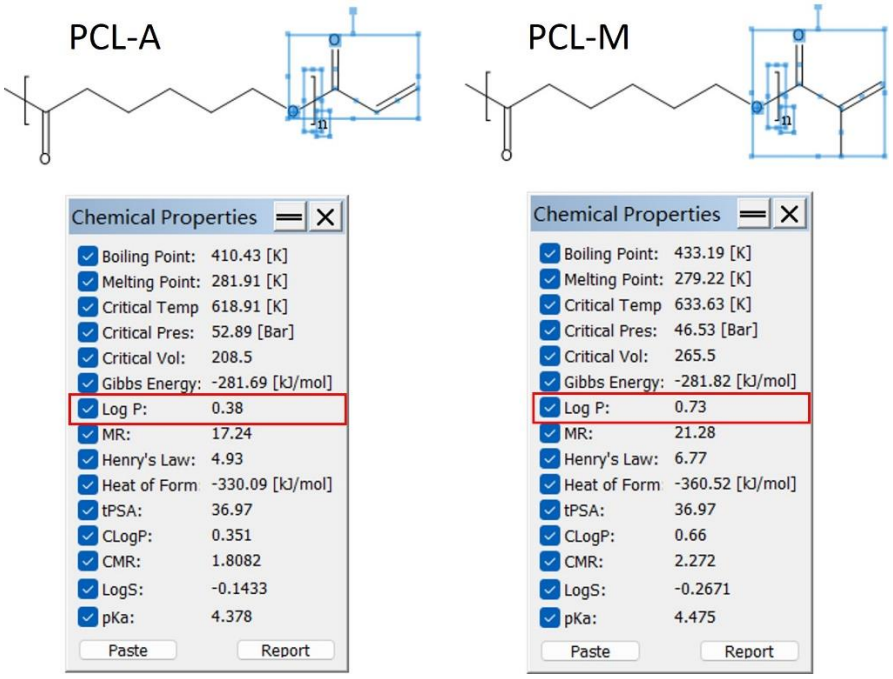

Figure 12. Estimated polarities of PCL-A (left) and PCL-M (right), of which the values are in the red boxes as log P.

$$\log P = \log \frac{c_{octanol}}{c_{water}} \tag{6}$$

In Equation (6), log P is defined as the logarithm of the ratio of the concentrations of substrate dissolved in a bi-phasic solvent containing a non-polar and a polar solvent, which are usually octanol ($c_{octanol}$) and de-ionised water (c_{water}), respectively [110]. According to Equation (6), if the value of log P is closer to 0, the ratio of $c_{octanol}/c_{water}$ is closer to 1, meaning that the substrate shows less difference of solubility in this non-polar and polar solvents. Since acrylate groups show a much closer value of log P to zero than methacrylate group on PCL does, it can be hypothesised that PCL-A might be a promising amphiphilic emulsifier for fabricating surfactant-free emulsion-templated materials. The main factor contributing to this result could

be one less -CH3 group on the chemical structure, which is a non-polar functional group, leading to a higher overall polarity of PCL-A.

1.6. An Alternative Method to Synthesise PCL Acrylate

1.6.1. Conventional Method and Possible Optimisations

Conventionally, acrylation is performed *via* acryloyl chloride/triethylamine (AC/Et_3N) reaction system as shown in Scheme 2. Acryloyl chloride is a commonly utilised acylation reagent, where there is an electropositive C on the -C=O- to be attacked by the -OH group and the -C=C from acryloyl chloride can be introduced to the substrate [111]. However, HCl will be generated as the by-product in this reaction, which has to be removed to acquire a higher degree of conversion. Due to the excellent solubility of triethylamine (Et_3N) in most organic solvents and its nucleophilic property, it is usually selected as the 'acid absorber' in this reaction to help improve the final yield of final acrylate product [112, 113].

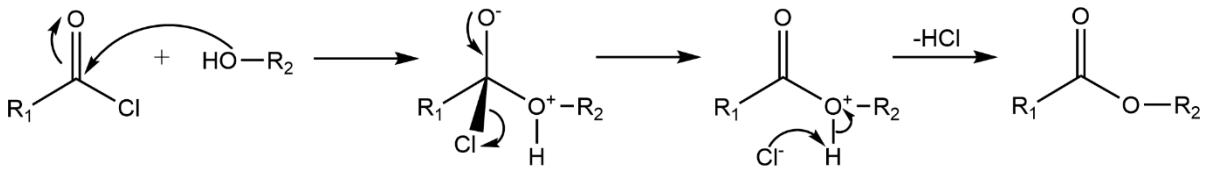

Scheme 2. Esterification between acyl cloride and alcohol.

However, it has been reported that a yellow final product is always generated after acrylation *via* this conventional method [40, 114]. A study has been conducted and concluded that this yellow colour comes from a complex compound between acryloyl chloride and Et_3N [114]. And this

yellowish colour can hardly be removed thoroughly from the final product [40, 114]. Due to its yellow colour, the performance of light absorbance could be limited during photocuring, certain wavelengths of incident light would be mostly absorbed by this impurity rather than the photoinitiator or photo-sensitive monomers, thus, the curing result could be affected. On the other hand, the report conducted the cytotoxicity of this impurity which demonstrated that this impurity could show significant cytotoxicity with concentration higher than 0.01g/L in the cell culture media [114]. Thus, this risk has to be avoided when relative acrylate resins are going to be employed as biomedical materials.

To improve this defect, multiple alternative methods have been suggested. One approach it to use inorganic compounds as the 'acid absorber', such as potassium carbonate [114]. However, these compounds usually have poor solubility in organic solvents, so, they might have very limited improvement on the conversion rate. A direct polycondensation between acrylic acid and -OH is not considered to be suitable as well due to that high temperatures, which is usually over 100°C, is normally an essential condition to remove the generated water from the reaction system to acquire high conversion rate, but such high temperatures will trigger crosslinking which might lead to explosive temperature increase in this exothermic reaction[115], which can ruin the product and also can be dangerous. In summary, an alternative way to perform high degree of acrylation without introducing toxic impurities but safe enough to protect the required -C=C functional group has become a challenge.

1.6.2. Steglich Esterification

In 1978, a novel method of performing esterification, Steglich Esterification, was discovered and named after Prof. Dr. Wolfgang Steglich [116]. As shown in Figure 10, this reaction allows esterification to happen directly between acid and alcohol with mild conditions by using

carbodiimide (coupling agent, compound in red in Scheme 3) and 4-dimethylaminopyridine (DMAP, catalyst, compound in blue in Figure 10) [116], which could completely avoid introducing the yellowish impurity generated from the AC-Et_3N reaction system. In this reaction, the N on carbodiimide, as a nucleophilic atom with unsaturated bond with C, attacks and captures the H from R_1-COOH and becomes ionised. Subsequently, the electron on the π orbital of -C=N- transfers to $-NH^+$ and forms an -NH group, leaving the central carbon being attacked by R_1-COO^- and forms an intermediate ester with a residual -C=N- structure. Following, this residual -C=N- performs similar reaction by attacking the H from an R_2-OH group and forms another $-NH^+$ and a ^-O-R_2. Subsequently, the engagement of DMAP will ensure the reaction to follow the correct direction by attacking the π orbital of -C=O- ad form an unstable intermediate product [22]. However, the strong induction effect of N and O atoms on the $-H^+N$=C-O- structure has a trend of breaking π orbital of N=C, and the O^- and N^+ on the pyridine side show a trend of withdrawing electron as well. As a result, the -O-C- bond of -O-C-R is weakened and broken by the strong induction effect from both sides, leading to a stable urea product and a DMAP-(C=O)-R_1 structure, of which the π orbital on the ketone structure is to be attacked by the ^-O-R_2 generated before. Hence, another unstable intermediate compound is formed with an ^-O-C-O- structure. Since the orbit of O atom on -OR_2 has already been saturated and, the O^- needs another electron to fill in all the orbitals and it has a stronger induction effect than N does, the C-N bond is broken and an ester R_1-(C=O)-O-R_2 is produced leaving DMAP as the original form.

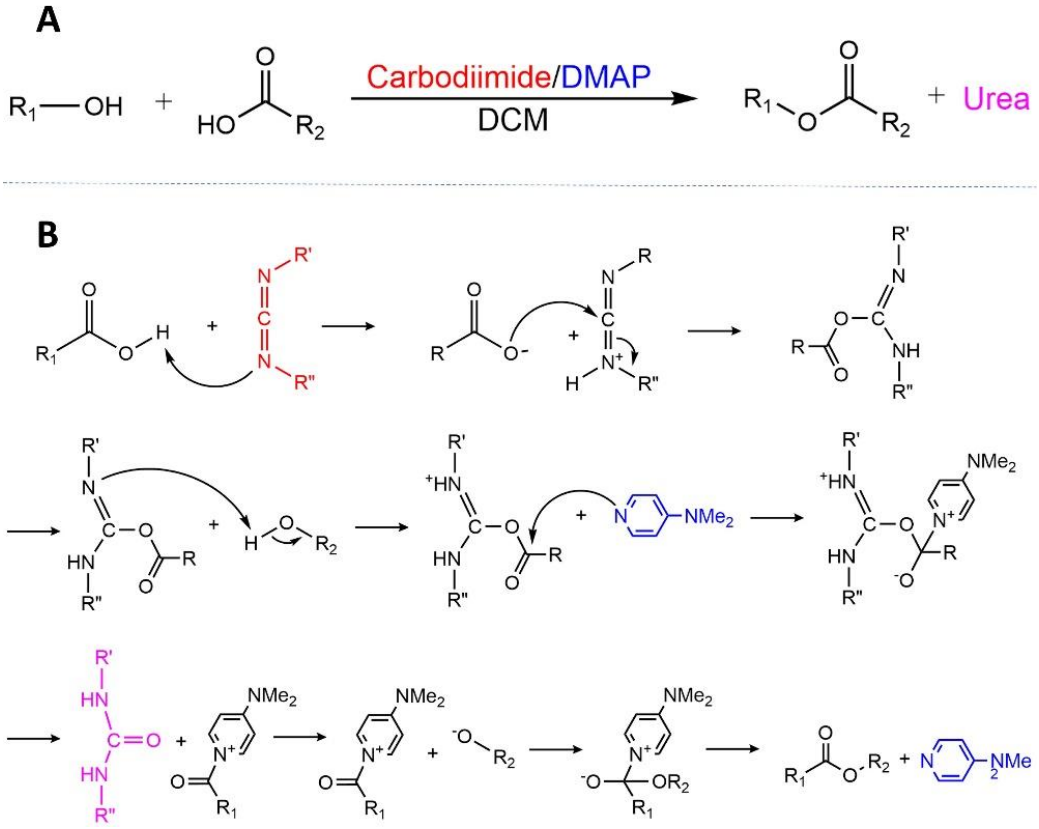

Scheme 3. A) Reaction scheme of Steglich Esterification, where the coloured compounds correspond to the chemical structures with same colours in B. B) Detailed mechanism of Steglich Esterification, where R′ and R′′ are the radicals of carbodiimide which are succeeded by urea so that they should have some similar properties, e.g., water solubility.

In the original reaction system reported by Bernhard and Wolfgang, dicyclohexylcarbodiimide (DCC) was used as the coupling agent [116]. However, the by-product urea dicyclohexylurea (DCU) generated from DCC has a poor solubility in water, hence, it can be difficult to remove thoroughly from the final product [22]. Nevertheless, a water soluble one, such as 1-ethyl-3-(3-dimethylaminopropyl)carbodiimide (EDC) used in Lutjen *et al.*'s work [117], can be selected from the carbodiimide family so that the by-product urea should be water soluble as well. Additionally, DMAP is regarded as an essential catalyst to be introduced in this reaction system,

which is a water soluble reagent and only to be used up to 5 mol% [22, 118]. Since acrylation on PCL is in fact a type of esterification, Steglich Esterification is eligible for this functionalisation. Therefore, if acrylic acid-EDC-DMAP reaction system is applied for acrylation on -OH groups, a clean final product can be expected, as all the by-product, catalyst, and excess acrylic acid can be easily removed by simple water washing.

Steglich esterification provides multiple advantages such as high selectivity, mild reaction conditions, and high yield of product. More importantly, this reaction can also apply to substrates with low sensitivity, which are normally large or complex-structured molecules. Norouzi *et al*. presented a work of functionalising polyhedral silsesquioxane pre-polymer with hydroxyl groups (POSS-OH) directly with acrylic acid *via* Steglich Esterification [119]. The POSS-OH with a molecular weight of 900 g/mol (M_w) used in this work showed successful acylation on the hydroxyl groups attached to a saturated hexagonal ring [119], which inspired our work to carry out acrylation on multi-arm PCL *via* Steglich Esterification. However, Steglich Esterification can also be applied to amination reactions as well. Since -NH_2 has higher nucleophilicity than -OH, the catalyst DMAP is not an essential reagent added in the reaction system. Furthermore, Steglich Esterification would possibly be an approach to control molecular weight and to reduce the reaction time of some polycondensation reactions. For example, the synthesis of poly(glycerol sebacate) (PGS), which is an excellent elastomeric biomaterial, is usually performed under 120 °C with 24 hours of nitrogen flow and 24 hours of vacuum (40 mTorr) successively [120]. However, the performance of maintaining such harsh conditions, such as high temperature and high vacuum, strongly depends on the capability of equipment. And the polydispersity index (PDI), which demonstrates the width of molecular distribution, would show a large value, particularly when high molecular weights are needed [121]. Deploying Steglich Esterification would help optimise such an issue because the reaction could be carried out under mild conditions rather than high temperature, which could possibly

bring oxidation and oil contamination to the polymer if an oil bath is used. Besides, the degree of esterification depends on the added amount of carbodiimide, which means that the process of esterification should be ceased once the carbodiimide is consumed up and the degree of esterification could be precisely controlled. Since the carbodiimide is a coupling agent taking off -OH and hydrogen from -COOH and -OH groups with a ratio of 1:1, there would be no water introduced into the reaction system, allowing the synthesised pre-polymer to stay in the solution for further functionalisation with water sensitive reagents such as anhydrides or acyl chlorides. Additionally, the reaction time would be significantly reduced due to the sensitivity of carbodiimides against -COOH and -OH.

1.7. Summary

PCL has been developed for years as a biomaterial due to its excellent physical properties and biocompatibility but also has potential for further functionalisation. Preparing photocurable multi-arm PCL would be an approach to overcome some of its natural defects. Moreover, introducing reinforcements into photocurable multi-arm PCL would possibly bring extra properties beside enhanced physico-chemical properties, such as self-healing or shape-memory, which could further broaden the application range of this material. To fabricate objects with complex structures for various of applications, additive manufacturing would be a promising approach including extrusion-lased and light-based. The extrusion-based additive manufacturing is more suitable for large-scale structuring while the light-based one is more suitable for building fine structures. Specifically, an up-to-date light-based additive manufacturing, two-photon laser direct writing, is able to fabricate ultra-fine 3D structures. Photoinitators (PIs) are normally used in light-based additive manufacturing. But selecting PIs would potentially affect biocompatibility of the cured material. So, more biocompatible PIs, or

even PI-free photocuring process, would be intriguing for exploration. Another way of fabricating porous biomaterials is called emulsion-templating, where surfactants are commonly used but could preferably be avoided to have less risk of cytotoxicity. Thus, surfactant-free emulsion-templated material would be worthwhile to explore. Interestingly, acrylates could potentially carry the duty of performing PI-free photocuring, specifically for 2PP, and surfactant-free emulsion-templating. However, the conventional method of acrylation would bring yellow cytotoxic impurity the final product, which would lower its biocompatibility and capability for PI-free 2PP structuring. Steglich Esterification shows a potential of performing acrylation withour bringing extra risk, which is worthy to be employed in this work.

AIMS AND OBJECTIVES OF THE THESIS

The main aim of this thesis is to explore the properties and potential applications of novel formulations based on photocurable multi-arm polycaprolactone.

The objectives of this project are:

1) To synthesise photo-curable polycaprolactone and functionalise it *via* methacrylation and acrylation.
2) To reinforce photocurable polycaprolactone with different types of additives.
3) For acrylation, a conventional method and an alternative method (Steglich Esterification) are to be used and compared.
4) To prepare samples by photocuring: dog-bone-shaped samples, films, and complex structures *via* additive manufacturing (both extrusion-based and light-based).
5) To characterise the samples properties: chemical structures, mechanical properties, thermal properties, microstructures, biocompatibility, and degradability.

2. Photocurable polycaprolactone-methacrylate (PCL-M) composites reinforced with linear polycaprolactone.

2.1. Introduction

Polycaprolactone is a commonly used biomaterial with interesting properties for implant applications [122, 123]. The common available PCL is a linear polymer with molecular weights ranging from 530 to 120000 Da [124]. Nowadays, there are commercially available PCL products which normally have linear chemical structures being widely utilised for medical research as it has been an FDA-approved material [125, 126]. PCL has an elastic modulus of ~350 MPa, and a melting temperature of ~60 °C [6]. The low melting temperature makes it quite applicable for melt deposition-based 3D printing applications, and its Young's Modulus (YM) is higher than typical soft tissues, which is in between 0.1 kPa to 1 MPa [127]. Its thermal and mechanical properties make itself a promising candidate for tissue engineering.

Recently a few reports have highlighted photocurable forms of the polymer to be used in light-based 3D printing, *via* a number of different strategies. Elomaa *et al.* reported the production of a photocurable 3-arm PCL resin *via* a ring-opening reaction of ε-caprolactone with trimethylolpropane and a following functionalisation with methacrylic anhydride [128]. Dikici *et al*. successfully synthesised a photo-curable 4-arm PCL (PCL-M) *via* a similar reaction route but using pentaerythritol as the initiator, which can also form chemically crosslinked structures after being exposed to UV light [15]. This was further explored by Field *et al*., who reported the

3-arm photocurable PCL showed relatively low YM and low ultimate tensile strength (UTS) (~3.5 MPa and ~4 MPa respectively, when the degree of methacrylation was over 75%) [13]. And the mechanical properties of polyHIPEs based on 4-arm PCL reported by Dikici *et al*. showed potential brittleness of this material, of which the YM, UTS and ultimate elongation were up to ~0.5 MPa, ~0.5 MPa, and ~100%, respectively [23]. For these materials to be implemented in commercial applications, and in particular as implant materials, one would need better mechanical properties. Recently, Melchels' group reported combining linear methacrylated PCL formulation with pentaerythritol tetraacrylate crosslinker, which increased the toughness up to 65 times than that of pure crosslinker [129]. In this study we followed an alternative approach to Melchels to obtain a photocurable resin *via* adding linear PCL in different ratios to a 4-arm photocurable PCL resin. This approach was similar to former approaches to produce crosslinked PCL with linear PLA composites [130].

Compared with PCL-M/PLA composites. PCL-M and linear PCL have the same repeating units, which is hexanoate, on their chains, they should show excellent compatibility to each other after being mixed. Thus, composites consist of PCL-M and linear PCL should be able to cover the disadvantages of both sides and acquire enhanced properties. Moreover, compared to using PLA as the reinforcement, which would bring higher stiffness but might not overcome its brittleness, using PCL to reinforce PCL-M could increase both stiffness and flexibility [131].

In this work, we synthesised 4-arm PCL-M and fabricated composites by doping it with a series amount of linear PCL. The mechanical properties, thermal properties, and the microstructures of these composites were characterised. *In vitro* cell work was carried out to explore the biocompatibility of these composites.

2.2. Materials and Methods

2.2.1.Materials

Pentaerythritol, ε-caprolactone, tin(II) 2-ethylhexanoate (stannous octoate), triethylamine (Et_3N), methacrylic anhydride (MAA), polycaprolactone (PCL, average M_n 80,000 g/mol), and diphenyl(2,4,6-trimethylbenzoyl)phosphine oxide/2-hydroxy-2-methylpropiophenone blends (photoinitiator, PI) were purchased from Sigma-Aldrich. Dichloromethane (DCM), hydrochloric acid (HCl), methanol, tetrahydrofuran (THF), and sodium hydroxide (NaOH) were purchased from Fisher Scientific, UK.

2.2.2.Methods

2.2.2.1. Synthesis of PCL-M

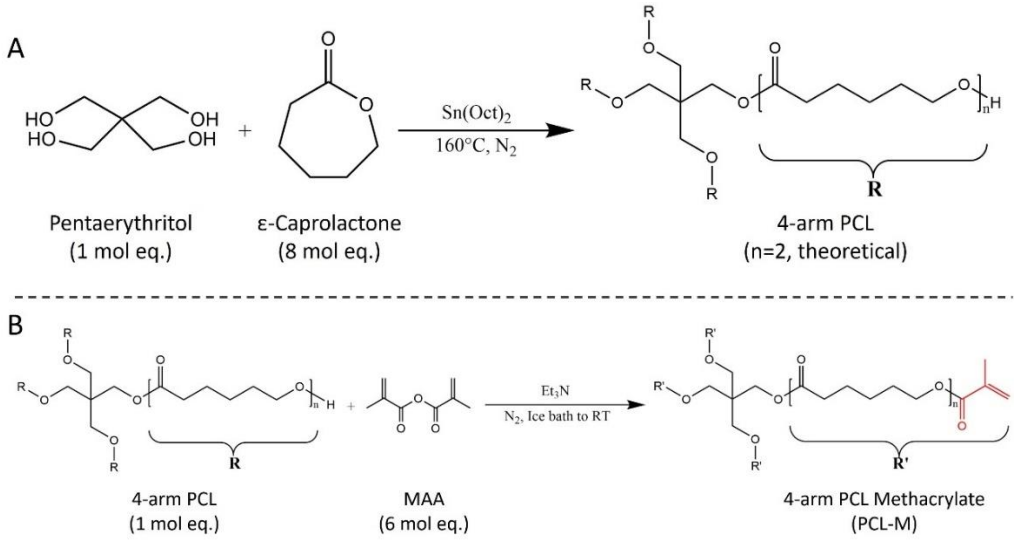

Scheme 4. Synthesis of PCL-M. A) Synthesis of 4-arm PCL which was kept running overnight under nitrogen flow at 160°C. B) Methacrylation of 4-arm PCL with MAA to prepare PCL-M, which was kept under nitrogen flow but in a dark condition for 20 hours [15].

The synthesis of PCL-M (Scheme 4) was done by following the work by Diciki *et al* [15]. Briefly, the first step of synthesis was a ring-opening reaction between pentaerythritol (1 mol eq.) and ε-caprolactone (8 mol eq.) under 160°C and nitrogen flow overnight with 1 drop of catalyst stannous octoate (approx. 30 μL) added when the liquid showed a homogeneous status being stirred at 200 rpm at 160°C. A 4-arm PCL pre-polymer was then obtained for further functionalisation. For the second step, this 4-arm PCL pre-polymer was dissolved in DCM (ratio: 100 g 4-arm PCL in 600 ml DCM) with Et_3N (6 mol eq.). The solution was kept stirring with continuous nitrogen flow and cooled in an ice bath. MAA (6 mol eq.) was then added into the solution dropwise. This reaction was performed in dark condition for 20 hours, during which it was allowed to raise to room temperature. The solution was then washed by HCl (1 M) and de-ionised water to remove residual reagents and by-products. The solution was rotary-evaporated to remove DCM as much as possible. Then the condensed solution was poured into methanol (approx. 10× volume) and kept under -80 °C to precipitate PCL-M to further purify the PCL-M from residual DCM and remnant reactants. The PCL-M precipitation was purified under another roto-evaporation and a high-vacuum line.

2.2.2.2. Fabrication of PCL-M/PCL80k Composites

PCL-M and PCL (80 kDa) were dissolved in DCM (1:3, w:v) with PI (2 wt% of PCL-M) in sealed vials and mixed thoroughly for at least 30 min. Then the PCL-M solution was mixed different weight ratios of linear PCL to form up PCL-M/PCL composite resins. The resins were loaded in syringes and injected into dog-bone-shaped PDMS moulds and also prepared as films on glass slides, respectively, which were then cured under UV lamp (OmniCure S2000, 40

W/cm^2) for 5 min each side. The cured samples were then washed in methanol and dried in a vacuum oven overnight.

2.2.2.3. Nuclear Magnetic Resonance Spectroscopy

Proton Nuclear Magnetic Resonance Sectroscopy (^{1}H NMR, Bruker AVIII 400 MHz, $CDCl_3$ as the solvent) was used for characterising the chemical structures of PCL and PCL-M. And the spectra were analysed *via* MestReNova.

2.2.2.4. Fourier-transform Infrared Spectroscopy

Attenuated Total Reflection - Fourier-transform Infrared Spectroscopy (ATR-FTIR, Thermo Scientific Nicolet 380 FT-IR Spectrometer) was performed for characterising the change of functional groups after 4-arm PCL being functionalised to PCL-M and the change after PCL-M and PCL-M/PCL composite resins being cured. The scanned wavenumber range was between 4000 cm^{-1} to 400 cm^{-1}.

2.2.2.5. Gel Permeation Chromatography

The molecular weights of 4-arm PCL and PCL-M were characterised *via* gel permeation chromatography (GPC, Agilent 1260 Infinity, calibration: polystyrene standard). Samples were dissolved in THF as solvent with a concentration of 2 mg/mL.

2.2.2.6. Mechanical Testing

The dog-bone shaped samples were tensile-tested on Mecmesin MultiTest 2.5-dV testing machine with a tensile speed 1 mm/min. Nine replicates were used for each type of samples.

2.2.2.7. Differential Scanning Calorimetry

Differential scanning calorimetry (DSC, Perkin Elmer Diamond DSC) was used to characterise the thermal properties and crystallinities of different types of samples. The heating profile was performed as follows: the samples were heated from 30°C to 100°C, held at 100°C for 5 min, cooled to -60°C at 10°C/min, held at -60°C for 5 min, and heated to 100°C at 10°C/min. This heating profile was carried out under nitrogen for each sample.

2.2.2.8. Scanning Electron Microscopy

Bulk samples were cut into cubic shapes. One group of samples remained as original, while another group was soaked in DCM and left on a shaker overnight to leach the linear PCL molecules out from the PCL-M matrix. The leached ones were dried in a vacuum oven overnight. Subsequently, all samples were gold-coated for SEM imaging.

2.2.2.9. *In Vitro* Biocompatibility Assay

The cured films were cut with a biopsy punch into circular discs (diameter 9 mm) for cell culture. NG108-15 cells were used to perform cell culture. The initial concentration of cell was 10,000 cells per well. Resazurin assay was carried out on day 1, 4, and 7 respectively to characterise the cell growth.

2.2.2.10. Accelerated Degradation

To examine and compare the degradability of PCL-M and PCL-M/PCL composites, an accelerated degradation was performed using NaOH solution (5 M) and de-ionised water (DI water, control). Briefly, the ends of the dog-bone-shaped sample were cut off into cubes with the same size and configuration. Three of each type of sample were randomly selected for this test. Empty bijous were weighed as w_0 and weighed as w_1 after loading the samples, and the initial weights of samples were recorded as (w_1-w_0). Each of the bijous were then filled with 2 ml NaOH solution and left in an incubator (37 °C), caps sealed to prevent water evaporation. Every 15 hours, NaOH solution was extracted from all the bijous which were then gently rinsed with 5 ml of DI water three times. The samples were left in the bijous and dried under vacuum (50 °C) for 2 hours to remove the residual moisture inside. After drying, each bijou containing sample was weighed as w_1', so the residual weight of sample is (w_1'-w_0). Subsequently, all bijous were filled with 2 ml fresh NaOH, sealed, and left in the incubator for further degradation. The bijous were labelled, and the weights were recorded accordingly. All the weighing process mentioned above was carried out without caps and this monitoring was conducted for 60 hours.

2.2.2.11. Data Analysis and Statistics

Data analysis was conducted in Origin Pro 2020 (mechanical testing, FTIR, and DSC data) and GraphPad Prism (version 10) (cell work data). Statistics was carried out by using One-way ANOVA (mechanical testing data) and Two-way ANOVA (cell work and degradation data). Error bars on graphs indicate standard deviation and statistical significance on graphs is represented as p-value < 0.033 (*), 0.002 (**) and 0.001 (***).

2.3. Results and Discussion

2.3.1. Chemical Structures

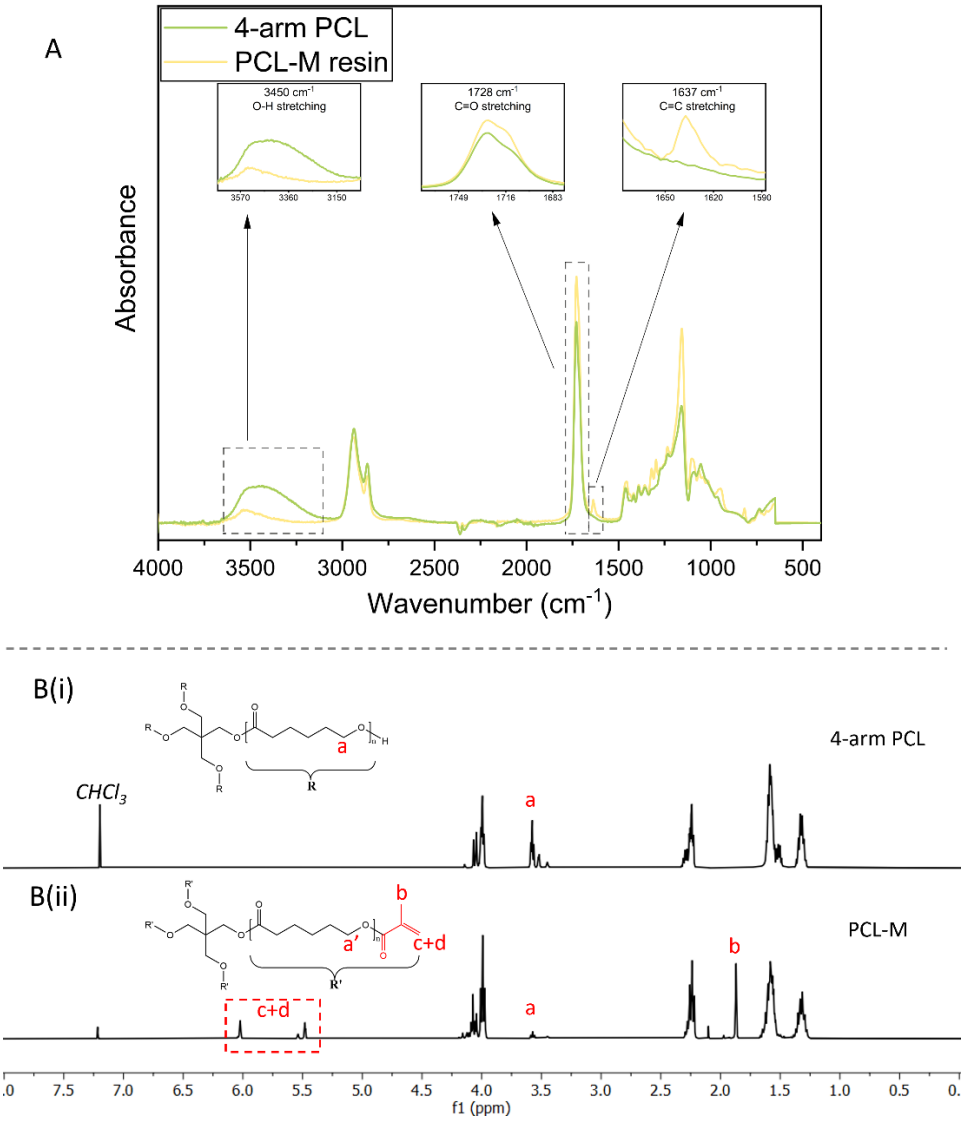

Figure 13. a) ATR-FTIR spectra of 4-arm PCL and PCL-M, where peaks at 3450 cm^{-1}, 1728 cm^{-1}, and 1637 cm^{-1} representing -OH, ester, and C=C functional groups respectively show significant change after 4-arm PCL being methacrylated to PCL-M. b(i & ii) NMR spectra of 4-arm PCL and PCL-M, where peak a at 3.58 ppm shows a significant reduction of intensity but peaks b, c, and d at 1.87 ppm, 5.48 ppm, are 6.02 ppm, respectively.

As shown in the ATR-FTIR spectra of Figure 13a, a significant reduction of infrared absorbance intensity of O-H stretching at 3450 cm^{-1} can be observed, which indicates that the -OH groups, at the ends of 4-arm PCL have been consumed, but not thoroughly. An increased absorbance intensity at 1728 cm^{-1} and a new peak at 1637 cm^{-1}, which represents the C=O and C=C groups respectively, indicate that the consumption of -OH groups is a result of esterification of MAA and -OH which have formed new ester bonds and introduced C=C bonds from MAA to the ends of 4-arm PCL molecules.

The NMR spectra of 4-arm PCL and PCL-M are shown in Figure 13b (i & ii). It can be confirmed that the methacrylate group, represented by peaks b, c, and d, have been successfully introduced onto the 4-arm PCL. As there is a linear relationship between the number of protons with the same chemical environment and the integral areas of their peaks, it can be calculated that the ratio between peaks (c+d) and b is 2:3, which matches the theoretical numbers of protons on the groups respectively. After methacrylation, some of carbon a have been attached with methacrylate groups and transformed to a', while the rest of them at the same location remained connecting with -OH as a. To calculate the degree of methacrylation, initially, the number of methylene carbons directly connecting with the methacrylate groups, labelled as a', can be set as X. The number of methyl groups on methacrylate groups equals to X. And the number of residual carbons still with the -OH groups, which is labelled as peak a on PCL-M's spectrum and located at the same position on PCL's spectrum, can be set as (4-X). And the integral area ratio between b and a on PCL-M's spectrum is 1:0.3. Multiplied by the numbers of protons attached on these methylene/methyl groups respectively, the equation of this peak integral area ratio is as follows:

$$\frac{3X}{2(4-X)} = \frac{1}{0.3} \quad (7)$$

By solving this equation, X is 2.76 approximately. If this 4-arm PCL molecule is fully methacrylated, X should be 4. Thus, the degree of methacrylation can be calculated as follows:

$$\mathbf{\frac{2.76}{4} \times 100\% = 69\%} \quad (\mathbf{8})$$

The degree of methacrylation is approximately 69%.

The PCL-M/PCL resins were prepared as shown:

Table 2. Weight ratios of PCL-M and linear PCL.

Name	Weight ratio (PCL-M : PCL)
PCL-M	PCL-M only
PCL-M-10	1:0.1
PCL-M-20	1:0.2
PCL-M-30	1:0.3

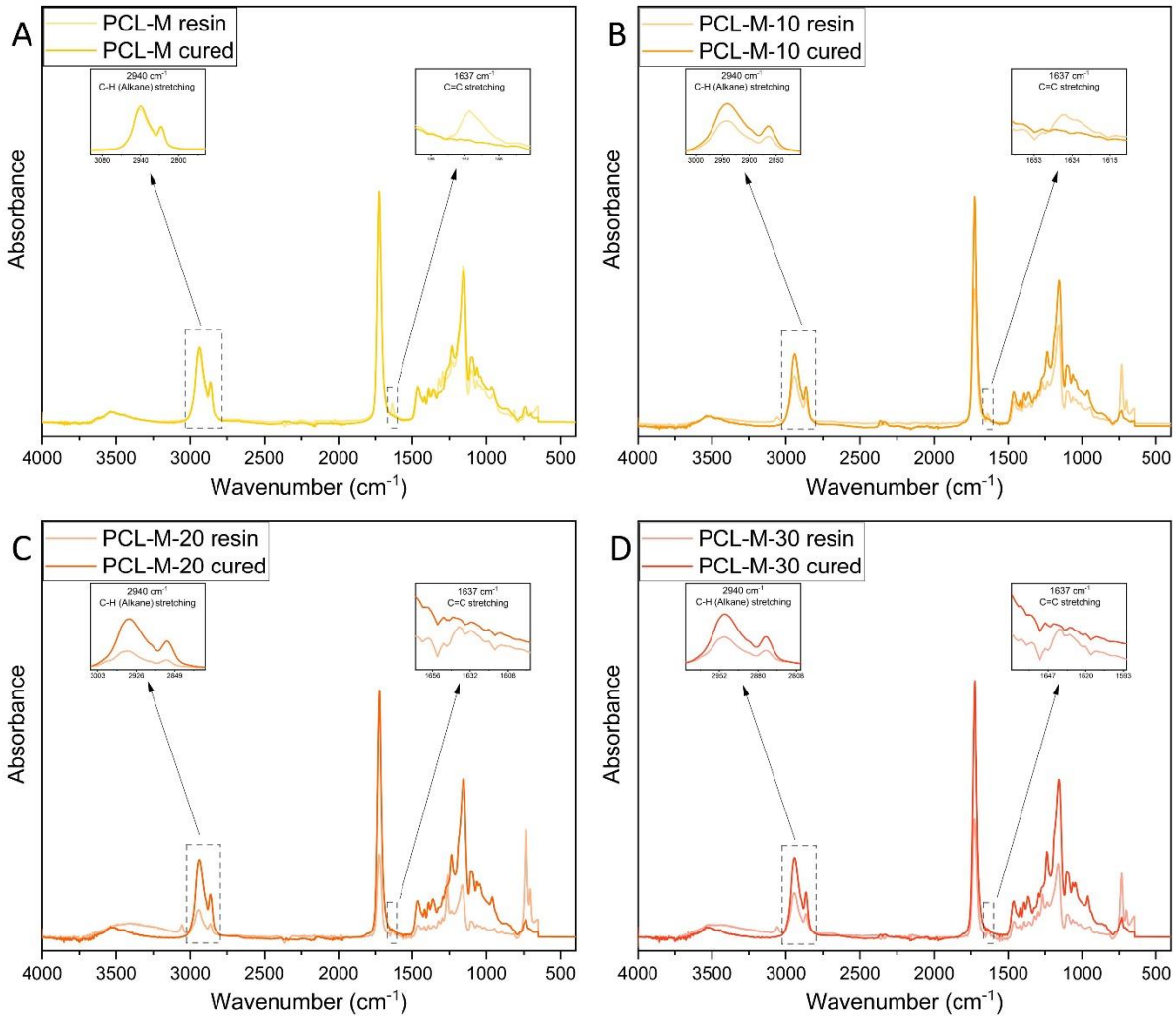

Figure 14. The ATR-FTIR spectra of PCL-M and PCL-M/PCL composites before and after curing.

Figure 14 shows FT-IR spectra of the resins before and after photocuring for the different resins. The spectra show that peaks at 1637 cm^{-1} have reduced in intensity in the spectra of all PCL-M and PCL-M/PCL composites upon curing, which indicates a consumption of C=C bonds. Furthermore, the peaks at 2940 cm^{-1} representing sp^3 C-H stretching have shown increased intensity after curing, which indicates that C=C bonds have been transformed to C-C bonds to form a cross-linked structure. However, due to the strong similarity of chemical structures of linear PCL and PCL-M, both of which contain caprolactone as the major repeating units where

there are lots of methylene groups, the peaks at 2940 cm-1 and 1460 cm-1 representing sp3 C-H stretching and C-H bending did not show significant difference between PCL-M, PCL-M-10, PCL-M-20, and PCL-M-30.

2.3.2. Molecular Weights

GPC results show that molecular weights of PCL and PCL-M are as follows:

Table 3. Molecular weights of 4-arm PCL and PCL-M.

Name	M_n (g/mol)	M_w (g/mol)	PD
4-arm PCL	1616	2167	1.341
PCL-M	2347	2637	1.124

According to the reaction recipe and the degree of methacrylation calculated from NMR result, which is 69%, the theoretical value of 4-arm PCL and PCL-M is calculated as follows:

$$M_{4-arm\ PCL} = M_{pentaerythritol} + 8M_{\varepsilon-caprolactone} = 1049 \text{ g/mol}$$

$$M_{PCL-M} = M_{4-arm\ PCL} + 4\left(M_{methacrylate\ group} - 17\right) \times 69\% = 1239 \text{ g/mol}$$

However, from the GPC results, a generally larger average molecular weight has been acquired than the theoretical value. The molecular weight discrepancy is likely because of a loss of unreacted and low molecular fragments during the washing steps, or potential sublimation of the pentaerythitol. Indeed, the GPC results show that PCL-M's molecular weight is also

generally higher than the theoretical value, of which both M_n and M_w are over 2000 g/mol but with a lower PD value 1.124. Such deviation could be a result of the washing steps, during which the low molecular weight PCL-M could be washed away by acid, DI water, and methanol more easily leaving the heavier fraction in the final product with a lower distribution width. Additionally, due to that PCL and PCL-M used in this work have multi-arm molecular structures, they would occupy larger space in the solution than linear molecules with the same theoretical molecular weight, which would make them spend more time running through the columns so that GPC results showed a higher value [132].

2.3.3. Mechanical Properties

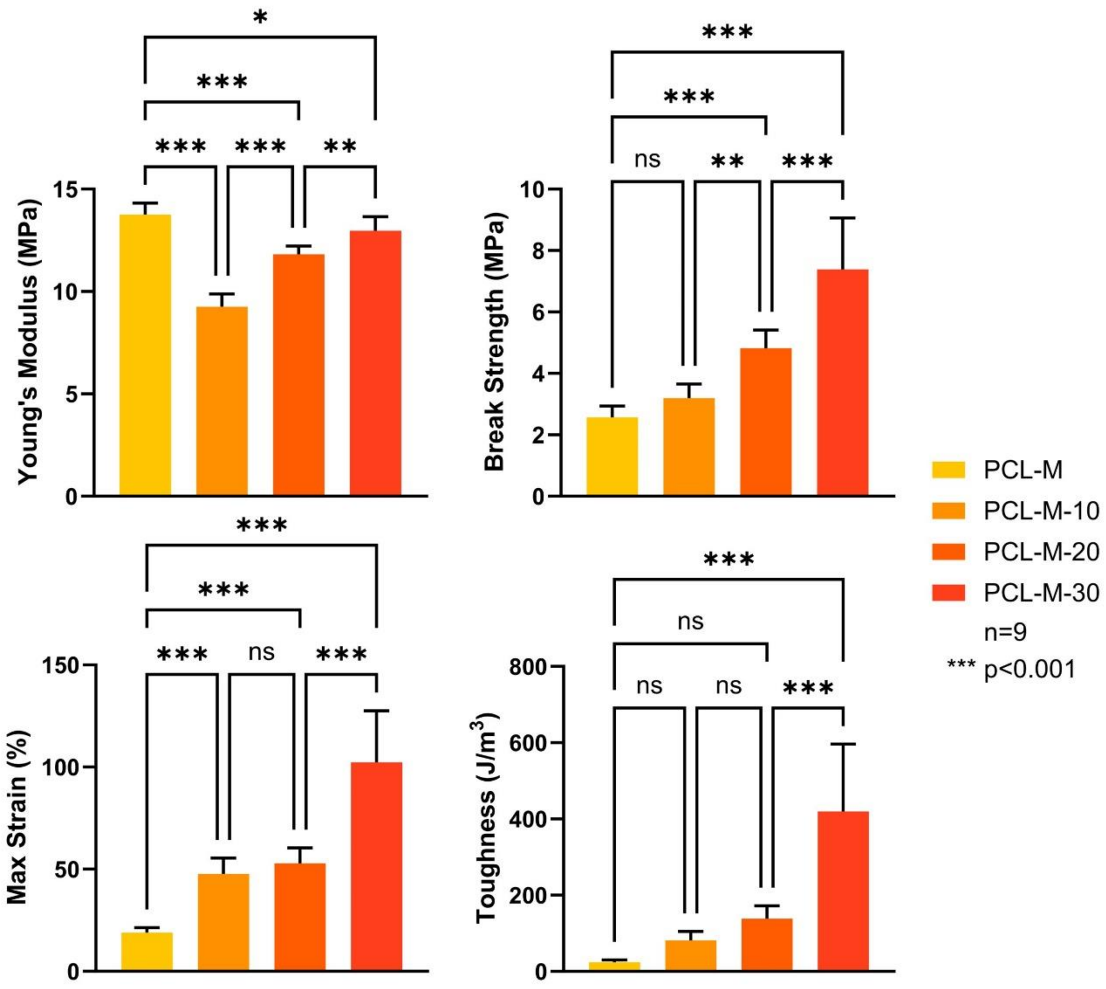

Figure 15. Plots of Young's Modulus, break strength, max strain, and toughness of PCL-M and PCL-M 10, 20, and 30 composites. 9 samples of each group were tested (n=9).

The Young's Modulus of PCL-M (~13.8 MPa) shows the highest value among all types of samples, although increasing the amount of PCL from 10 to 30% increases the YM from ~9.3 MPa to ~13 MPa (Figure 15). After adding 10 wt% of linear PCL, PCL-M-10 shows lower YM compared to PCL-M. This could be a result of the introduction of linear PCL broke the highly crosslinked structure and lowered the crosslink density, but the added amount of linear PCL

was too low to compensate the lost YM value, which led to a lower stiffness [133]. But as the added amount of PCL increased, the degree of crystallised linear PCL increased (as calculated in Section 2.3.4), which contributes an increasing value of Young's Modulus to the materials [134].

As a reinforcement, PCL also provides extra break strength, max strain, and toughness. This is largely contributed by the added linear PCL, of which its mobility is highly restricted due to its high molecular weight (80,000 g/mol). Additionally, the entanglement and crystallinity of these large linear molecules would also introduce extra intermolecular interactions into the composites so that higher stress is required to break them [135]. Furthermore, the large volume and entanglement of linear PCL molecule also would allow a longer molecular moving distance of being stretched from entangled to straightened, and to completely moved away from each other [135]. Accompanying this, more energy is required during this process, which leads to the higher toughness [129, 135]. Accordingly, this composite could be suitable for scenarios which may require heavy loads, high flexibility, or impact absorbance.

2.3.4. Thermal Properties

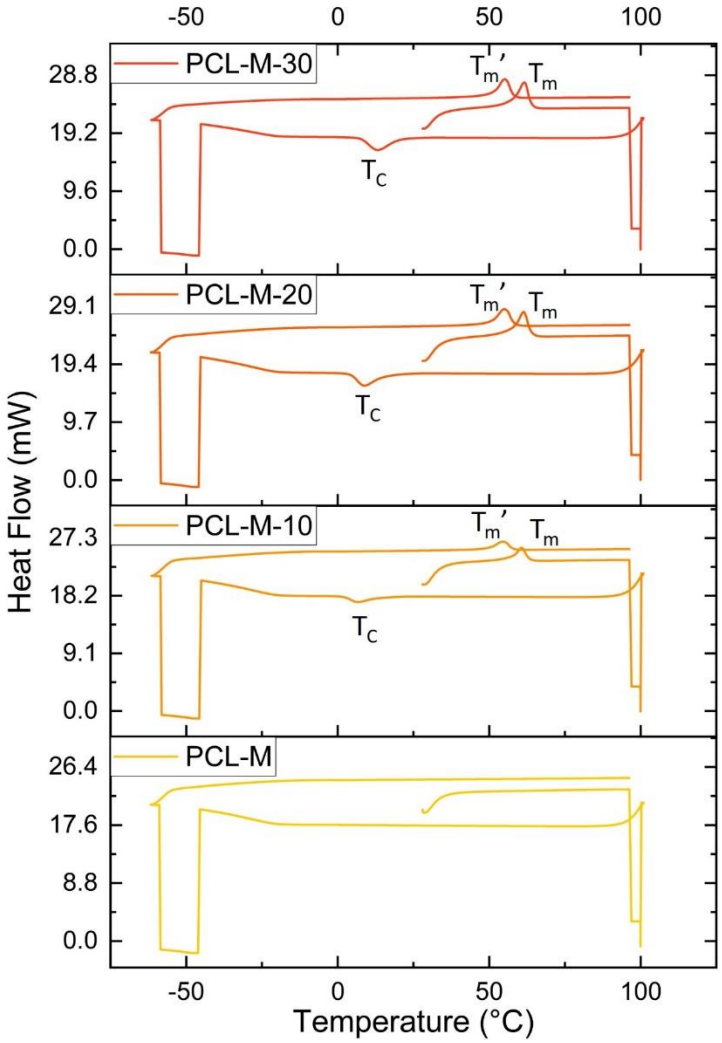

Figure 16. DSC thermograms of PCL-M and PCL-M/PCL80k composites, where peaks refering to melting points (Tm and Tm') and crystallisation points (T_C) can be found on PCL-M/PCL80k composites but cannot be found on PCL-M sample.

Table 4. Thermal properties of PCL-M and PCL-M/PCL composites.

Sample Name	T_m/°C	ΔH_m/(J/g)	T_c/°C	ΔH_c/(J/g)	T_m'/°C	ΔH_m'/(J/g)
PCL-M	N/A	N/A	N/A	N/A	N/A	N/A
PCL-M-10	57.11	6.82	6.87	-5.07	54.47	4.88
PCL-M-20	61.38	12.47	8.90	-9.92	54.93	9.72
PCL-M-30	61.55	17.58	13.21	-13.75	55.10	13.05

All samples used in DSC were completely cured with all residual solvent removed under high vacuum.

As shown in Figure 16, DSC curves show that no peaks can be seen from PCL-M's thermogram, indicating that the photocured PCL-M is an amorphous material, which is expected given that the low-molecular weight pre-polymer will likely form a heavily cross-linked thermoset polymeric network upon cross-linking.

However, peaks can be obtained from PCL-M/PCL samples, and the melting temperatures basically match with PCL's melting point, which is approximately 60°C [6]. These peaks indicate that there are crystallised phases brought by the added PCL, which is a semi-crystalline polymer. Thus, PCL-M-10, 20, and 30 samples can be defined as composites due to this phase separation. The crystallinity of PCL in PCL-M/PCL composites can be calculated as follows:

$$X_c = \frac{\Delta H_m}{\Delta H_0} \times 100\% \quad (9)$$

where ΔH_m is the melting enthalpy measured from each sample's DSC result and ΔH_0 is the standard melting enthalpy of 100% crystallised PCL (M_w 80,000 g/mol), which is 136 J/g [136]. The result of calculated crystallinity of PCL in the composites is shown in Table 5 below, where X_c and X_c' are the crystallinity values before and after thermal history erasing, respectively.

Table 5. Degrees of crytallinity of PCL-M and PCL-M/PCL composites.

Sample Name	X_c/%	X_c'/%
PCL-M	N/A	N/A
PCL-M-10	5.01	3.59
PCL-M-20	9.17	7.15
PCL-M-30	12.93	9.60

From the calculated results, generally, the crystallinity of the linear phases shows a rising trend along with more added PCL, and a same trend could also be found from the samples after thermal history erasing. These results indicate that crystallinity is able to restore in these PCL-M/PCL composites after heating is withdrawn, which makes the linear PCL encapsuled in crosslinked PCL-M a thermally reversible phase. This would probably bring these composites thermoresponsive shape-memory capability [137], of which the testing result is further discussed in Section 2.3.6.

2.3.5. Microstructural Properties

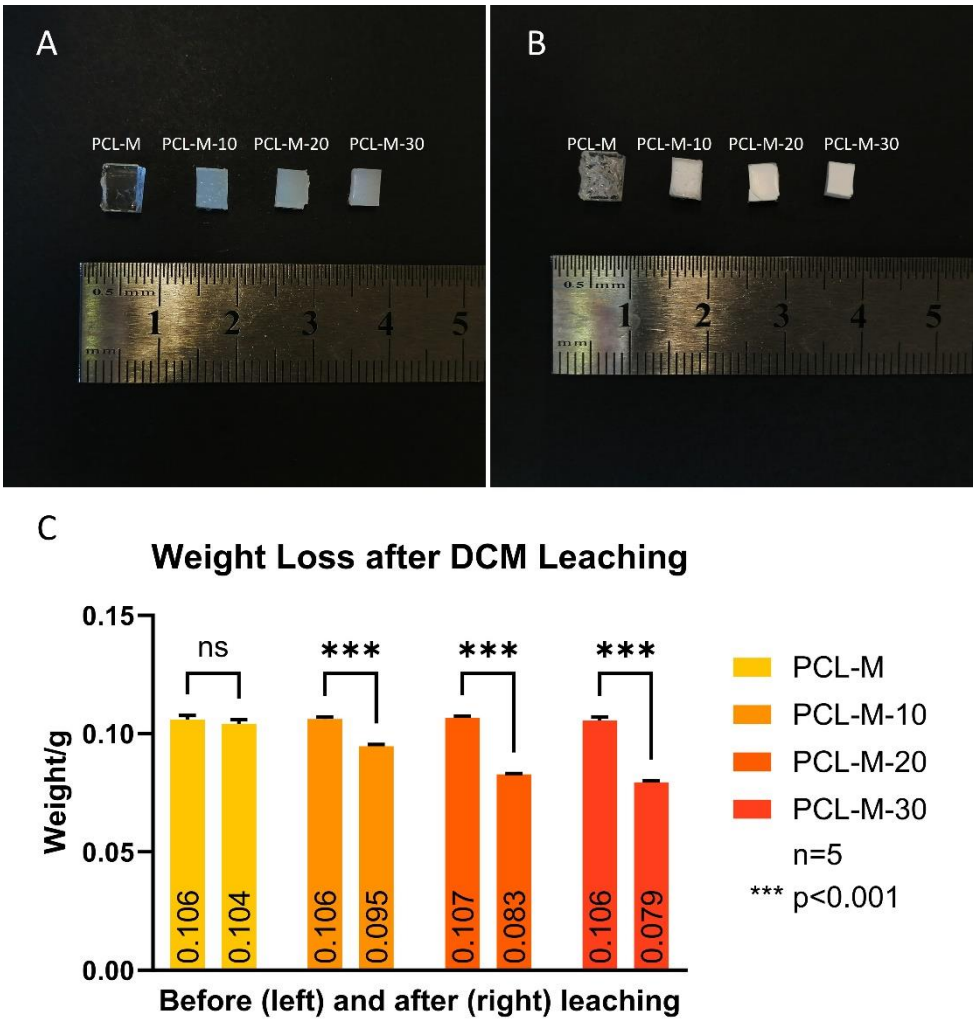

Figure 17. A) Appearances of PCL-M to PCL-M-30 before DCM leaching. B) Appearances of PCL-M to PCL-M-30 after DCM leaching.

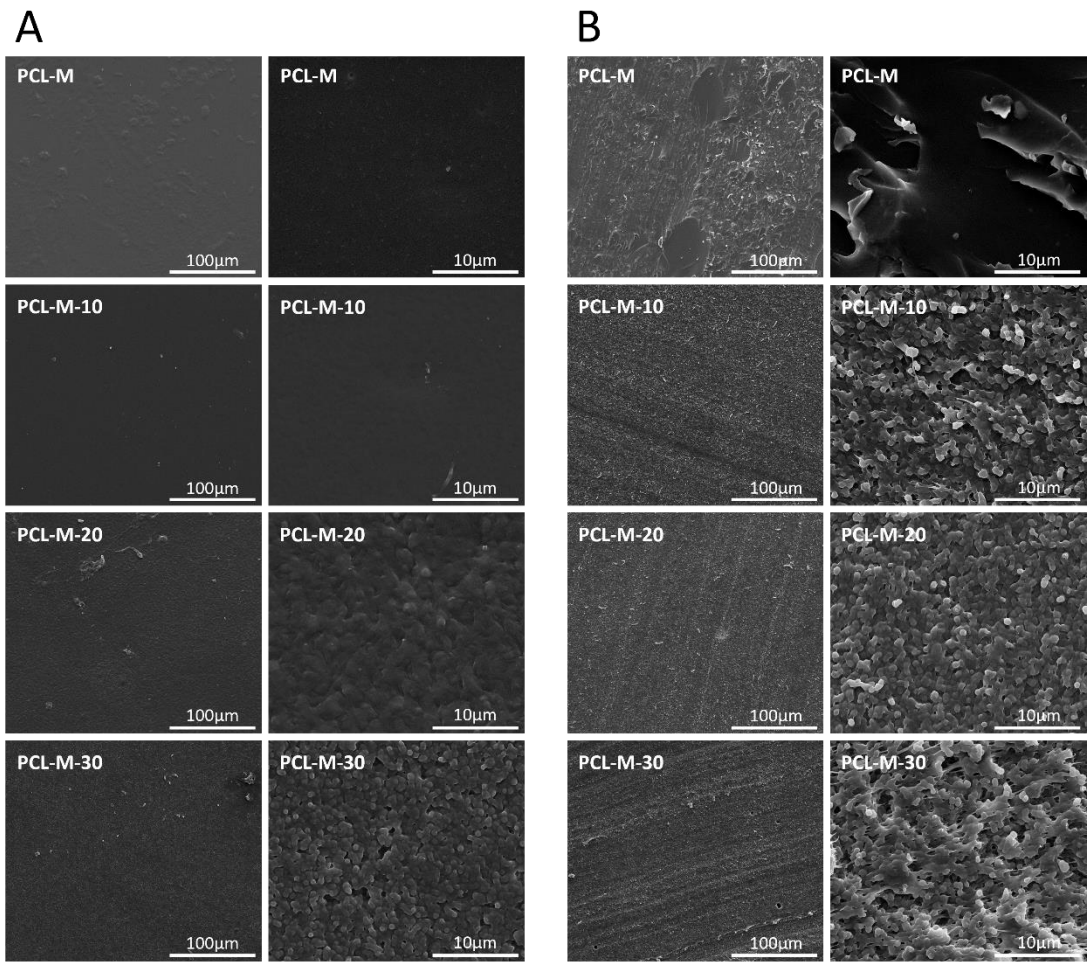

Figure 18. A) Surface PCL-M to PCL-M-30 before DCM leaching. B) Cross-sectional area of PCL-M to PCL-M-30 before DCM leaching.

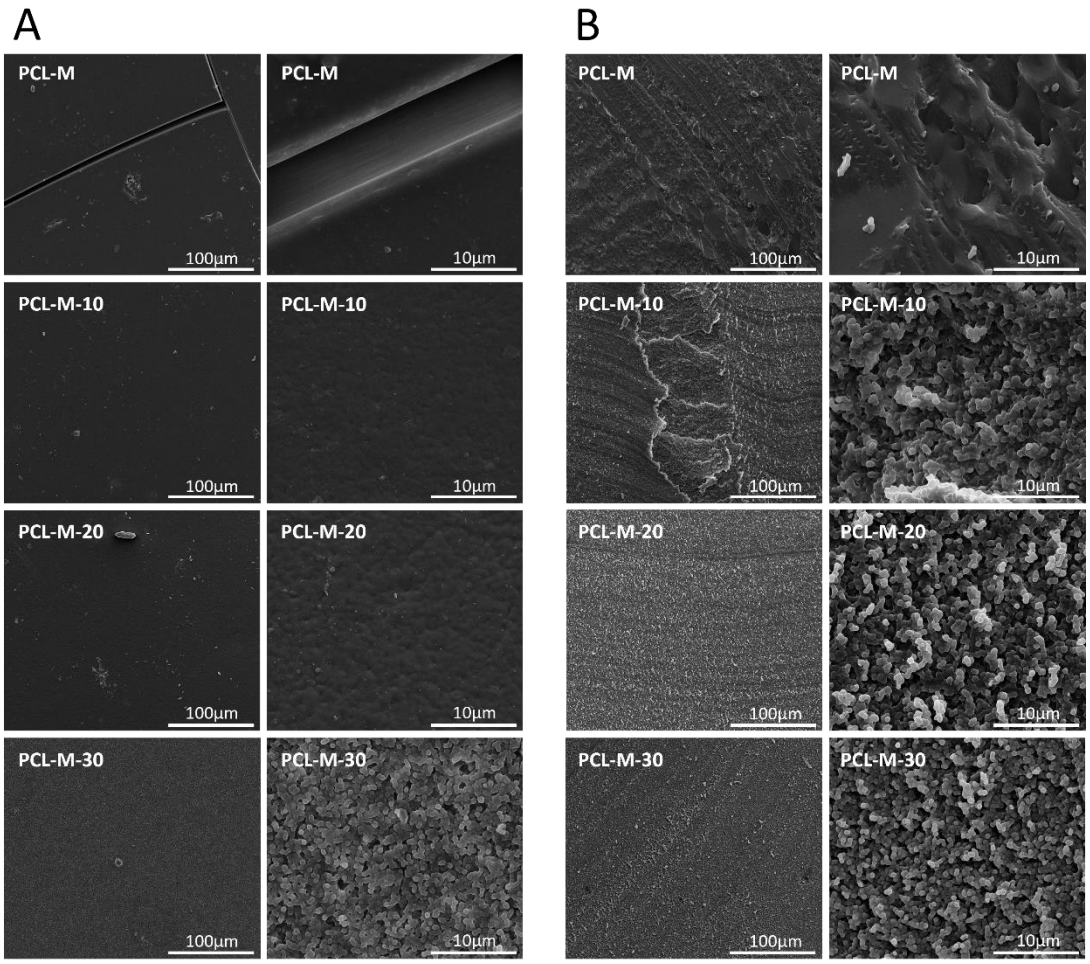

Figure 19. A) Surface of PCL-M to PCL-M-30 after DCM leaching. B) Cross-sectional area of PCL-M to PCL-M-30 after DCM leaching. Scale bars: 100 µm (left columns) and 10 µm (right columns).

Figure 17A shows a set of cured PCL-M materials , the PCL-M samples are transparent, which indicates a phase segregation and a composite structure instead of a mixed polymer structure. To further investigate the microstructure of these materials DCM was used to leach the linear PCL phase out of the PCL-M matrix.

The appearance of PCL-M/PCL leached samples (Figure 17B) look more pale and less reflective on the surfaces, indicating that the leached samples might have porous structures

after leaching. From each type of material, 5 samples were selected randomly and cut into cubic shape with approximately 0.1 g as their initial weight. After DCM leaching, all the samples were dried under vacuum and weighed to record the weight loss. According to the results (Figure 17C), the weight loss shows compliance with the added ratio of PCL. Such results indicate that the distribution of PCL after solvent casting was considerably homogeneous in the composites. The mass loss Fig 5C showed that the 10% PCL-M/PCL materials lost 10.4%, the 20%-PCL-M/PCL lost 22.4% and the 30% PCL-M/PCL lost 26.5%, indicating that most of the linear PCL can be eluted from these objects. As expected, the PCL-M did not lose any significant weight upon DCM treatment. PCL-M did exhibit cracking after DCM treatment, which was due to the mechanical stresses on the materials during swelling and subsequent drying.

Before DCM leaching, SEM images show that the cured PCL-M/PCL composites generally acquired bumpy surfaces compared to PCL-M's surface which is a rather smooth one (Figure 18A). Some spherical structures can be observed on the surface of PCL-M-20 and PCL-M-30 sample. The samples were cut through by a scalpel so that the cross-sectional areas can be observed. Under SEM, a smoother cross-sectional area can be seen compared to PCL-M/PCL composites (Figure 18B). However, a massive number of spherical structures, which appear to be immersed in a matrix, can be observed, which indicates a composite structure, driven by a phase separation between the linear and 4-arm PCL materials. To further explore the phase separation of these composites, all samples were washed in DCM overnight to leach the linear PCL out from the matrix. In Figure 19A and particularly in the cross-sectional areas shown in Figure 19B, porous structures formed by the spherical structures can be seen, of which the size is basically homogenously distributed, and the approximate average diameter of spheres is below 1 micron. Since these structures have not been washed away, it can be confirmed that these structures are PCL-M matrix. These structures indicate a well-mixed structure micro-

composite obtained by solvent casting, which might be able to be combined with other manufacturing techniques (e.g. stereolithography or emulsion templating).

2.3.6. Shape-memory Testing

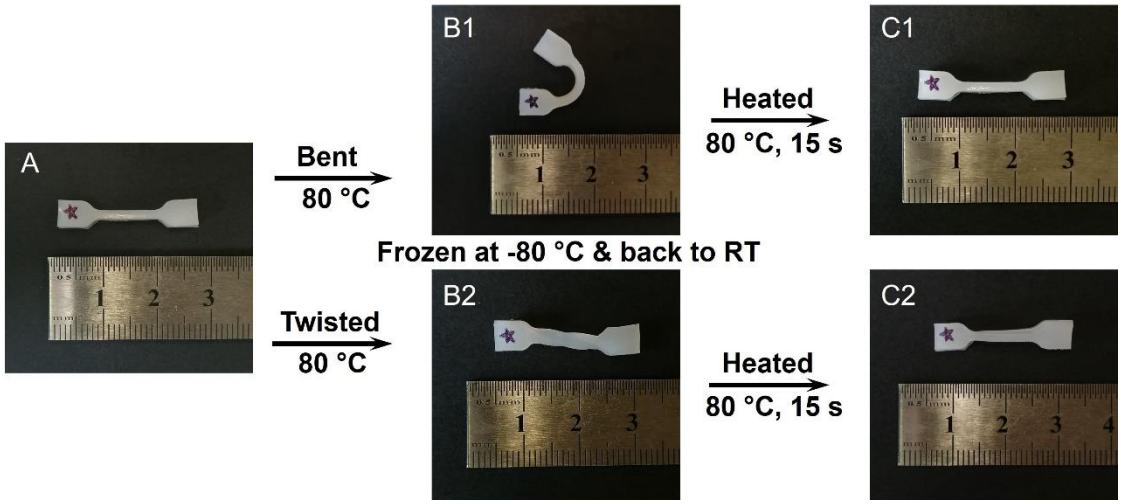

Figure 20. A) The original configuration of PCL-M-10 dog-bone shaped sample. B1 & B2) Bending and twisting of this sample, respectively. C1 & C2) The restoration of configuration after heat applied. All pictures were taken under room temperature (RT).

A PCL-M-10 sample was selected to test the shape memory property. The initial configuration is shown as a dog-bone shaped sample in Figure 20A. The sample was heated at 80°C in an oven for at least 10 minutes. Then, the sample applied with bending (B1 in Figure 20) or twisting stress (B2 in Figure 20), separately, and fixed on a glass slide with tapes to maintain the configurations. The sample was then frozen at -80 °C for 5 minutes and taken back to RT. The fixing tapes and glass slides were removed, and it was found that the deformation could

be maintained (Figure 20 B1 & B2). Subsequently, the sample was moved to the 80°C oven, and the shape restoring process could be accomplished in 15 seconds.

Such a shape-memory property could be explained by its two-phase composite structure. After photo-curing, PCL-M forms a chemically cross-linked thermoset network but combined with a thermoplastic semi-crystalline matrix of linear PCL semi-crystallised. When the temperature is below the melting point of PCL (60°C), due to its crystallised structure, its linear molecules do not exhibit mobility but offer much higher stiffness to deformation (PCL YM: 343 MPa vs, PCL-M YM 15 MPa, approximately) which means that PCL dominates the internal stress thus the deformation can be maintained under RT. When the temperature is above 60 °C, these linear molecules de-crystallise and exhibit mobility, however, the PCL-M phase still maintains chemically cross-linked structures. This also provides a mechanism of storing mechanical energy. Energy input by applied external stress can be stored within the deformed PCL-M network and also can be released when the deformed sample is heated over 60°C where the PCL-M phase dominates the internal stress, the stored external energy can be released, and the shape can be restored. This was also observed by Melissa's group working on a thermoresponsive PCL-DA/PLA shape-memory materials [73].

2.3.7. Biocompatibility (Resazurin Assay)

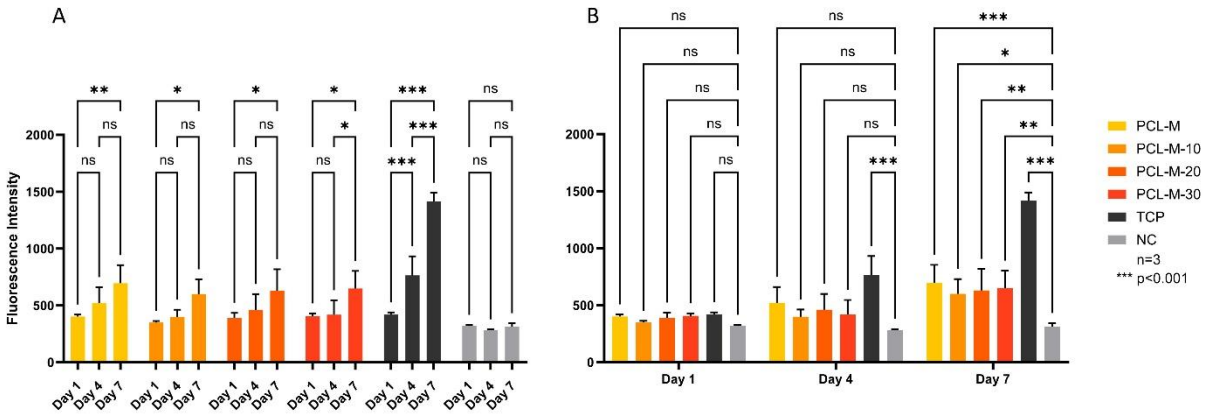

Figure 21. Resazurin assay results of PCL-M and PCL-M/PCL composites. a) Comparison between days within groups. All groups (except the negative control, NC) show significant cell growth on Day 7 compared to Day 1. b) Comparison of each group against NC on each day. On Day 7, a significant difference can be observed from all other groups against NC.

The result of NG108-15 cell culture (resazurin assay) (Figure 21) shows that there is a significant cell growth on all types of materials after 1 week. The composite groups generally show slightly less increase in cell growth compared to the PCL-M results. Due to that PCL has less polar functional groups, such as the -(C=O)- group of methacrylate group (Figure 22), PCL is overall more hydrophobic than PCL-M and adding linear PCL will slightly reduce cell adhesion and proliferation.

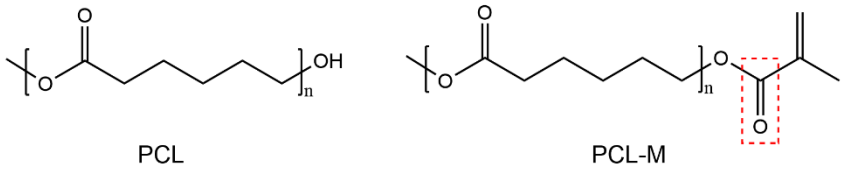

Figure 22. Chemical structures of PCL and PCL-M, where the -(C=O)- group of methacrylate group (in the red dashed box) provides additional polarity thus more hydrophilicity.

To optimize the cell attachment performance, some surface modification can be considered, such as air plasma treatment which could bring a more hydrophilic surface for better cell adhesion, thus, a better biocompatibility. Regarding that these composites shows quite similar or even better mechanical properties than some natural tissues, such as cartilage (YM 5 – 25 MPa), it could potentially be applied as a biomaterial [138, 139].

2.3.8. Degradability

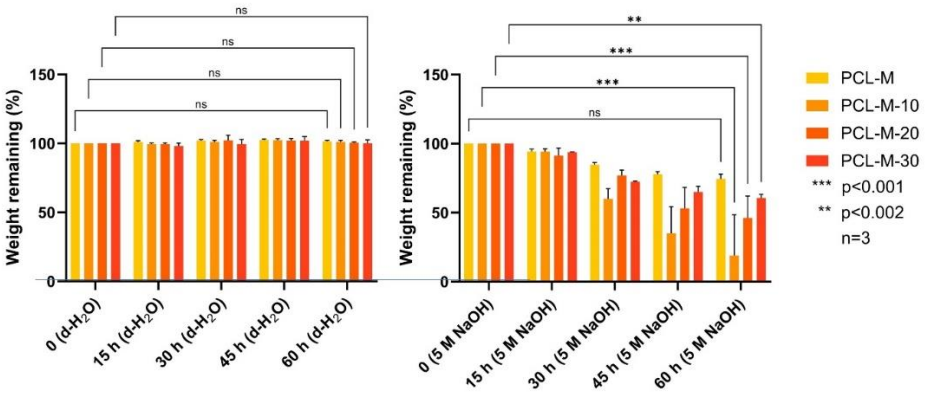

Figure 23. Degradation results of PCL-M and PCL-M/PCL composites in de-ionised water (d-H_2O) and 5 M NaOH solution (remaining weight percentage after 60 h, weights recorded every 15 hours).

From the degradation results shown in Figure 23, it can be seen that generally all types of samples had weight loss after 60 hours of immersion in 5 M NaOH solution. Interestingly, pure PCL-M exhibits the least significance among all samples indicating its stability under aqueous condition even with high concentration alkali, which should be a result of its relatively low hydrophilicity. Such phenomenon was also observed by Woodard *et al*., who conducted accelerated degradation on PCL-DA/PLLA semi-interpenetrating networks (semi-IPNs) in NaOH solution, where PCL-DA showed much lower degradation than the semi-IPNs [130]. Possibly, this is on one hand due to the phase separation of PCL-M and linear PCL, meaning that there are no actual strong covalent bonds in between, water molecules would have higher probability to diffuse into these composites than into pure PCL-M, which leads to higher degradation rates [73]. On the other hand, according to the crystallinities, the doped linear PCL shows much less degree of crystallisation (3.6% to 9.6%) compared to the crystallinity of pure linear PCL (~60%) allowing much higher water diffusion for hydrolysis leading to a higher rate of degradation than pure PCL, which could take 4 weeks in 5 M NaOH [73, 140]. Along with the increased amount of linear PCL, the degradation rate slows down, which would be contributed by the increased crystallinity [8, 141]. Such results indicate that by doping linear PCL, a tunable degradation rate could be obtained, which would be beneficial for applications requiring different degradation rates.

2.4. Conclusions

PCL-M/PCL composites can be fabricated *via* solvent casting. These composites have PCL-M with an interconnected spherical structured matrix which has linear PCL droplets as reinforcing inclusions. The composites have shown significantly enhanced mechanical properties

compared to pure PCL-M material. Moreover, the composites have also shown shape-memory properties due to the added PCL. Additionally, the addition of linear PCL is capable of tuning the degradation rate of PCL-M/PCL composites. Meanwhile, we have discovered that these composites are biocompatible and could be potentially used as biomaterials.

3. *In vitro* study of 3D printed photocurable PCL-M/HAp scaffolds

3.1. Introduction

Previously, researchers have successfully synthesised photocurable multi-arm PCL (PCL-M) and used to fabricate cell scaffolds for tissue engineering, and several cell culture experiments have been conducted on these scaffolds and shown positive results of biocompatibility [13, 15]. Since this is produced in a liquid resin, which could be easily combined with particles to form a composite, it would be interesting to explore its potential application for hard tissue engineering, such as bone tissues.

Hydroxyapatite (HAp), as a naturally existing inorganic compound in bone tissues, plays a vital role in providing ability of bearing loads and promoting bone regeneration [142]. It has been extensively used as a reinforcement in polymeric biomaterials and has shown excellent capability of introducing higher biocompatibility to the polymeric matrix [69, 143]. In practical scenarios, the scale of bone damage could vary a lot which requires customised geometries and tuned degradation rate of cell scaffolds if tissue engineering is applied as the treatment [143]. Photocurable materials, such as PCL-M, are able to offer complex structures as required *via* additive manufacturing, and the addition of hydroxyapatites could bring tuned degradation rate of the polymer matrix. Thus, hydroxyapatite-reinforced PCL-M could be a potential material for biological issues, such as tissue engineering.

Instead of using pure hydroxyapatite, some other ions which naturally exist in bone tissues have drawn researchers' attention, such as Sr^{2+} and Mg^{2+}, due to their ability of promoting bone

formation [144, 145]. Therefore, using hydroxyapatites doped with other ions (substituted hydroxyapatites) as reinforcements in a polymer matrix would hopefully increase biocompatibility, specifically for bone cells. These substitution dopants would also change the grain size of HAp due to their different atomic radius [146], which would further influence its physical properties and relative performance under certain conditions, such as changing the viscosity when being used as a reinforcement of a 3D printing ink [124].

In this work, we aim to synthesise a 4-arm PCL-M as the matrix and use different types and ratios of HAp as reinforcements. And three types of samples are fabricated, films, dog-bone-shaped samples, and 3D printed scaffolds *via* extrusion-based additive manufacturing. Water contact angle testing is to be performed on some of the film samples to examine their hydrophilicity. Tensile testing was performed on the dog-bone-shaped samples. And an *in vitro* assay is to be conducted on all types of samples to evaluate their biocompatibility. An accelerated degradation is also performed to characterise PCL-M/HAp composites' degradability.

3.2. Materials

Pentaerythritol, ε-caprolactone, tin(II) 2-ethylhexanoate (stannous octoate), triethylamine (Et3N), methacrylic anhydride (MAA), hydroxyapatite (HAp), 3-(Trimethoxysilyl)propyl methacrylate (MAPTMS), diphenyl(2,4,6-trimethylbenzoyl)phosphine oxide/2-hydroxy-2-methylpropiophenone blend (photoinitiator, PI), 37% formaldehyde solution, 6-diamidino-2-phenylindole dihydrochloride (DAPI), and phalloidin were purchased from Sigma-Aldrich. Dichloromethane (DCM), hydrochloric acid (HCl), and methanol were purchased from Fisher Scientific, UK. Silica (HDK H30, hydrophobic) was purchased from Wacker Chemicals UK. Substituted HAp (C4, 5 mol% Mg and 5 mol% Sr) was acquired from Finceramica (Italy).

3.3. Methods

3.3.1. Preparation of Film Samples and Dog-bone Samples

PCL-M resin were synthesised by using exactly the same method described in Section 2.2.2.1.

To prepare film samples, coverslips (dia. 13 mm) were washed by piranha solution, which was a mixture of H_2SO_4 (97%) and H_2O_2 (30%) (3:1, v/v), to remove any residual organic contaminants and bring -OH groups on the surface. Subsequently, the coverslips were rinsed by methanol to remove residual acid and H_2O_2. A MAPTMS solution (10 wt% in toluene) was then to immerse the coverslips for at least half an hour, after which the surface of coverslips is to be added with -C=C groups so that after photocuring, the films could form covalent bonding with the glass surface and be able to maintain flat without falling off the coverslips.

Non-substituted HAp (SigmaAldrich) was selected to fabricate the films for a preliminary experiment to evaluate the biocompatibility of PCL-M/HAp composites, due to limited availability of the substituted one. Initially, PCL-M was blended with PI (2 wt% of PCL-M) for at least 5 min to obtain homogenous mixtures. Subsequently, different ratios of HAp were added into individual PCL-M resins. An ultrasonicator (UP100H, Hielscher) was used to help break large particles of HAp until no aggregation could be observed in the mixtures.

Drops of fabricated PCL-M/HAp mixture onto glass slides individually. The inks were covered by surface treated coverslips which were allowed to compress by gravity. When the coverslips were fully covering the ink and horizontal ‘sandwich’ structures were fabricated, the samples were taken to a UV light source (OmniCure S2000, 40W/cm^2) for UV exposure for 5 min each side. The coverslips were then removed, and the film samples were peeled off the glass slide substrate. The films were then washed in methanol to remove the residual photoinitiator and

unreacted PCL-M. And these samples were used under the biocompatibility assay protocol described in Section 3.3.3.4.

For tensile testing, dog-bone-shaped samples were also prepared. Briefly, the photocurable PCL-M and PCL-M/HAp (SigmaAldrich, 10, 20, 30 wt% against PCL-M) composites were prepared by the method above, loaded into individual syringes, injected into PDMS moulds, and cured under the same UV light source as for the films for 5 min each side.

3.3.2. Additive Manufacturing (3D Printing)

To prepare 3D printing 'inks', PCL-M was mixed with PI (2 wt%) for at least 5 min under dark conditions to obtain a homogenous mixture. Subsequently, 10, 20, 30, 40, and 50 wt% HAp (C4, weight percentage against PCL-M) was added into PCL-M individually. During the mixing process, an ultrasonicator (UP100H, Hielscher) was used to break the large particulates until no aggregation could be found in the 'inks'. Then, with the assistance of the same ultrasonicator, all inks with HAp were doped with 1.5 wt% silica (weight percentage against HAp), which is typically added to make the inks shear-thinning specifically at low flow rate [81, 147], and allow for better 3D printing performance. The inks were loaded into syringes individually (BD, 10 ml with Luer-lock), on each of which a dispensing tip (METCAL, taper tip, pink, gauge 20, inner diameter 0.61 mm) was fixed. A syringe was loaded and tightened into BioBots 2 3D printer (now Allevi 2).

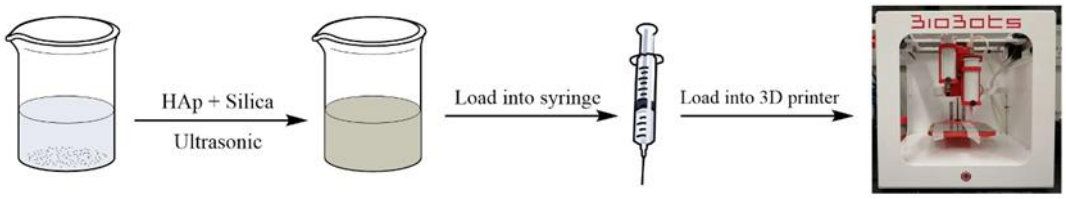

Figure 24. Schematic of preparing 3D printing on Biobots (now Allevi 2).

A 2-layer lattice structure we aimed to print was downloaded from 3D printer's website (https://www.allevi3d.com/sample-files/), which can be used as sample printing files freely. And after trials and optimizations, the printing parameters were chosen as follows:

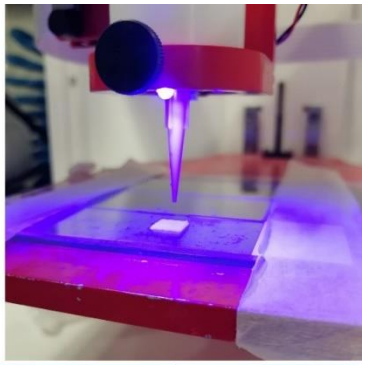

wt% of HAp	Pressure/psi	Temperature/°C	Speed/(mm·s^{-1})
0	5	25	1
10	15	25	0.8
20	20	25	0.8
30	30	25	0.8
40	40	25	0.8
50	75	30	0.6

Figure 25. Structure to be printed (top left), photocuring during 3D printing (top right), and printing parameters for each concentration of HAp (bottom).

The scaffolds were printed on a glass slide and cured by the LED light (wavelength: 405 nm) fixed on the 3D printer (top right of Figure 25). And the printed scaffolds were gently removed from the glass slide by a scalpel and washed in methanol to remove unreacted PCL-M and photoinitiator.

3.3.3. Characterisation

3.3.3.1. Water Contact Angle

Film samples were used to test the wettability of PCL-M and the composite formulations. An additional group of samples, PCL-M doped with silica (named as PCL-M/Silica), were introduced into wettability test as a control due to that all PCL-M/C4 samples used for 3D printing and the following cell work were doped with 1.5 wt% of silica to increase 3D printability from silica's shear-thinning effect [81, 147, 148]. Since the amount of HAp was used as 10, 20, 30, 40, and 50 wt% against PCL-M and the doped silica was 1.5 wt% against hydroxyapatite, the concentration of silica against PCL-M should be 0.15, 0.3, 0.45, 0.6, and 0.75 wt% against PCL-M, respectively. To simplify the process of experiments, PCL-M with 0.15, 0.45, and 0.75 wt% silica was selected, which were chosen as the controls for comparison with PCL-M with 10, 30, and 50 wt% hydroxyapatites respectively. Kruss DSA 100 was used to conduct water contact angle tests. On each type of sample, ~ 30 μL of de-ionised water was placed on 5 locations respectively, which were selected randomly without overlapping each other. The shapes of water droplet and contact angles were recorded and analysed by the machine automatically by its monitoring software. Data analysis was performed *via* GraphPad

Prism 10.0.1, where two-way ANOVA was used for statistical analysis. Films reinforced by normal hydroxyapatite (SigmaAldrich) were named as PCL-M/N, and those reinforced by substituted HAp were named as PCL-M/C4.

3.3.3.2. Mechanical Testing

Mechanical testing was performed on the dog-bone-shaped samples. The samples were loaded individually on a tensile testing machine (Mecmesin MultiTest 2.5-dV) with a tensile speed 1 mm/min. Five replicates were used for each type of samples. Tensile testing results were analysed in GraphPad Prism (version 10), and statistics was carried out by using One-way ANOVA.

3.3.3.3. Scanning Electron Microscopy (SEM)

The microstructures of 3D printed scaffolds and cross-sectional area of PCL-M/HAp dog-bone samples were imaged by SEM (FEI Nova NanoSEM 450)

3.3.3.4. *In Vitro* Biocompatibility Assay

Biocompatibility test was conducted by seeding Y201 cells on to the films and 3D printed scaffolds. Before cell seeding, all samples were washed by pure methanol for 3 days to remove the residual unreacted monomer and photoinitiator. Following that, a sterilisation process was performed by immersing samples in 70% ethanol solution for 3 days (discs for 1 week, 3D scaffolds for 4 days). Then the samples were washed twice by sterile de-ionised water to remove residual ethanol. Prior to the actual cell seeding, all samples were immersed in 300 μL

growth media for 45 min, which was used to improve cell attachment by introducing media-bound proteins to the samples. The media was then removed from culture plate and the cells were seeded onto the samples (cell concentration: 4000 cells/cm^2). Standard cell culture conditions were used (37°C, 5% CO_2, and 95% humidified). Two groups of control were used in this work and cultured under the same conditions, which were tissue culture plate (TCP) where there were no samples but only cells seeded in the plates with media, and a negative control (NC) where there were only samples and media, but no cells seeded in the plates.

Resazurin assay was used to test the metabolism of cells on Day 1, 4, and 7. Briefly, before adding resazurin solution, media was withdrawn from the culture plates which were then washed by Hanks' Balanced Salt Solution (HBSS) twice. For films and discs, resazurin solution was added directly to the culture plates. For the 3D printed scaffolds, they were transferred to a new plate so that only the cells attached to the scaffolds were examined. 650 μL of resazurin solution was added to each well under minimum light condition. Then, the well plates were placed in an incubator (37°C, 5% CO_2) with aluminium foil cover for 2 hours. Subsequently, 200 μL solution from each well was transferred to 96-well plate which was then placed in a plate reader to obtain the fluorescence intensity (excitation at 540 nm, emission at 590 nm). The intensity data was analysed *via* GraphPad Prism 10.0.1, with two-way ANOVA as the statistical method.

Confocal microscopy was also used in this assay to image the cells' morphology on the 3D scaffolds of PCL-M/C4 (30 wt%, with 1.5 wt% silica). Formaldehyde solution was initially used to fix the cell on the scaffolds (500 μL, 30 min) after media removal and two times of PBS washing. Subsequently, the formaldehyde solution was removed, and the scaffolds were rinsed in PBS for 2 times. 500 μL permeabilization solution was then used to treat the scaffolds for 10 min and removed. After the treatment, the scaffolds were washed in PBS twice. Then, 4',6-diamidino-2-phenylindole dihydrochloride (DAPI, 1 μg/ml in PBS) was added to the

scaffolds, which were then covered in dark condition and incubated for 15 min at room temperature. Following that, the DAPI solution was removed, and the scaffolds were washed in PBS twice. The scaffolds were then added with phalloidin solution (10 μg/ml in PBS) for 30 min in dark condition and room temperature. Phalloidin solution was then removed, and the scaffolds were washed in PBS twice, which were kept in PBS under dark conditions until confocal microscopy imaging was performed. The images were captured *via* MetaMorph® Microscopy Automation & Image Analysis Software (Molecular Devices4 LLC, UK).

3.3.3.5. Accelerated Degradation

Due to the limited availability of substituted HAp, accelerated degradation was performed on PCL-M and PCL-M with normal HAp (Sigma Aldrich, 10, 20, and 30 wt%) cubic samples, which were cut approximately with the same configuration and size from the ends of dog-bone-shaped samples, to evaluate the effect that HAp could bring on the degradation rate of PCL-M. 6 of each type of samples were immersed in 2 ml NaOH solution (3 M) in individual bijous (7 ml, polystyrene) to monitor the accelerated degradation process. Each empty bijou was weighed as w_0 and weighed as w_1 after loading the sample, and the initial weights of samples were recorded as (w_1-w_0). The bijous were sealed and left in an incubator (37 °C). Every 5 days, NaOH solution was extracted from all the bijous which were then gently rinsed by 5 ml of de-ionised water for 3 times. The samples were left in the bijous and dried under vacuum (50 °C) for 2 hours to remove the residual moisture inside. After dying, each bijou containing sample was weighed as w_1', so the residual weight of sample is (w_1'-w_0). Subsequently, all bijous were filled with 2 ml fresh NaOH, sealed, and left in the incubator for further degradation. All the weighing process mentioned above was carried out without caps and this monitoring

was conducted for 15 days. Data analysis was performed *via* GraphPad Prism 10.0.1, where a two-way ANOVA was used for statistical analysis.

3.4. Results and Discussion

3.4.1. Mechanical Properties and Microstructures of Dog-bone Samples

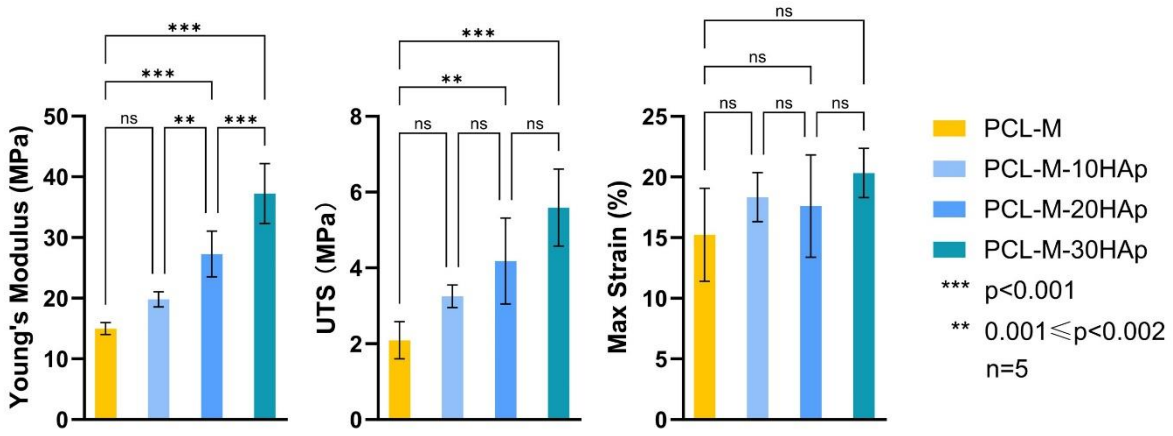

Figure 26. Tensile testing results of PCL-M and PCL-M/HAp composites, left to right: Young's Modulus, ultimate tensile strength (UTS) and max strain.

Tensile testing results show that the Young's Modulus (YM) of PCL-M/HAp composites gradually increase along with the added amount of HAp. Particularly after being doped with 20 and 30 wt% HAp, there is a significant increase of stiffness, indicating that compared to PCL-M only, under the same stress PCL-M/HAp composites are more capable to maintain their shape, which is beneficial for applications of hard tissue engineering. Compared to cancerous

bones, of which their Young's Modulus normally falls within 20-500 MPa [149], PCL-M-20HAp and PCL-M-30HAp show appropriate YM values (27 MPa and 38 MPa respectively, mean values) exactly in this range, which brings them potential applications for this type of tissue. Moreover, the UTS also shows an increasing trend after adding 20 and 30 wt% HAp, which indicates that the additional HAp in the PCL-M matrix provides higher strength so that the composites can resist higher stress along the long axis of the material until breaking. The increase of YM and UTS could possibly be a result of extra hydrogen bonds formed between the -C=O and -OH groups of PCL-M and P-OH groups of HAp molecules which has been confirmed by Zhou *et al.*'s and Zhang *et al.*'s work on HAp-reinforced poly(lactic acid) and polyamide 66 [150, 151]. However, the maximum strain does not show significant changes after adding HAp. It is largely due to that HAp, as a ceramic, is stiff but brittle, so the flexibility of the composite is mainly dominated by the flexibility of the polymer matrix, which makes this reinforcement unable to contribute much to composite's maximum strain. But with the stiff crystalline structure, the composites' anti-compression properties would hopefully be increased [149], which are yet to be examined in the future.

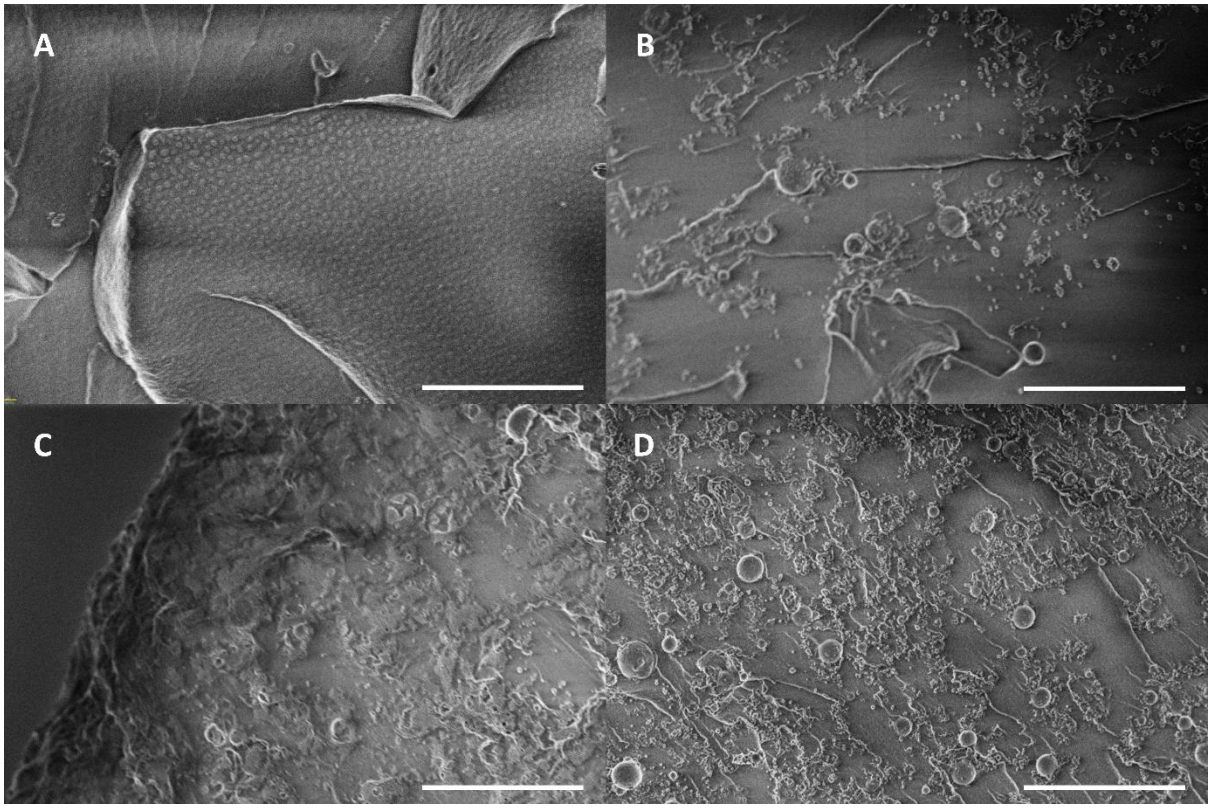

Figure 27. SEM images of cross-sectional area of A) PCL-M, B) PCL-M-10HAp, C) PCL-M-20HAp, D) PCL-M-30HAp (magnification 10000x, scale bar: 4 μm)

All four types of samples were cut to image their cross-sectional area. SEM images (Figure 27) show that along with the increased amount of HAp addition, more sub-micron scale particulates can be found in the matrix, which further enhanced the YM and UTS of composites. The distribution of HAp particulates in PCL-M-10HAp to 3PCL-M-30HAp show relatively homogeneous status. However, as a ceramic, HAp particles have charged surface due to their ionic nature, which resulted in they still slightly aggregated in PCL-M matrix, even with the help of ultrasonicator to mix.

3.4.2. Microstructures of 3D Printed Scaffolds

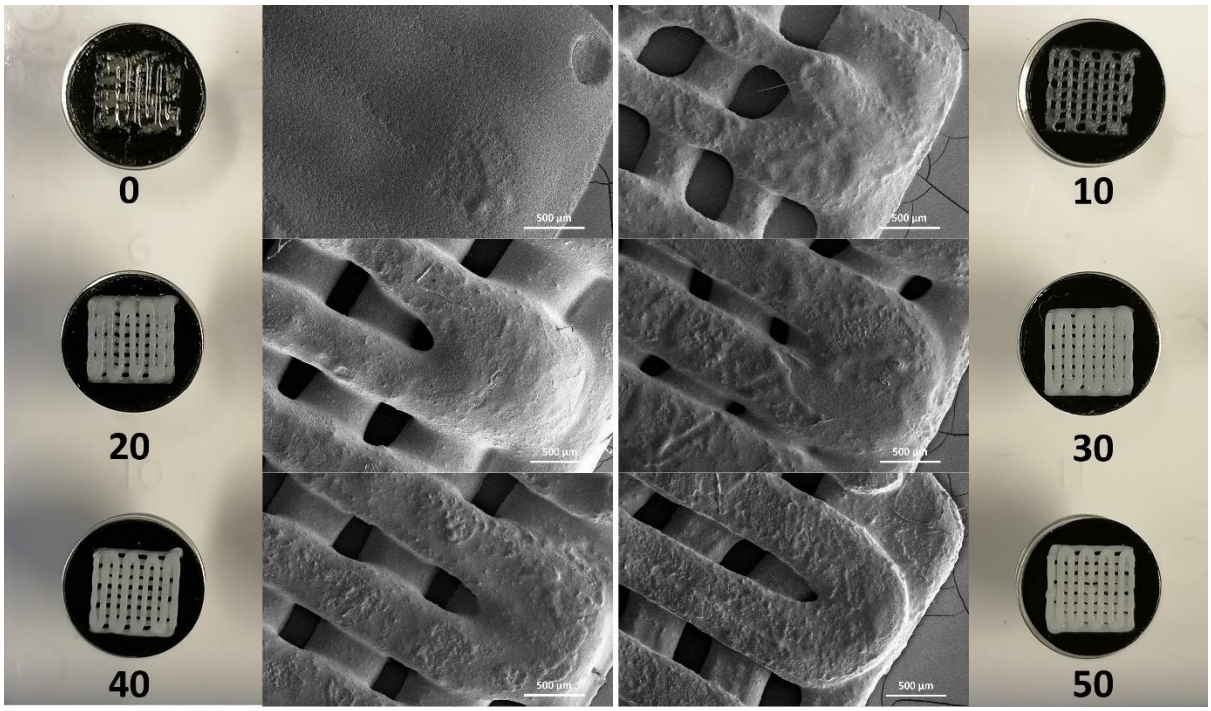

Figure 28. 3D printed scaffolds with different concentrations of C4 substituted hydroxyapatite (concentrations 0 - 50: 0 - 50 wt% C4 HAp, all with 1.5 wt% silica against C4 HAp except sample 0), scale bar 500 µm.

PCL-M without any hydroxyapatite does not show a well-printed 3D structure but the trace of printing can still be recognised. From 10 wt% to 50 wt% hydroxyapatite, the upper lines can be observed as partially merged into the bottom lines, but the resolution of printing is gradually improved. When the concentration reaches 50 wt%, sharp edges of lines can be observed, the printed two layers can be better distinguished from each other, and the width of turning point shows a proximity of the width of straight lines. This should be a result of increased added amount of hydroxyapatite leading to an increased viscosity [124], which gradually improved the ink's ability to maintain its configuration after being printed out rather than spread or merge

into each other. Additionally, more particulates can be observed on the surface, indicating that the surface roughness could be increased along with more added C4 HAp.

Additionally, during 3D printing, the pressure requirement was increased along with higher amount of HAp dopant. Particularly when the amount reached 50 wt%, 75 psi and higher temperature (30 °C) were both needed so that the ink could be extruded out but still the extrusion speed (0.6 mm/s) could not be as high as the ones used for lower concentration inks (0.8 mm/s). This should be a result of increased viscosity brought by higher concentration of HAp dopant [124]. However, as this 3D printer was driven by compressed air stored in a tank, while being used, the air was gradually consumed from the tank and the total pressure (maximum 100 psi) went down until it fell to 60 psi. Then an air pump started to refill the tank back to 100 psi. Thus, an over 60 psi pressure requirement might not be stably delivered into the ink and the printing performance and structural integrity would be influenced. To optimise this issue, more silica dopant, rather than a fixed ratio, could be used when high concentrations of HAp to be added, which could possibly bring more shear-thinning effect to the ink so that lower pressure could be required.

Among all 3D printed structures, 30 – 50 wt% C4 show preferable printing performance. But 30 wt% C4 required lowest printing conditions, this composition was used to fabricate 3D scaffolds for a biocompatibility assay.

3.4.3. Biocompatibility

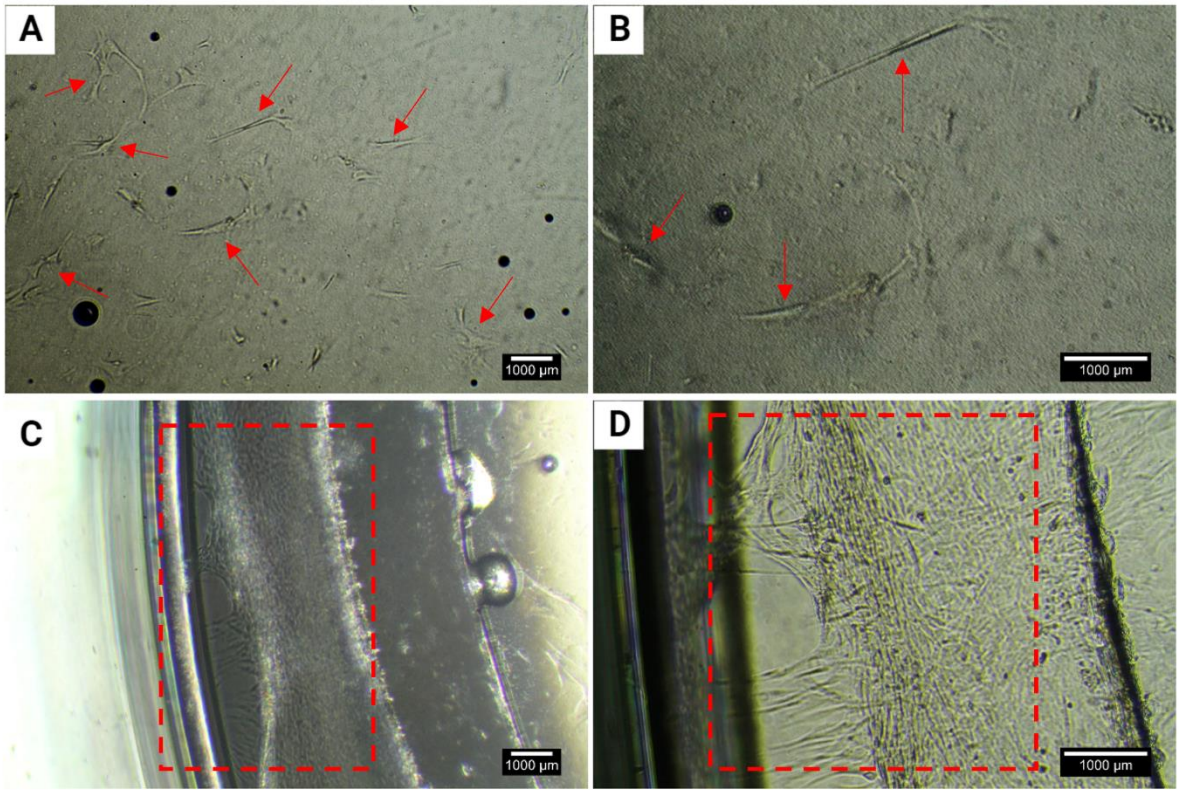

Figure 29. Images from optical microscopy: A & B: Y201 cells on the film (pointed by red arrows, magnification A: 50x, B: 100x), C & D Y201 cells at the edge of the film (in the red dashed boxes, magnification C: 50x, D: 100x) (PCL-M-30HAp, Day 7).

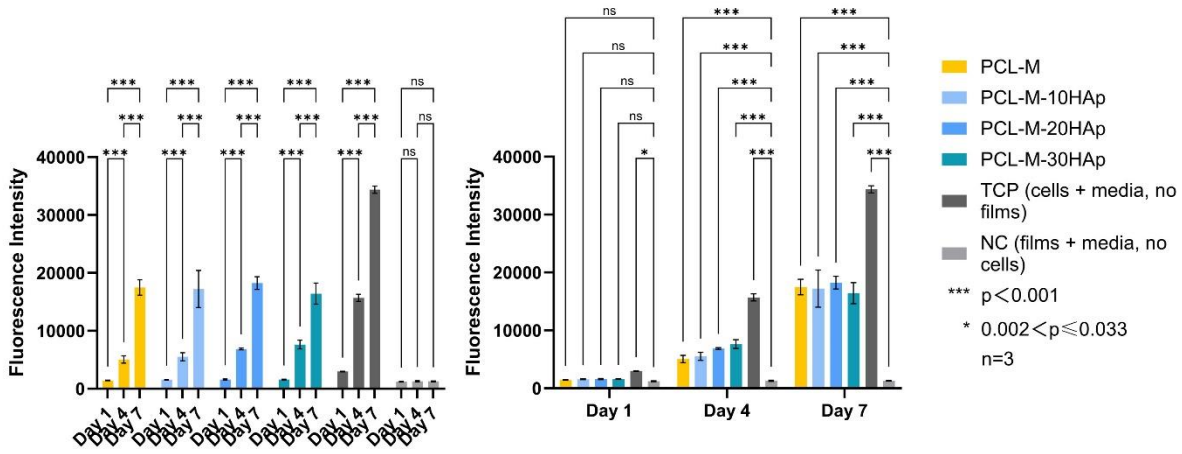

Figure 30. Resazurin assay (Day 1, 4, and 7) results of Y201 cells on PCL-M and PCL-M/HAp films.

After 1 week, cells can be observed under optical microscope (Figure 29) on the film samples with elongated feature and fibroblast morphology, from which it can be confirmed that Y201 cells have been successfully seeded on the films and proliferated [152]. Resazurin assay on film samples can also confirm that significant growth of Y201 cells could happen on all types of films (Figure 30). But HAp reinforced samples do not show higher metabolism than pure PCL-M. Additionally, the media did not become cloudy, which is usually a result of cell debris from dead cells but remained clear indicating that PCL-M and PCL/M/HAp samples are not cytotoxic. According to the images, the cells tend to proliferate more around the edge of the films rather than in the central areas (Figure 29). This would a consequence of roughness difference between the top and edge surfaces. Since the samples were cured on glass slides, the surface of glass slides actually limited the exhibition of surface roughness brought by HAp, but the edge area was not limited which allowed the protrusion of HAp particle and led to a higher roughness, which is preferable for cell attachment and proliferation [153]. Such phenomena could be further investigated by curing samples on substrates with different softness to allow HAp to protrude on surfaces with different degrees and obtain surfaces with different roughness. And cells could be cultured on these surfaces to further explore the influence of HAp as a reinforcement in a polymer matrix.

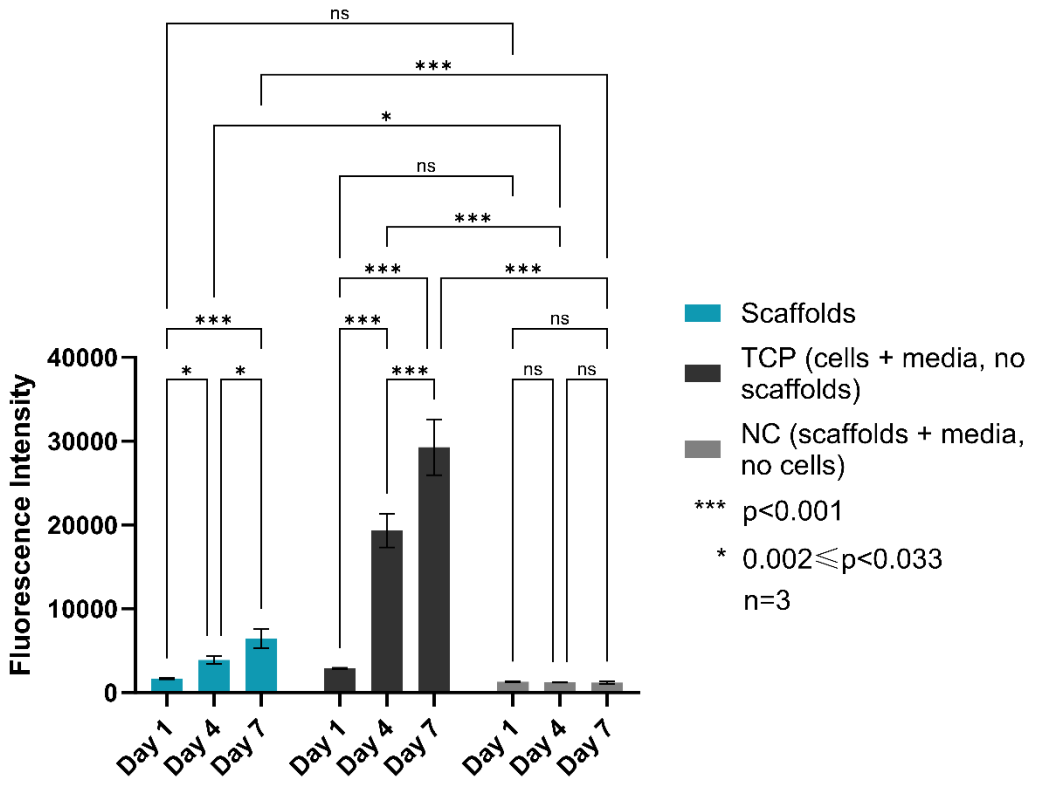

Figure 31. Resazurin assay results (Day 1, 4, and 7) of cell culture (Y201 cells) on the 3D printed scaffolds (C4 HAp)

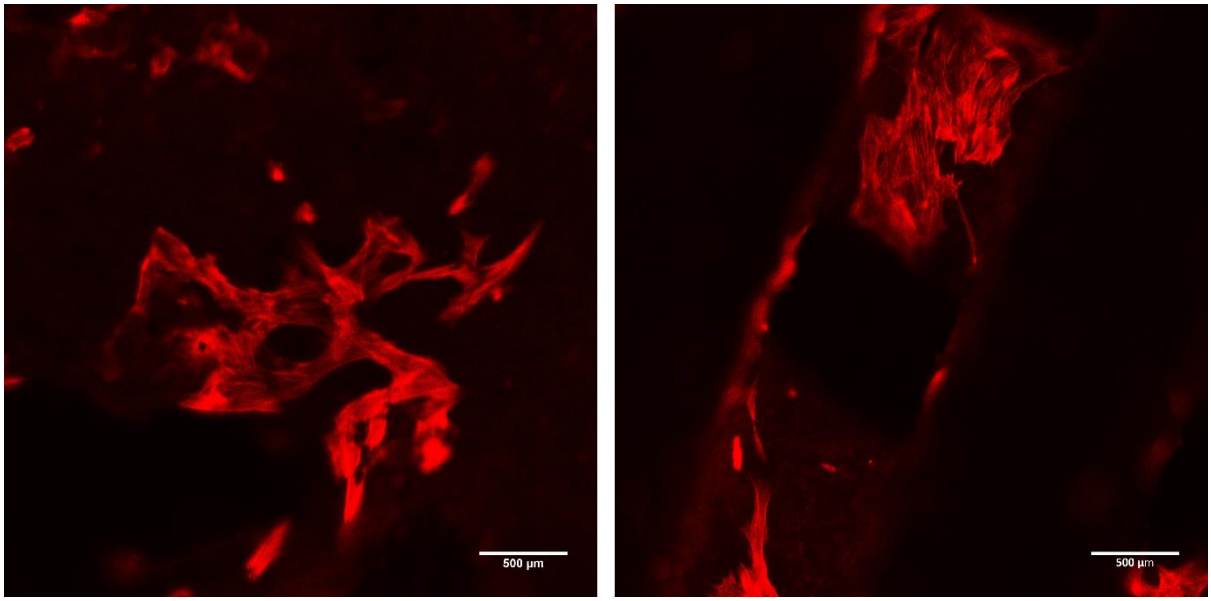

Figure 32. Confocal microscope images of Y201 cells on 3D printed scaffold (C4, 30 wt% of PCL-M).

After confirming that the PCL-M matrix and PCL-M/HAp composites did not exhibit cytotoxicity and allowed cell growth. 3D printed PCL-M/C4 (30 wt%) scaffolds were used for further cell work. The resazurin assay results show that there is a significant cell growth on the 3D printed scaffolds from Day 1 to Day 7 (Figure 31). And the cells under confocal microscope also exhibit elongated shapes on the scaffold indicating cell attachment (Figure 32). The scaffold allows cell proliferation but exhibits relatively lower metabolism activity than that on the films on Day 7 (compared to the fluorescence intensity of TCP on Day 7). Multiple factors could possibly lead to this result, such as surface morphology and surface chemistry. However, since hydroxyapatite additives would normally increase surface roughness of a polymer matrix thus increase cell attachment [70], surface chemistry of these compositions should be investigated to analyse this phenomenon, such as hydrophilicity test.

3.4.4. Wettability

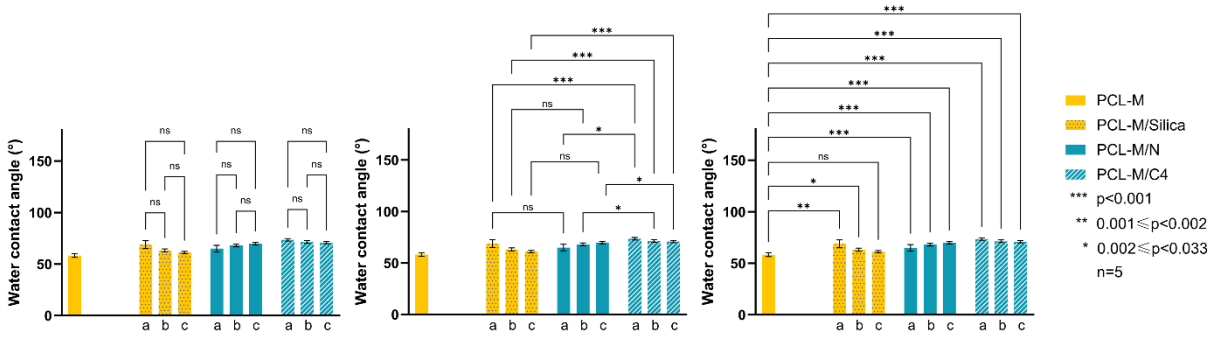

Figure 33. Water contact angles of different types of samples, where a, b, and c mean different concentrations of additives (weight percentage against PCL-M). PCL-M/silica (dotted yellow plots): a—0.15 wt%, b—0.45, c—0.75 wt% silica. PCL-M/N (blue plots): a—10 wt%, b—30 wt%, c—50 wt% HAp. PCL-M/C4 (left-hashed blue plots): a—10 wt%, b—30 wt%, c—50 wt% substituted C4 HAp.

The wettability test shows that all samples have water contact angles lower than 90°, which indicates that the hydrophilic feature has remained after adding several types and amounts of dopants, and that they should be suitable for biological applications. However, the increased amount of silica/HAp (N)/HAp (C4) has not brought significant change on the water contact angle. This should be largely due to that there might not be significant change of surface roughness, which is limited by the glass slide's surface where they were cured. Compared to PCL/silica samples, PCL-M/N samples do not exhibit significant change in water contact angles as well, but PCL-M/C4 shows significantly increased values. This should be resulted from a different average particle size that C4 has, which could possibly bring a different surface morphology, such as roughness, along with the hydrophobic feature of doped silica, the water

contact angle slightly but significantly increased. This phenomenon would also indicate that silica particles could dominate the hydrophilicity on the surface. Such results could be a potential explanation for cellular activity on C4 3D scaffolds (30 wt%), on which there should be higher surface area and surface roughness but poorer cell attachment and metabolism activity than that on films. As such, hydrophilic silica, which is also capable for shear-thinning the organic matrix[154], would be preferable to be added to obtain a more hydrophilic surface and improved biocompatibility. However, Gashti *et al.*'s work on comparison between the dispersity of hydrophilic and hydrophobic silica in a polyethylene terephthalate (PET) matrix demonstrated that hydrophilic silica is more likely to aggregate at the surface area and the hydrophobic silica would have a more homogenous distribution in the polymer matrix [155]. So, adding hydrophilic silica into PCL-M/HAp composites would lead to a non-homogenous mixture which would benefit less from shear-thinning so that it might require higher pressure printing or clogging printing tips frequently. More practically, surface treatment, such as O_2 plasma treatment [156], would be a preferable method to improve hydrophilicity of PCL-M matrix thus increase the composites' biocompatibility.

3.4.5. Degradability

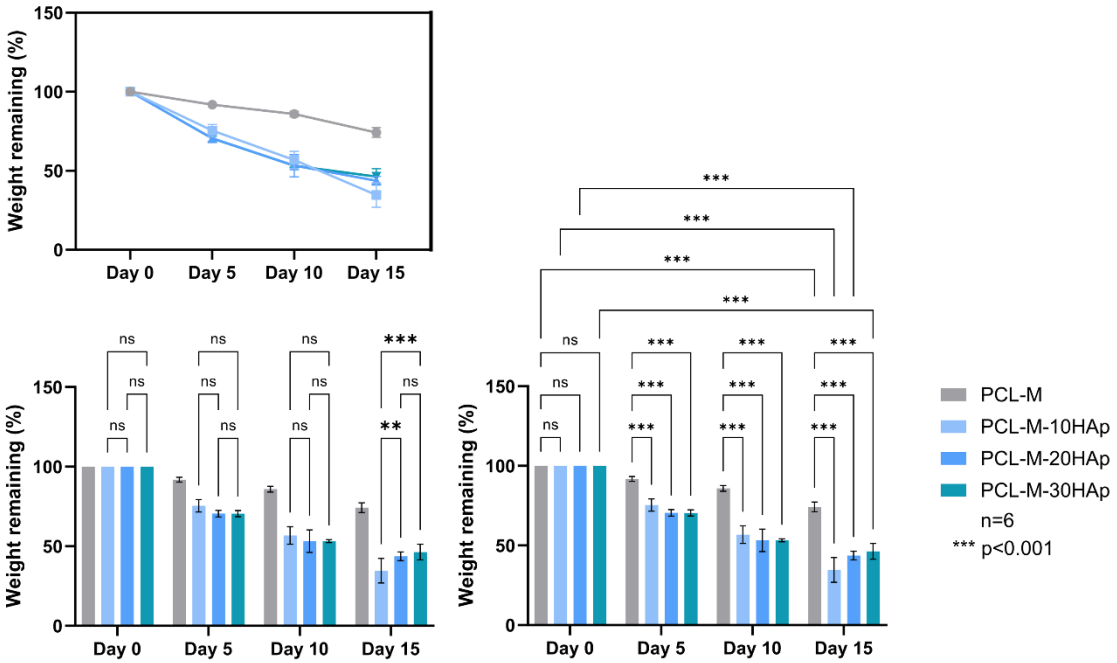

Figure 34. Accelerated degradation of PCL-M and PCL-M/HAp composites (15 days in 3 M NaOH solution).

The results of accelerated degradation in Figure 34 show that all samples show significant degradation in 3 M NaOH after 15 days. From Day 0 to Day 5, the weight between PCL-M and PCL-M/HAp samples did not show significant differences but on Day 10 and Day 15, a more obvious weight loss acquired on samples doped with HAp showed a more significant trend of degradation. HAp, as a ceramic powder, would bring more charge on the surface of the composites, which helps attract OH- and water molecules to perform hydrolysis on the ester bonds. Furthermore, on Day 15, the residual weight of PCL-M-30HAp had the highest value and PCL-M-10HAp had the lowest one. And the remaining weight percentage of PCL-M-10HAp showed significant difference with both PCL-M-20HAp and PCL-M-30HAp on Day

15. During degradation, PCL-M network was broken into degraded product and rinsed away leaving HAp structure in the sample so that when the degradation process was close to the end, samples doped with more HAp showed higher value of residual weight. However, the degradability of PCL-M/HAp with silica dopant has not been investigated yet. Since the silica used in this work is hydrophobic, a lower degradation rate could be expected. Thus, adding silica would be a feasible approach to adjust the degradability of these composites. Additionally, Gu *et al.* discovered that doping Sr in HAp could lead to a higher degradation rate of HAp [157]. Thus, a different degradation rate could be expected on polymer reinforced by Mg-Sr substituted HAp, which would be another potential method to adjust the degradability of polymer matrix. Furthermore, it would be interesting to investigate whether silica would bring an effect on the degradability of PCL-M matrix composites.

3.5. Conclusions

Photocurable PCL-M with 69 % methacrylation can be synthesised *via* a ring-opening reaction followed by methacrylation for 20 hours. HAp reinforcement can bring extra stiffness and ultimate tensile strength to the PCL-M matrix, which could make this composite as a potential candidate for some hard tissue engineering, such as cancerous bones. Photocured PCL-M, and PCL-M reinforced by normal and substituted hydroxyapatites (Mg-Sr substitution) are biocompatible. However, a very low amount of silica dopant would bring a relatively strong effect on the surface chemistry, thus affect biocompatibility. PCL-M and PCL-M/HAp composites are all degradable. The degradation process can be accelerated with the presence of hydroxyapatites, but the amount of doped HAp might not bring impact to the degradability.

Acknowledgements

All cell work was assisted by Denata Syla, who is a PhD student at the University of Sheffield. GPC and NMR data collection was assisted by Dr Simon Parker and Dr Khalid Doudin, who are technicians at the Department of Chemistry of the University of Sheffield.

4. Synthesis of Multi-arm PCL Acrylate *via* An Alternative Method and Exploration of Its Applications

4.1. Introduction

As an FDA-approved material for clinical use, polycaprolactone (PCL) has become a promising material for biomedical research due to its biocompatibility and degradability [1]. Researchers have been working on further functionalising PCL as a photocurable material so that high-resolution and highly customised 3D structures can be obtained, which are beneficial for biomedical applications, such as tissue engineering [13, 23].

To acquire photo-curable properties, acrylation and methacrylation are the most common approaches. Previously, methacrylated 3 and 4-arm PCL have been successfully prepared by Field *et al.* and Dikici *et al.*, both of which showed excellent photo-curability and capability of light-based additive manufacturing [14, 15]. However, due to hyperconjugation between CH_3 and its neighbouring C=C group, the methacrylate groups on these multi-arm PCL molecules should be more stable than acrylate groups [158]. Thus, we can have a hypothesis that PCL acrylates, which do not have these methyl groups, should have lower photo-stability but higher photosensitivity to have a higher probability of being cured *via* two-photon polymerisation (2PP) to fabricate ultra-high resolution structures, which are beneficial for scenarios requiring hyperfine structures such as biomedical microfluidics devices and biochips [159-161].

Additionally, we explore the hydrophilic/hydrophobic character of the produced resins. It was observed in Johnson *et al.*'s study which mentions that during the washing multi-arm PCL acrylate, a thick emulsified layer formed between the organic phase and aqueous phase, which was stable and could hardly be separated without high-speed centrifugation[40]. This indicates that the multi-arm PCL acrylate could potentially be amphiphilic or even water soluble. Therefore, we explored the possibility of surfactant-free emulsion-templated porous material and water-based 3D printing resins.

In this work, we report the synthesis of 4-arm PCL acrylate (PCL-A) *via* Steglich Esterification (SE) and comparison with conventional methods. Curing performance and mechanical properties of bulk PCL-A material are investigated. An initial biocompatibility test *via* cell culture was carried out and light-based additive manufacturing, *via* both single-photon and two-photon polymerisation (1PP and 2PP respetively), was applied to explore PCL-A's potential of structuring.

4.2. Materials

Pentaerythritol, ε-caprolactone, tin(II) 2-ethylhexanoate, acryloyl chloride (AC), triethylamine (Et_3N), Celite® Hyflo, acrylic acid (AA), 4-dimethylaminopyridine (DMAP), and Diphenyl(2,4,6-trimethylbenzoyl)phosphine oxide/2-hydroxy-2-methylpropiophenone blend (photoinitiator, PI), and tetrazine were purchased from Sigma Aldrich. Dichloromethane (DCM), acetone, methanol, ethanol, isopropanol (IPA), toluene, chloroform, ethylenediamine (EDA), sodium chloride (NaCl), sodium hydroxide (NaOH), potassium hydroxide (KOH), potassium carbonate (K_2CO_3), hydrochloric acid (HCl, 37%), and magnesium sulphate ($MgSO_4$) were purchased from Fisher Scientific. N-(3-Dimethylaminopropyl)-N'-

ethylcarbodiimide hydrochloride (EDC·HCl) was purchased from FluoroChem. NG108-15 cells and resazurin sodium salt were purchased from SigmaAldrich, UK.

4.3. Methods

4.3.1. Acrylation on PCL *via* Conventional Methods

To synthesise PCL acrylate (PCL-A) *via* the conventional way, we followed but slightly modified Johnson *et al.*'s method [40]. Our 4-arm PCL pre-polymer (1 mol eq.), which was synthesised by using the method in Section 2.2.2.1, was mixed with DCM (1:5, w:v) in a three-necked round bottom flask. Then Et_3N (8 mol eq.) was added into the solution. The reaction system was kept running in an ice bath with continuous stirring and nitrogen flow. After every component was well mixed in the solution, AC (10 mol eq.), which was prepared with DCM as a solution (1:3, w:v), was added dropwise. The reaction system was kept running for 18 hours in dark condition and allowed to raise to room temperature. The solution became amber and cloudy. Subsequently, the solution was filtered by Celite® Hyflo to remove most of the particles, washed by KOH solution (3 wt%) and HCl solution (1 v%) respectively, centrifuged, dried *via* $MgSO_4$, filtered, and dried again under vacuum. A yellow viscous resin was obtained as the final product, named as PCL-A-AC.

A proposed alternative method to synthesise PCL-A was carried out as well, following a protocol described by Cai and Wang [114]. Briefly, excess K_2CO_3 was utilised in the reaction to replace Et_3N as the acid absorber. Apart from K_2CO_3, this reaction was performed with exactly the same ratio of reagents stated in the AC/Et_3N method and with same conditions which were ice bath, continuous nitrogen inlet, dark condition, and 18 hours of reaction. The solution was

post-processed through exactly the same steps as the one performed in the AC/Et_3N method. A colourless and transparent resin was obtained as the final product, named as PCL-A-K.

4.3.2. Acrylation on PCL *via* Steglich Esterification

Inspired by Lutjen *et al*., we slightly optimised Steglich Esterification by choosing EDC·HCl, [117] rather than N,N'-dicyclohexylcarbodiimide (DCC) which was originally reported in Neises and Steglich's ground-breaking work,[116] as the coupling agent due to its own and its corresponding by-product urea's better solubility in water [162, 163]. Besides, DMAP and acrylic acid are also water-soluble [164]. Therefore, in theory, a clean final product should be obtained after being purified by using a straight-forward water washing.

Briefly, PCL (1 mol eq.) was dissolved in DCM (1:5, w:v) in a three-necked round bottom flask. Then EDC·HCl (6 mol eq.), was added and the solution turned cloudy. Subsequently, DMAP (0.1 mol eq.) was added as the catalyst. The flask was cooled in an ice bath with continuous stirring and nitrogen flow. Later, AA (6 mol eq., diluted in DCM, 1:3, w:v) was added into the solution dropwise from a dropping funnel. The entire reaction system was kept running under dark condition for 18 hours and allowed to raise to room temperature.

The solution was then washed by saturated NaCl solution twice and rotary-evaporated to remove DCM as much as possible. Afterwards, the solution became cloudy with some NaCl precipitations inside. Acetone was used to dissolve the resin again to precipitate NaCl from the final product. The solution was then filtered, and roto-evaporated. The final resin showed a colourless and transparent feature, named as PCL-A.

4.3.3. Dog-bone Samples and Films Fabrication

The final resin PCL-A was blended with PI (5 wt%) for at least 5 min to obtain homogeneous distribution. Then the resin was loaded to a syringe and injected into a PDMS mould, of which the dimensions were designed and forged in compliance with BS EN ISO 527-2:2012. The samples were then cured under UV lamp (OmniCure S2000) for 5 min each side. The excess parts at the ends of dog-bone samples were cut off for a proper mechanical testing condition.

For the film samples, one droplet (~50 μL) of the resin blended with PI (5 wt%) was placed on a glass slide and covered gently by a coverslip (dia. 13 mm) to form up a 'sandwich' structure. Until the coverslip was fully covered by the resin, the 'sandwich' was cured under UV lamp (OmniCure S2000) for 5 min each side and then the cured film was peeled off from the glass slide and coverslip carefully.

All samples stated above were washed in methanol to remove the residual monomer and PI on the surface. However, a slightly tacky surface was always obtained after photocuring. It was assumed to be result of oxygen inhibition which commonly happens in photocured acrylate-based resins [165]. Further characterisation by ATR-FTIR confirmed this phenomenon on the cured samples. This could provide an opportunity to further functionalise the surface with designed functionality. Therefore, a surface treatment following Junyi *et al.*'s work to reduce the unreacted C=C on the surface [36]. Briefly, EDA was diluted in methanol (10 wt%) and the samples were immersed in the solution for at least 10 min [36]. Subsequently, the films were taken out, washed in pure methanol for 2 times, and dried under vacuum.

4.3.4. Viscosity Characterisation

Viscosity of PCL-A and its corresponding water solutions (weight ratios and results are shown in Section 4.4.5) was carried out by using TA instruments AR 2000 (cone plate 40 mm, 2°, 25°C, ramping shear rate: 0.01 Hz to 100 Hz).

4.3.5. Additive Manufacturing *via* 1PP

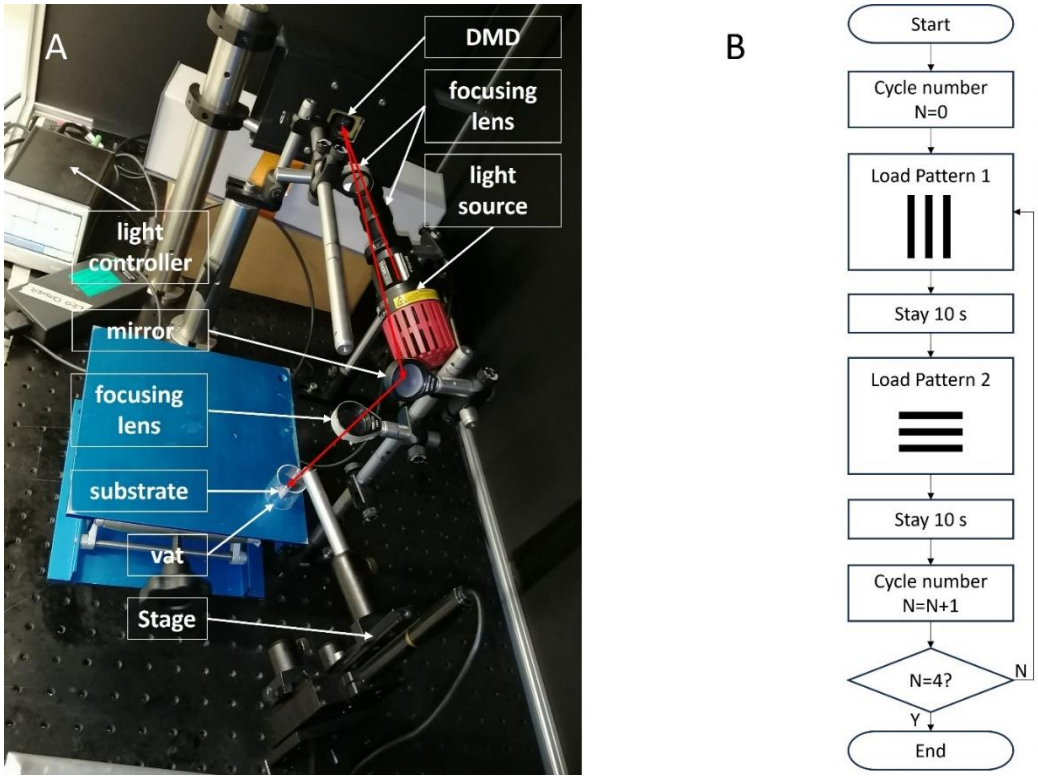

Figure 35. Light-based additive manufacturing of PCL-A. A) A built-in-house stereolithography set-up based on UV LED and DMD. B) Flow chart of programmed patterns for building wood pile structures displayed on DMD

Light-based additive manufacturing was performed by built-in-house UV LED (Thorlabs M405LP1, wavelength: 405 nm) additive manufacturing system (Figure 35A). This system worked on a programmable digital micromirror device (DMD, DLP® 0.7'' XGA, Texas Instruments Inc.), on which the '|||' and '≡' patterns (Figure 1B) can be displayed as a programmed cycle for 10 seconds for each pattern. The cycle was programmed to repeat four times (Figure 35B). There was a substrate connected to a motorised stage (Figure 35A,

Thorlabs one- axis stage MT1-Z8, controller: Thorlabs apt - dc servo controller tdc 001), which was programmed to move vertically at 0.05 mm/s. The light source was controlled by Thorlabs DC2200. UV light emitted from the light source was focused and reflected as the pattern displayed on the screen of DMD. Then the 'pattern beam' was reflected on a mirror and focused on the substrate. Initially, the stage was adjusted carefully to make sure that the pattern is precisely focused on the substrate. Subsequently, the substrate was loaded into the polymer vat (Figure 35A), of which the height was adjusted carefully by tuning the blue platform (Figure 35A) to make sure that the upper surface of the substrate touched the polymer liquid's surface. Once the UV was turned on, the programmes of running were switched on as well manually on the controlling computer. The fabricated structure was then peeled off the substrate carefully and washed by IPA.

4.3.6. Additive Manufacturing *via* 2PP

Due to the potential high reactivity of PCL-A along with the high energy density that multi-photon could bring, a PI-free additive manufacturing *via* 2PP using this PCL-A was considered as a potential intriguing fabrication route for high resolution structures. We collaborated with Jurga Jeršovaite and Prof Mangirdas Malinauskas (Laser Research Centre, Vilnius University, Lithuania) on this experiment by employing their built-in-house two-photon laser direct writing set-up, of which the structure and light route is shown in Figure 36. In this set-up, a Yb:KGW laser source was deployed (PHAROS Femtosecond Lasers, Light Conversion, Lithuania), which generated 300 fs pulsed laser with a 1030 nm wavelength.

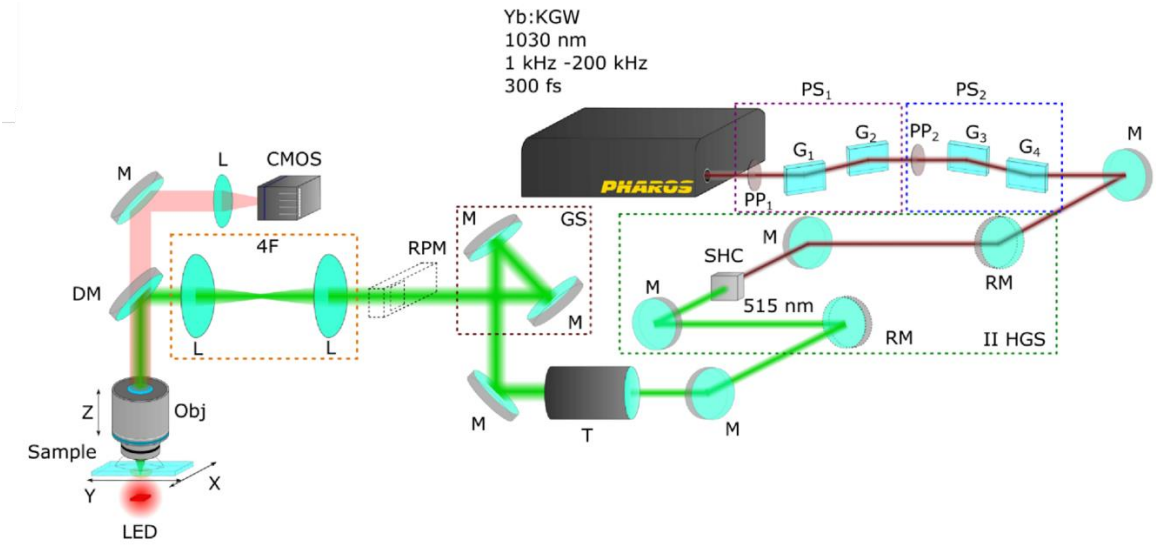

Pharos: laser source with specifications shown above	PS1 & 2: coarse (1) and precise (2) power control stage	PP1: manually rotatable phase plate
PP2: phase plate mounted in an attenuator	G1 – G4: glass plates	M: mirrors
II HGS: second harmonic branch	RM: removable mirrors	SHC: second harmonic crystal
T: telescope expanding laser's diameter	GS: galvanometric scanner	RPM: removable power meter
4F: lens system	L: lenses	DM: dichroic mirror
CMOS: monitoring camera	Obj: objective lens Olympus MPlan N 10x/0.25NA	LED: LED light source for sample illumination

Figure 36. Schematic of the 2PP set-up with annotations below (this figure was kindly provided by Prof Mangirdas Malinauskas' research group and adapted from Jonusauskas *et al.*'s work [166]).

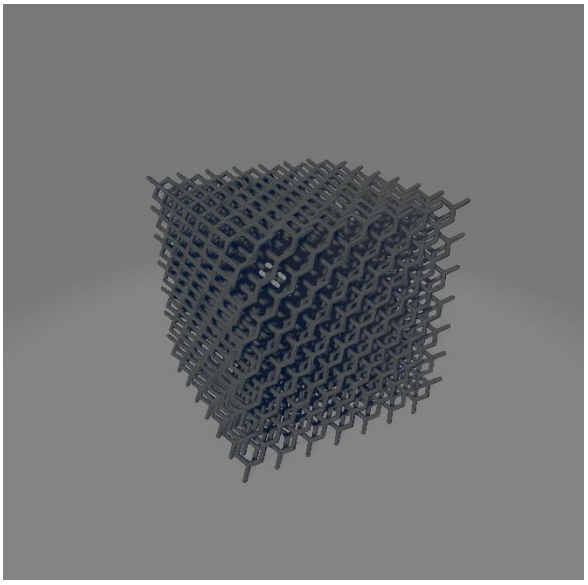

Figure 37. Lattice structure used for 2PP (free download from: www.thingiverse.com/thing:2788117, with license CC BY-NC-SA 4.0, creator: RobotMama (Anika Uhlemann)).

After initial trials on PCL-A without PI, it was found that 2PP could happen and structures could be built successfully. After optimising the operational parameters, we tried 2, 3, and 4 mW to fabricate a lattice structure shown in Figure 3. A scanning speed 25000 μm/s was chosen to fabricate the structure to acquire the fastest production rate. The fabricated samples were then carefully rinsed by IPA to remove residual PCL-A.

4.3.7. Surfactant-free Emulsion-templated Porous Material

PCL-A behaved as a surfactant and showed strong potential of emulsification during washing process [40]. A trial of using PCL-A to fabricate surfactant-free emulsion-templated porous material was carried out. Briefly, by following Dikici *et al*.'s protocol performed on PCL methacrylate [15], 0.4 g PCL-A and 5 wt% of PI was added into 0.6 g solvent mixture (0.36 g

toluene + 0.24 g chloroform) in a closed EPA vial under room temperature. The solution was mixed at 300 rpm for 5 min to ensure homogeneity. 5 vials of such solution were prepared for different types of added aqueous phase. Subsequently, 4 ml of deionised water, NaCl solutions (2.5, 5, 7.5, and 10 wt%) were loaded into separate syringes with needles. These different aqueous phases were added dropwise into the vials respectively through the seals of vials. The mixtures were kept stirring at 300 rpm while the aqueous phases were being added. The mixtures were left being stirred for a further 5 min for homogeneity. Then, all emulsions were removed from stirring and left still for 2 hours to evaluate stability. The most stable one without phase separation was loaded to a syringe and cured under an UV spotcurer (OmniCure S2000, 5 min each side). Then, the sample was withdrawn from the syringe and washed in methanol and deionised water successively to remove residual solvent mixture, PI, and NaCl. The cured emulsion-templated material was frozen under -20 °C then freeze-dried (Edwards Modulyo 4K Freeze Dryer) overnight.

4.3.8. Characterisation

4.3.8.1. Chemical Structures

Chemical structures 4-arm PCL, PCL-A-AC, PCL-A-K, PCL-A were characterised *via* Proton Nuclear Magnetic Resonance (NMR) Spectroscopy (^{1}H NMR, Bruker AVIII 400MHz, $CDCl_3$). Spectra analysed on MestreNova. Attenuated total Reflectance-Fourier transform infrared spectroscopy (ATR-FTIR, Thermo Scientific Nicolet 380 FT-IR Spectrometer, scanning range: 4000 cm^{-1} to 600 cm^{-1}, 64 scans) was used to characterise the performance of photocuring and surface treatment of film samples.

4.3.8.2. UV/Vis Spectroscopy

UV/Vis Spectroscopy was performed to explore the difference of UV/Vis absorbance between PCL-A-AC and PCL-A. Shimadzu UV-2600 UV-Vis spectrophotometer was used for this characterisation. Individually, 2 resins were dissolved in a methanol/acetone solvent mixture (1:1, v:v) with a concentration 0.033 g/ml. Each of the samples was loaded into the UV/Vis spectrometer along with the pure solvent mixture as the reference, of which the baseline was subtracted automatically by the controlling software. A 200 nm to 800 nm wavelength range was selected for the scanning. The wavelength resolved spectra were analysed in OriginPro 2020.

4.3.8.3. Tensile Testing

Tensile testing was performed on Mecmesin Multitest 2.5-dV with a tension speed 1 mm/min. The data was analysed in OriginPro 2020. Nine replicates were tested.

4.3.8.4. Cell Viability Assay

Film samples were further washed in 70% ethanol for sterilisation and washed in PBS 3 times to remove the residual ethanol. A specific type of neuro cell NG108-15 was chosen for 2D cell culture on the films sample to assess the biocompatibility of PCL-A. On Day 0, 10000 cells (in 20 μL droplet) were seeded on the films in each well and cultured in an incubator for 1 hour initially. Triplicate samples were cultured along with tissue culture plate (TCP) and a negative control (media only). Cells were cultured in an incubator under 37 ℃ and for 1 week. On day 1, 4, and 7 respectively, resazurin assay was utilised to characterise the cell growth status. A spectrofluorometer (FLX800, Bio-TEK Instrument) was used to read the intensity of

fluorescence. On day 7, the dead/alive status of cell were imaged under confocal microscope (Zeiss LSM800 Airyscan). Data were analysed *via* GraphPad Prism and ImageJ.

4.3.8.5. Accelerated Degradation

PCL-A samples were cured as disc-shaped samples in a PDMS mould (5wt% PI, dia. 9 mm, thickness 3 mm) and weighed as 0.1 g approximately for each. The samples were then soaked into bijous with 2 ml NaOH (1 M) in each to characterise the rate of accelerated degradation. All the empty bijous were weighed beforehand, recorded as w_0. After being loaded with samples without NaOH solution, they were weighed again as the initial weights, recorded as w_i. Thus, the initial sample weight was recorded as (w_i - w_0). Then the samples were added with NaOH solution and left with caps sealed in a 37°C incubator. Every hour, the liquid phase was removed carefully by a pipette gun, and the solid phase was kept in bijous and gently rinsed with deionised water. The rinsing water was then disposed. Following, the bijous with leftover solid parts were dried in a warm vacuum to get rid of the residual water and weighed individually, recorded as w_1, w_2, w_3, and so on. Thus, the weight of remaining solid parts after each hour was recorded as (w_1 - w_0), (w_2 - w_0), (w_3 - w_0), and so on.

4.4. Results and Discussion

4.4.1. Comparison of PCL-A Synthesised *via* Different Methods

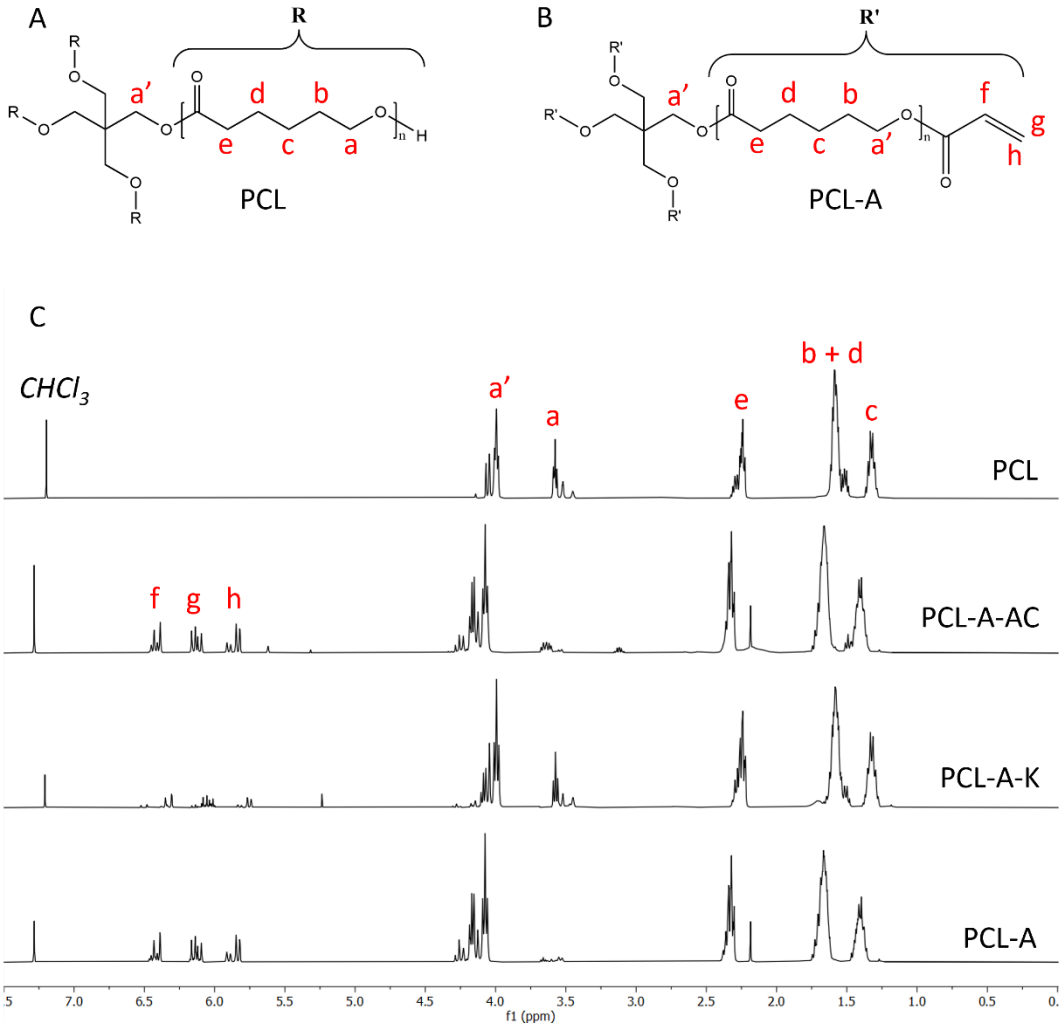

Figure 38. Chemical structures of PCL (A) and PCL-A (B) with proton sites labelled, (C) ^{1}H NMR spectra of PCL (4-arm PCL pre-polymer), PCL-A-AC (resin synthesised via AC/Et_3N), PCL-A-K (resin synthesised via AC/K_2CO_3), and PCL-A (resin synthesised via SE), where all peaks are labelled according to the proton sites on the chemical structures respectively.

From the spectra in Figure 38, it is clear that the intensity of peak a at 3.6 ppm has reduced and a series of peaks f, g, and h at 5.8, 6.1 and 6.4 ppm, respectively, have occurred on the spectra of PCL-A-AC, PCL-A-K, and PCL-A, which confirms that acrylate groups have been successfully introduced onto the PCL molecules *via* all methods [40].

After acrylation, the chemical environment of protons at site a has changed to the same one as site a'. To calculate the degree of acrylation, on each PCL molecule, we set X as the average number of converted carbon atoms directly connected the acrylate groups. As the number of acrylate groups, on each of which there are 3 protons shown as peaks f, g, and h, equals to the number of converted carbons, we can have the number of protons on acrylate groups as 3X. And we can have the number of non-converted carbon atoms, still remaining as -C-OH, as (4 - X), where there are 2 protons. Since the integral area has a linear relationship with the number of protons, we can have an equation as follows:

$$\frac{\int peak_a}{\int peaks_{f+g+h}} = \frac{2(4-X)}{3X} \quad (X \neq 0) \tag{10}$$

And the degree of acrylation is follows:

$$\eta = \frac{X}{4} \times 100\% \tag{11}$$

From the software analysis, we can have the integral ratio between peak a and peak f-h are 0.13/0.53, 0.19/0.30, and 0.07/0.42 for PCL-A-AC, PCL-A-K, and PCL-A respectively. So, we can have the calculated results shown in Table :

Table 6. Calculated results of acrylated PCL resins.

Name	X	η
PCL-A-AC	2.92	73%
PCL-A-K	1.19	29.8%
PCL-A	3.2	80%

Thus, the degree of acrylation of PCL-A-AC, PCL-A-K, and PCL-A are 73%, 29.8%, and 80% respectively.

Acrylation *via* AC/Et_3N method provides relatively high conversion rates, but still lower than SE method. Acrylation *via* potassium carbonate method results in a significant lower degree of conversion due to its poor solubility in organic solvents such as DCM. As the degree of acrylation is 29.8%, it indicates that there are only slightly over 1 acrylate group on each of the 4-arm PCL molecules averagely, which means after curing, the final resin will unlikely form a chemically crosslinked network, which normally requires at least 2 acrylate groups on a single molecule. However, under the same reaction time and conditions, acrylation *via* SE leads to a decent degree of acrylation 80%. It indicates that there are more than 3 acrylate groups being introduced onto each PCL molecules on average. Thus, after curing, a highly chemically crosslinked structure can be expected.

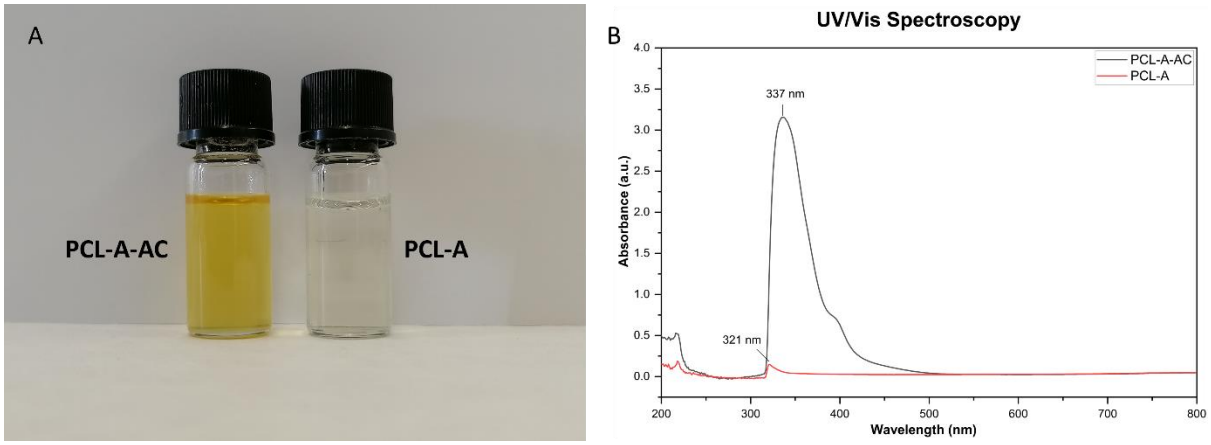

Figure 39. A) Colour difference between PCL-A-AC and PCL-A. B) UV/Vis spectroscopy of PCL acrylates *via* both methods, where there is tall and sharp peak at 337 nm on the spectrum of PCL-A-AC but only a much weaker peak can be found at 321 nm from PCL-A.

From the results of UV/Vis spectroscopy (Figure 39B), compared to PCL-A synthesised *via* SE, the yellow-coloured sample synthesised *via* the AC/Et_3N shows a much stronger absorbance between 300 nm and 500 nm, which agrees with the yellow colour caused by the impurity. Unfortunately, this is also within wavelength range of common photocuring wavelengths, i.e. 360 and 405 nm. Particularly, for light-based additive manufacturing, the impact of this yellow impurity cannot be ignored, because it absorbs strongly in the near-UV and blue region of the spectrum which means that commonly used light sources for photocuring (300 – 500 nm) will be strongly absorbed by this impurity rather than photoinitiator to trigger photo-polymerisation. When fine structures being fabricated *via* micro-stereolithography such as two-photon 3D printing, it will likely lead to a poor polymerisation performance. In addition, since this yellow impurity cannot be completely removed from the final product, its concentration and effects on photoabsorption and biocompatibility cannot be controlled effectively. In contrast, PCL-A synthesised *via* SE presents a visibly clear compound which ensures that the incident light can be efficiently absorbed by added photoinitiator during

photocuring rather than any impurities. If the light needs to be attenuated to improve printing resolution, a light absorber, e.g., tartrazine, can be added to provide tuneable light absorbtion [91].

Therefore, compared to conventional AC/Et_3N and alternative inorganic compound methods, SE should be the preferable one to acquire clean PCL-A resin with high degree of acrylation.

4.4.2. Assessment of Mechanical Properties of PCL-A Bulk Material

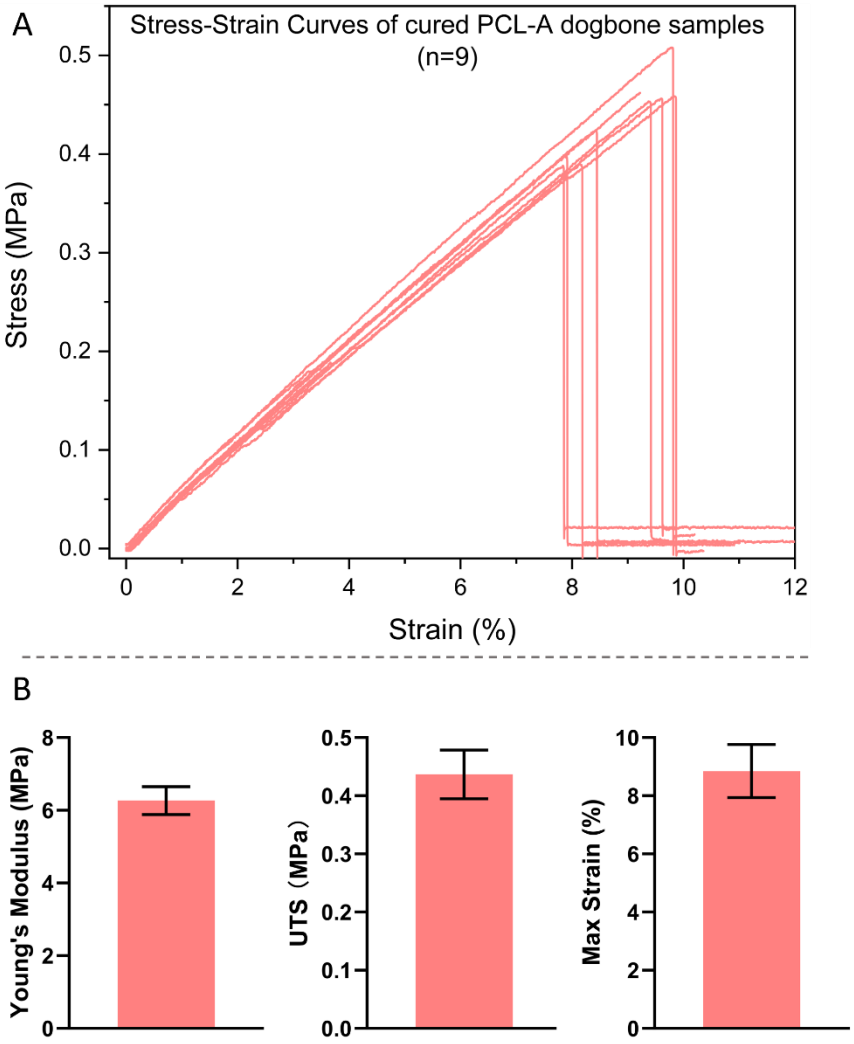

Figure 40. Tensile testing results of cured PCL-A dog-bone samples (n = 9). A) Strain-stress curves. B) Mechanical properties PCL-A: Young's Modulus (YM) 6.27 MPa, ultimate tensile strength (UTS) 0.44 MPa, and max strain 8.85% (mean values).

After analysing tensile testing results, PCL-A dog-bone samples present average Young's Modulus (YM) 6.27 MPa and ultimate tensile strength (UTS) 0.44 MPa. Such mechanical properties can be regarded as elastic. Compared to some natural tissue, such as human tibial nerve which has YM 9.5 MPa and UTS 3.9 MPa [167], PCL-A shows potential to be applied in soft tissue engineering applications. However, the samples broke when their elongation reached 8% - 10% approximately, which indicates the brittleness of this cured PCL-A. Such low stiffness could be a result of low crosslinking density due to oxygen inhibition during photocuring process, which usually happens when photocuring acrylate-based resins with presence of oxygen [38]. To reduce the influence of oxygen inhibition, several approaches were suggested, such as curing under nitrogen, performing 'thiol-ene' click chemistry, and amine chemical modification. Furthermore, PCL-A would have better mechanical properties thus a broader range of applications if the oxygen inhibition issue is reduced. When compared to PCL-M of the same molecular weight discussed in the PCL-M/PCL composite work, PCL-A's YM (6 MPa approximately) is about half of PCL-M's YM (13 MPa approximately), which indicates lower cross-linking density. Generally, oxygen inhibition is considered to happen more easily during curing acrylates than methacrylates due to that firstly oxygen could have a higher solubility in acrylates leading to a stronger oxygen inhibiting effect [168], and secondly an abstractable tertiary hydrogen rather than a $-CH_3$ on carbon -C= makes acrylate's radical less stable and easier to be attacked by oxygen performing a chain transfer reaction and leading to an termination to crosslinking [169, 170].

4.4.3. Photocuring and Surface Treatment Performance

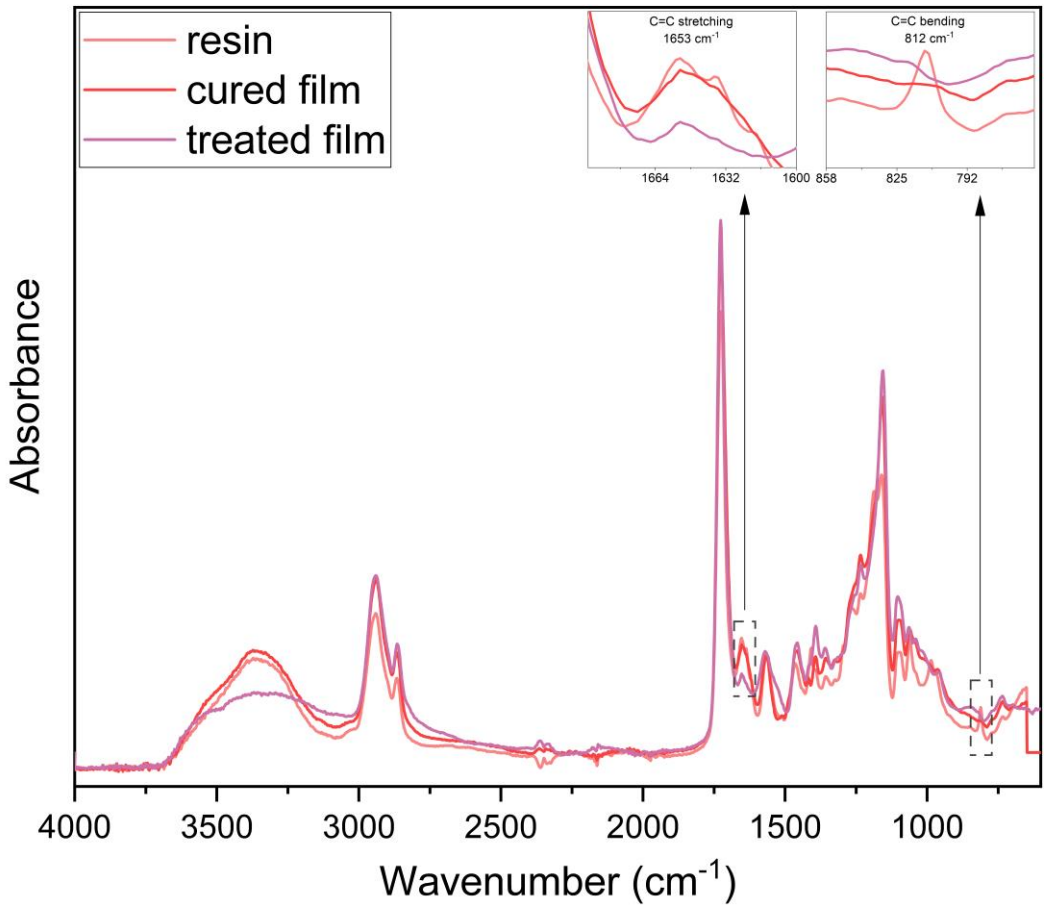

Figure 41. ATR-FTIR spectra of PCL-A resin (liquid, pink spectrum), cured film before treatment (red spectrum), and surface-treated film (purple spectrum).

To reduce the amount of residual -C=C on the surface, an EDA solution (10 wt% in methanol) treatment was introduced to this work. PCL-A film was characterised by ATR-FTIR before and after this treatment.

In Figure 41, ATR-FTIR spectra shows that after curing, the peak at 812 cm^{-1} becomes flattened indicating that -C=C groups have been consumed [36]. However, the peak at 1653 cm^{-1} still shows strong intensity indicating that there are -C=C groups remaining. The residual -C=C groups could be result of oxygen inhibition. As the photocuring in this work is a free radical polymerisation process, -C=C groups can be triggered by PI into free radicals, but with the presence of oxygen, the free radicals can be oxidised by oxygen and turn into carbon centred free radical peroxide which terminates the process of polymerisation and leaves unpolymerised -C=C on the surface or even inside the sample, which is called oxygen quenching. And from the spectra in Figure 41, the intensity of peak at 1653 cm^{-1} significantly decreased, which indicates that the residual -C=C groups have been consumed by -NH_2 groups and EDA molecules have been introduced to the surface of PCL-A films. Moreover, this surface modification method could be used to create more cell-adhesive surface, such as using butanediamine [171, 172].Interestingly, the rapid oxygen quenching of this resin could allow it to be explored for continuous liquid interface production (CLIP), which is to make use of this oxygen quenching effect to fabricate fine 3D structures rapidly, which was reported by Tumbleston *et al* [39].

4.4.4. Assessment of Cell Viability on PCL-A Films

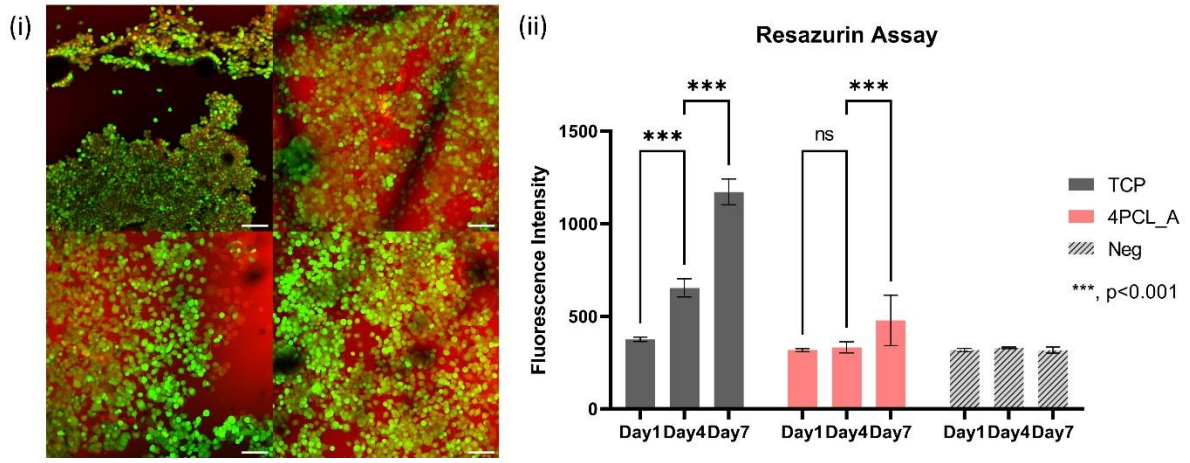

Figure 42. (i) Confocal microscope images of live-dead stained NG108-15 cells on 4PCL-A films on Day 7, where green fluorescence indicates living cells and red dead cells, (ii) resazurin assay results show that from Day 1 to Day 4, cell growth was not significant, but from Day 4 to Day 7, a significant growth can be observed (TCP: tissue culture plate, Neg: negative control).

Resazurin assay results (Figure 42ii) indicate that from Day 1 to Day 4 there is no significant cell growth but from Day 4 to Day 7, cells have grown on the film samples significantly. One possible reason for this phenomenon is that the films were still not that suitable for cell attachment as TCP which is usually treated to promote cell growth. Another possible reason is that oxygen inhibition during the curing process might not only result in residual -C=C groups but also peroxyl groups (-O-O-) on the surface [173], which could not be overcome by EDA treatment and would oxidise protein [174]. Thus, the general environment on the films' surface was not that preferable for cell attachment and growth.

Images from confocal microscopy on Day 7 (Figure 42i) show that basically all cells on the films are still alive and dead cell can hardly be found, which indicates that these PCL-A films are conducive to neuronal cell growth. Interestingly, we can further functionalise these surfaces with amine groups which should further increase the neuronal cell attachment and differentiation [175]. Accordingly, PCL-A synthesised *via* Steglich Esterification can be considered as a promising resin for further cell scaffold fabrication.

4.4.5. Light-based Additive Manufacturing (1PP)

PCL-A diluted with different weight ratios of DI water is shown as follows:

Table 7. Weight ratioes of water in PCL-A.

Name	PCL-A	DI water
PCL-A-0	1	0
PCL-A-25	1	0.25
PCL-A-50	1	0.5
PCL-A-75	1	0.75
PCL-A-100	1	1

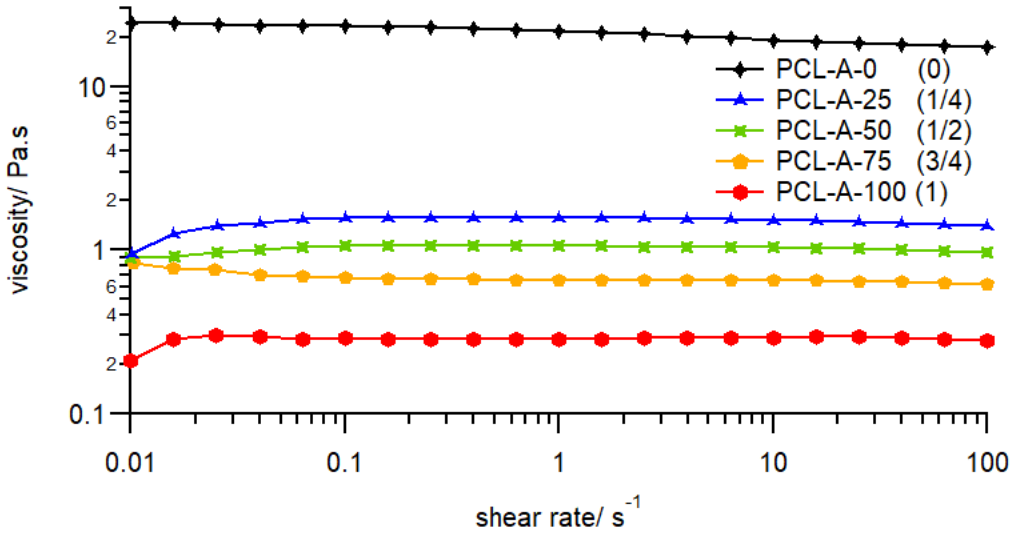

Figure 43. Viscosity of PCL-A and its water solutions (numbers in the parentheses are the water weight ratio against PCL-A, e.g., 1/4 means water : PCL-A = 1 : 4, w/w).

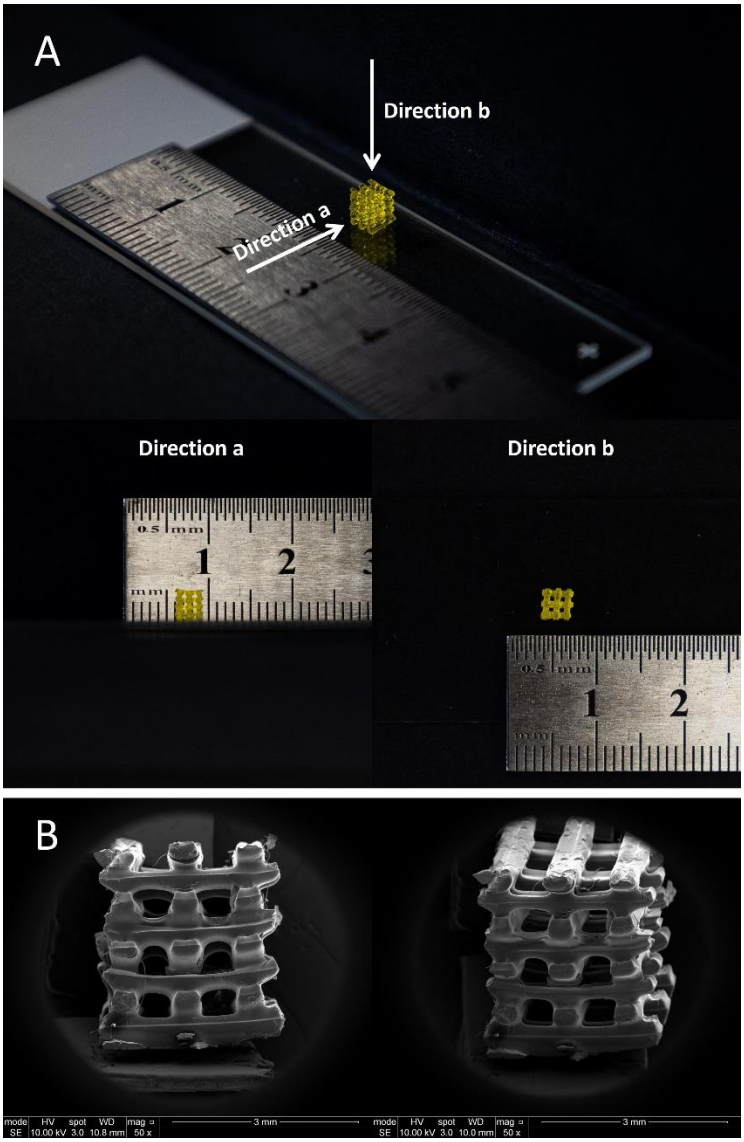

Figure 44. A woodpile structure fabricated *via* stereolithography. A) General appearance of the wood pile structure, approximately 3 mm x 3 mm x 3mm cubic shape. B) Structure details under SEM (scale bar: 3 mm), where the width of each line is approximately 0.35 mm and the horizontal distance between lines is approximately 0.4 mm, and the height of each line is approximately 0.35 mm.

Before running stereolithography, to optimise the printing performance of vat polymerisation, dilution of PCL-A to reduce its viscosity might be necessary. PCL-A exhibited good water

solubility. Therefore, we tested the viscosity of the PCL-A water solutions. After a few trials of stereolithography, resins with viscosity higher than PCL-A-50 in Figure 43 (weight ratio of water and PCL-A: 0.5:1) could not be properly structured due to high viscosity, which led to overly cured polymer rather than a designed structure. This is largely due to that when the viscosity is high, the stage has to move downwards with lower velocity to allow fluid compensation on the top so that the additive manufacturing can be continued. But the low velocity would allow the top surface to be exposed to UV for longer time resulting an overly cured polymer. But when then concentration of water was higher than PCL-A-50, the printed structures showed higher brittleness, which were extremely difficult to remove from the platform without being broken. Thus, we chose PCL-A-50, which showed decent viscosity (approximately 1 Pa·s), for further stereolithography.

Figure 44 shows the woodpile structure manufactured *via* stereolithography by using PCL-A-50. The yellow colour is a result of doped tartrazine to acquire the optimum resolution of light-based stereolithography. From two directions of observation (Figure 44A), both vertically and horizontally, the cubic wood pile structure can be seen through meaning that a proper 3D structure has been fabricated. Under SEM (Figure 44B), some curvy surfaces can be observed on each layer of wood pile. Such curvy surfaces should be a result of slow compensating flow of resin which could not cover the top of fabricated structure while the stage being moved downwards. Thus, resins with lower viscosity should be used for stereolithography, such as PCL-A-75 and PCL-A-100 to acquire higher resolution structures.

4.4.6. Light-based Additive Manufacturing (2PP)

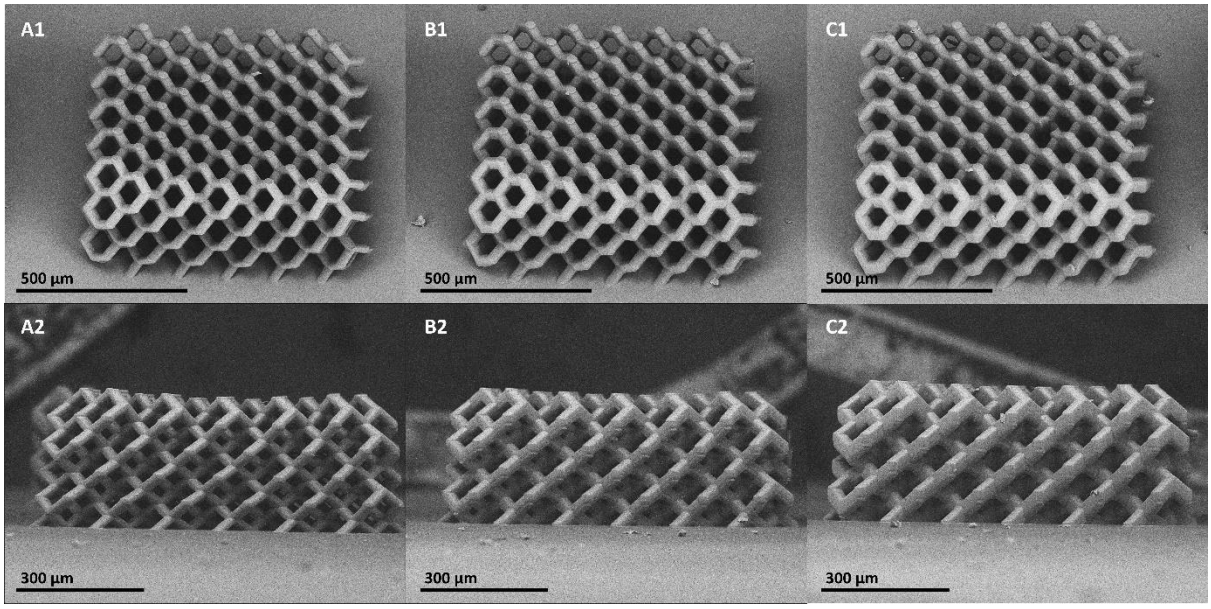

Figure 45. SEM images of lattice structures fabricated by 2PP without photoinitiator with different powers: A) 2mW, B) 3mW, C) 4mW. Imaging directions: 1) 45°, 2) horizontal.

The SEM images (Figure 45) show that ultra-high resolution lattice structures have been fabricated, where the wanted patterns with sharp edges can be observed. The structural integrity has also been maintained after IPA washing. These exciting results exhibit the capability of this PCL-A for PI-free 2PP structuring with a relatively wide laser power window under fast direct writing speed. Besides, this PCL-A resin was synthesised *via* Steglich Esterification which should leave much fewer toxic impurities in the final product, along with the PI-free 2PP fabrication process, these PCL-A scaffolds with ultra-fine structures would be promising materials for future cell work. As can be observed in the horizontally imaged structures, the line thickness increases with higher power. This is largely due to that the light spatial confinement, in which 2PP happens, normally increases along with the light intensity, which

delivers larger voxels during fabrication and lower resolution [166]. However, the curing performance and surface chemistry is uknown at the moment, but can be examined *via* state-of-the-art characterisation techniques, such as nano-FTIR.

4.4.7. Surfactant-free Emulsion-templating Porous Material Fabrication

We also tested the potential of the PCL-A as an amphiphilic compound to be used in emulsion templating.

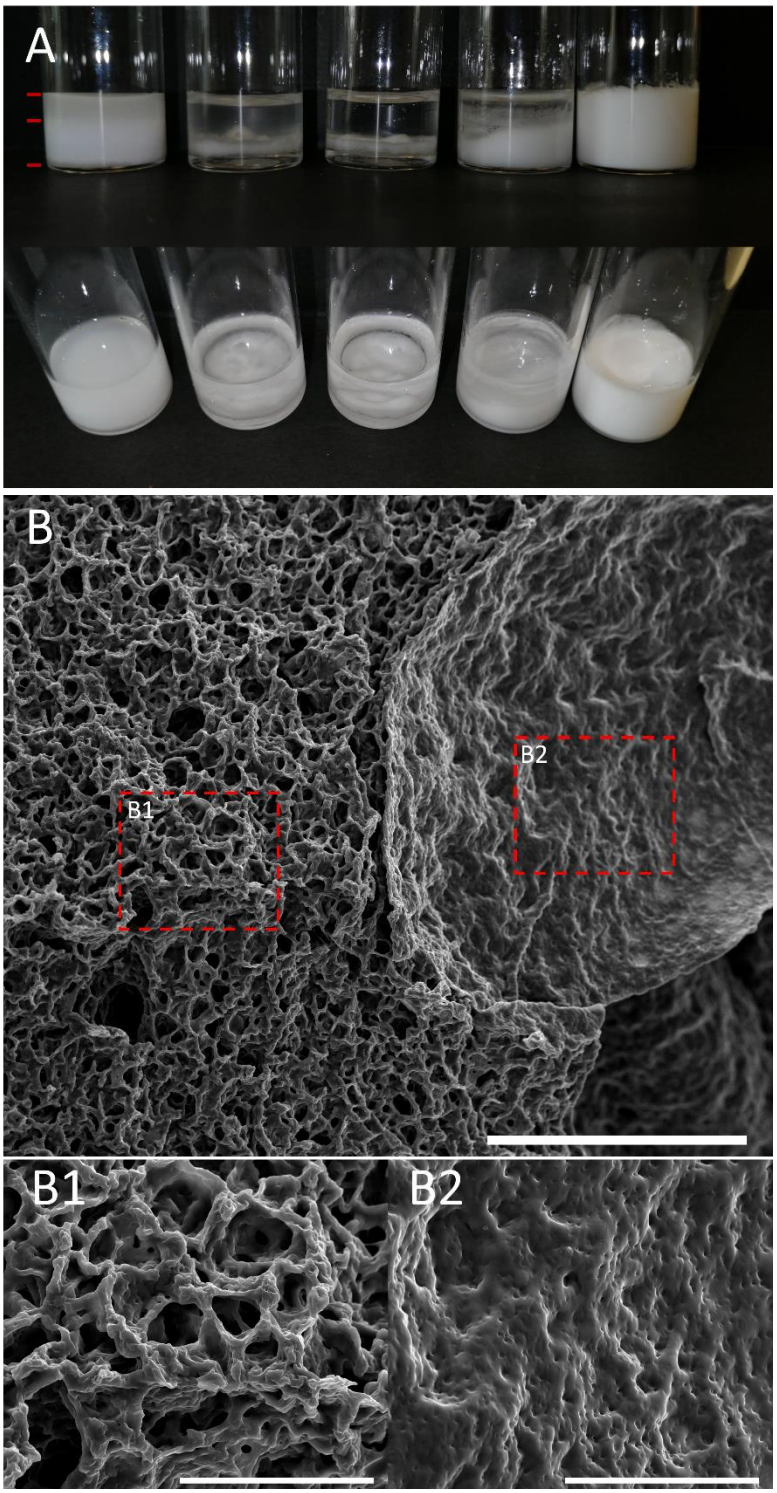

Figure 46. A) Stability of emulsions left still for 2 hours (aqua phase from left to right: deionised water, 2.5 wt%, 5 wt%, 7.5 wt%, 10 wt% NaCl). B) Microstructures of freeze-dried PCL-A emulsion-templated porous material (made with 10 wt% NaCl) under SEM (scale bars: B: 100 μm, B1 and B2: 30 μm).

In Figure 46A, pure deionised water forms a cloudy suspension with phase separation marked by short red lines, where the upper part of the mixture shows a less cloudy phase than the bottom one. This indicates that pure deionised water formed an oil-in-water emulsion where organic solvent droplets are wrapped by PCL-A molecules. When the ionic concentration of the aqueous phase in increased by adding NaCl, Na^+ and Cl^- rapidly increase the polarity leading a clear phase separation. However, when the amount of NaCl reaches 7.5 wt%, phase separation still occurs but begins to show a trend of being less obvious. When the concentration of NaCl reaches 10 wt%, the emulsion becomes able to maintain stability for 2 hours. After curing, washing, and freeze drying, the material shows a highly porous internal structure with interconnected microscale pores. However, the surface of the material shows a much less porous feature with smaller pore sizes. This promising result shows that the potential of PCL-A being applied as surfactant-free emulsion-templated material for cell scaffolds, which could help avoid the cytotoxicity brought by residual surfactant to a large extent [176].

Additionally, from the configuration of the porous structures it can be seen that it is not highly stabilised compared to surfactant-stabilised emulsion-templated materials with micro-spherical voids [15]. To enhance its stability and obtain decent micro-porous structures but without using surfactant, Pickering emulsions, which uses solid particles rather than surfactants, could potentially be applied to PCL-A to fabricate surfactant-free emulsion-templated materials [107].

4.4.8. Accelerated Degradation

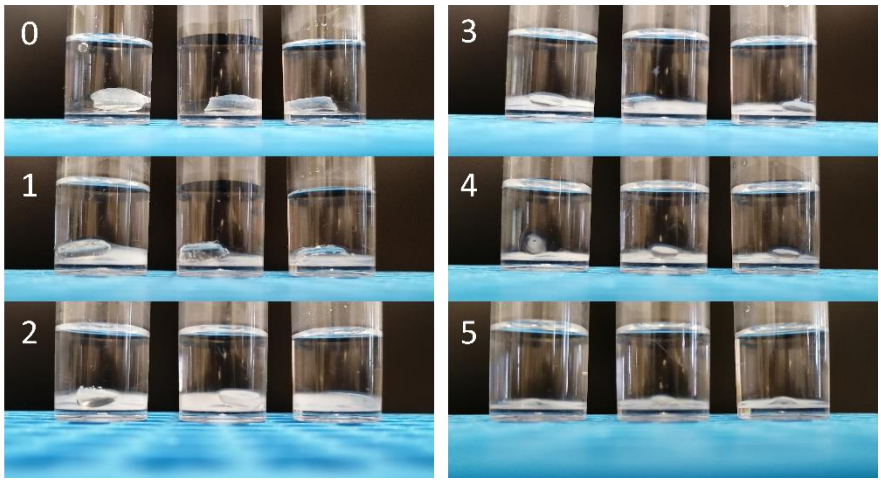

Figure 47. A) Visual progress of PCL-A's accelerated degradation in 1M NaOH solution from 0 to 5h, B) weight losing trend of 0.1 g sample in 1M NaOH with samples in d-H2O as control (n=3).

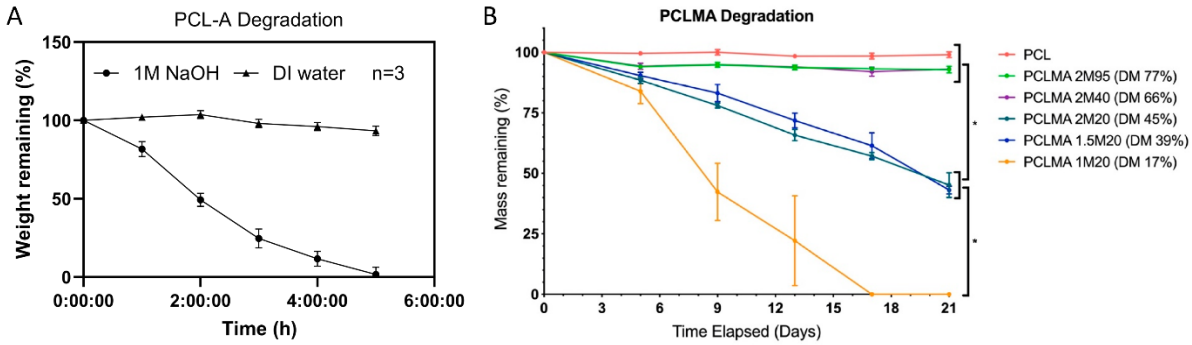

Figure 48. Comparison of degradation rate comparison between A) PCL-A and B) PCL-M (PCLMA used in Field *et al.*'s work), among which PCLMA 1M20 shows the lowest degree of methacrylation (DM) and the fastest degradation process but the degradation time is still over 2 weeks [13].

The result of accelerated degradation shows that PCL-A disc samples were be fully degraded within 6 hours in 1M NaOH solution. Compared to the commercial PCL products, which usually have linear molecular structures with 60% crystallinity and can be degraded in 5M NaOH over 6 weeks [177], this PCL-A material shows much higher degradability even in a lower concentration of NaOH solution. Moreover, a study of 3-arm PLC methacrylate (PCL-M), which has similar star-shaped molecular structure, carried out by Field *et al*. shows that PCL-M disc samples with low degree of methacrylation (dia. 4 mm, thickness 1.3 mm) were degraded in 5M NaOH for 17 days (Figure 48B), which still took much longer time for a thorough degradation [13].

According to a study investigating the mechanism of degradation of PCL, its crystallinity contributes significant impact to the degradation time [178]. As this PCL-A has 2 repeating units on each arm which extremely limits the ability of crystallisation, we can assume that there is hardly any crystalline region in the cured material. Additionally, the methacrylate group is more hydrophobic because of the additional methyl group in its chemical structure which cannot be found on PCL-A. Thus, while PCL-A being degraded in aqueous solutions, water ingress in the polymeric structure is enhanced in the acrylate, which allows the hydrolysis of the ester groups to occur more rapidly [179]. On the other hand, the relatively low crosslinking density brought by oxygen inhibition could also be a reason for this rapid degradation.

Furthermore, this rapid degradation indicates the high water absorbance of cured PCL-A. This would also lead to some other applications, such as co-polymerising with hydrophilic monomers, e.g., poly(ethylene glycol), to further increase hydrophilicity and potentially fabricate hydrogels [180], and also tailored degradability by co-polymerising with less hydrophilic monomers, such as styrene, which could also tune its mechanical properties [181].

4.5. Conclusions

4-arm PCL can be functionalised with acrylate groups *via* SE with 80% conversion. Compared to conventionally synthesised PCL acrylate, PCL-A *via* SE is a highly purified colourless resin, which brought higher tunability of absorbing light. The bulk material showed an elastic property which indicates that it might be capable for soft tissue engineering. The PCL-A synthesised *via* this novel method has also shown biocompatibility for future cell work. PCL-A is also capable for high-resolution light-based additive manufacturing for both single and two-photon light sources. Additionally, this PCL-A shows capability of structuring *via* 2PP without PI. This PCL-A is also found to have an excellent degradability compared to other linear PCL and PCL methacrylate, of which the accelerated degradation process could take days even weeks.

Acknowledgement

We appreciate Louis Johnson for assisting with the cell work, and Jurga Jeršovaite and Prof Mangirdas Malinauskas (Laser Research Center, Vilnius University, Lithuania) for sharing equipment and expertise on the laser work.

General Conclusions

1. Photocurable 4-arm PCL (PCL-M) can be synthesised *via* ring-opening reaction of ε-caprolactone with pentaerythritol, and a following functionalisation with methacrylic anhydride. The degree of methacrylation can reach ~ 69% after 20 hours of methacrylation.
2. Doping linear PCL into PCL-M can obtain biocompatible composites with tuned mechanical properties and degradability, also with intriguing micro-scale spherical structures.
3. Linear PCL-reinforced PCL-M composite has thermoresponsive shape-memory property.
4. Doping HAp particles in PCL-M can also fabricate biocompatible materials with enhanced mechanical properties and accelerated degradation process.
5. Increasing HAp concentration in PCL-M matrix can bring better performance on extrusion-based additive manufacturing.
6. Acrylation on 4-arm PCL can be achieved *via* Steglich Esterification which produces highly purified polymers with 80% of conversion.
7. PCL-A shows biocompatibility but still there is a potential to further improve its surface and mechanical properties to by reducing oxygen inhibition during photocuring.
8. PCL-A is surprisingly water soluble, thus, shows a potential of formulate water-based 3D printing resin with tuned viscosity.
9. PCL-A is capable for photoinitiator-free 2PP structuring.
10. PCL-A can be used for fabricating porous material *via* emulsion-templating method without surfactant.

Future Work

1. Additive manufacturing of PCL-M/PCL composites, and relevant 3D cell culture.
2. Characterisation of dynamic thermo-mechanical properties of PCL-M/PCL composites.
3. Exploration of the chemical composition of the micro-spherical structures of PCL-M/PCL composites to examine whether it could have semi-interpenetrating network (semi-IPN) structures.
4. Trying to formulate PCL-M/PCL-based polyHIPE and also leached polyHIPE with meso-scale porous structures.
5. Trying to explore the possibility of fabricating PCL-M/PCL/HAp composites.
6. Characterising compressive mechanical properties of PCL-M/HAp scaffolds.
7. Further exploration of the effect of substituted HAp would bring to extrusion-based additive manufacturing and biocompatibility.
8. Further explore the possibility of increasing the degree of acrylation on 4-arm PCL.
9. Acrylation on other multi-arm polymers such as PLA *via* Steglich Esterification.
10. Further surface modification on PCL-A materials to acquire higher biocompatibility.
11. Cell work on 2PP-structured scaffolds.
12. Stabilising surfactant-free emulsion-templated PCL-A porous material *via* optimising emulsion recipe or Pickering method.

References

(1) Ghassemi, T.; Shahroodi, A.; Ebrahimzadeh, M. H.; Mousavian, A.; Movaffagh, J.; Moradi, A. Current Concepts in Scaffolding for Bone Tissue Engineering. *Archives of Bone and Joint Surgery-Abjs* **2018**, *6* (2), 90-99, Review.

(2) Nair, N. R.; Sekhar, V. C.; Nampoothiri, K. M.; Pandey, A. 32 - Biodegradation of Biopolymers. In *Current Developments in Biotechnology and Bioengineering*, Pandey, A., Negi, S., Soccol, C. R. Eds.; Elsevier, 2017; pp 739-755.

(3) Hiraishi, N.; Yau, J. Y. Y.; Loushine, R. J.; Armstrong, S. R.; Weller, R. N.; King, N. M.; Pashley, D. H.; Tay, F. R. Susceptibility of a Polycaprolactone-based Root Canal–filling Material to Degradation. III. Turbidimetric Evaluation of Enzymatic Hydrolysis. *Journal of Endodontics* **2007**, *33* (8), 952-956. DOI: 10.1016/j.joen.2007.05.004 (acccessed 2023/09/13).

(4) Lotfi, M.; Ghasemi, N.; Rahimi, S.; Vosoughhosseini, S.; Saghiri, M. A.; Shahidi, A. Resilon: a comprehensive literature review. *J Dent Res Dent Clin Dent Prospects* **2013**, *7* (3), 119-130. DOI: 10.5681/joddd.2013.020 From NLM.

(5) Yoshimoto, H.; Shin, Y. M.; Terai, H.; Vacanti, J. P. A biodegradable nanofiber scaffold by electrospinning and its potential for bone tissue engineering. *Biomaterials* **2003**, *24* (12), 2077-2082. DOI: 10.1016/s0142-9612(02)00635-x.

(6) Dwivedi, R.; Kumar, S.; Pandey, R.; Mahajan, A.; Nandana, D.; Katti, D. S.; Mehrotra, D. Polycaprolactone as biomaterial for bone scaffolds: Review of literature. *Journal of oral biology and craniofacial research* **2020**, *10* (1), 381-388. DOI: 10.1016/j.jobcr.2019.10.003 PubMed.

(7) Buwalda, S. J.; Boere, K. W. M.; Dijkstra, P. J.; Feijen, J.; Vermonden, T.; Hennink, W. E. Hydrogels in a historical perspective: From simple networks to smart materials. *Journal of Controlled Release* **2014**, *190*, 254-273. DOI: 10.1016/j.jconrel.2014.03.052.

(8) Pantani, R.; Sorrentino, A. Influence of crystallinity on the biodegradation rate of injection-moulded poly(lactic acid) samples in controlled composting conditions. *Polymer Degradation and Stability* **2013**, *98* (5), 1089-1096. DOI: 10.1016/j.polymdegradstab.2013.01.005.

(9) Hynes, C. G.; Morra, E.; Walsh, P.; Buchanan, F. Chapter 7 - Degradation of biomaterials. In *Tissue Engineering (Third Edition)*, De Boer, J., Blitterswijk, C. A. V., Uquillas, J. A., Malik, N. Eds.; Academic Press, 2023; pp 213-259.

(10) Xia, Y.; Zhou, P.; Cheng, X.; Xie, Y.; Liang, C.; Li, C.; Xu, S. Selective laser sintering fabrication of nano-hydroxyapatite/poly-ε-caprolactone scaffolds for bone tissue engineering applications. *International Journal of Nanomedicine* **2013**, *8* (null), 4197-4213. DOI: 10.2147/IJN.S50685.

(11) Wang, B.; Zhang, P.; Song, W.; Zhao, L.; He, C. Modification of polyglycolic acid and poly lactic-co-glycolic acid fibers by ultrasonic treatment for enhancing hydrophilicity and cytocompatibility. *Journal of Industrial Textiles* **2014**, *45* (4), 516-530. DOI: 10.1177/1528083714537104 (acccessed 2023/09/26).

(12) Woodruff, M. A.; Hutmacher, D. W. The return of a forgotten polymer-Polycaprolactone in the 21st century. *Progress in Polymer Science* **2010**, *35* (10), 1217-1256, Review. DOI: 10.1016/j.progpolymsci.2010.04.002.

(13) Field, J.; Haycock, J. W.; Boissonade, F. M.; Claeyssens, F. A Tuneable, Photocurable, Poly(Caprolactone)-Based Resin for Tissue Engineering-Synthesis, Characterisation and Use in Stereolithography. *Molecules* **2021**, *26* (5). DOI: 10.3390/molecules26051199.

(14) Dikici, B. A.; Dikici, S.; Reilly, G. C.; MacNeil, S.; Claeyssens, F. A Novel Bilayer Polycaprolactone Membrane for Guided Bone Regeneration: Combining Electrospinning and Emulsion Templating. *Materials* **2019**, *12* (16), 24, Article. DOI: 10.3390/ma12162643.

(15) Dikici, B. A.; Reilly, G. C.; Claeyssens, F. Boosting the Osteogenic and Angiogenic Performance of Multiscale Porous Polycaprolactone Scaffolds by In Vitro Generated Extracellular Matrix Decoration. *Acs Applied Materials & Interfaces* **2020**, *12* (11), 12510-12524, Article. DOI: 10.1021/acsami.9b23100.

(16) Khosravi, E.; Musa, O. M. Thermally degradable thermosetting materials. *European Polymer Journal* **2011**, *47* (4), 465-473. DOI: https://doi.org/10.1016/j.eurpolymj.2010.09.023.

(17) Szanka, A.; Szarka, G.; Iván, B. Multi-methacrylated star-shaped, photocurable poly(methyl methacrylate) macromonomers via quasiliving ATRP with suppressed curing shrinkage. *Polymer* **2013**, *54* (22), 6073-6077. DOI: https://doi.org/10.1016/j.polymer.2013.09.025.
(18) Zhang, X.; Liu, H.; Yue, L.; He, J.; Bai, Y. Mussel-inspired polymer: A photocurable and degradable polymer network for adhesives. *Polymer Degradation and Stability* **2019**, *167*, 130-138. DOI: https://doi.org/10.1016/j.polymdegradstab.2019.06.018.
(19) He, Y.; Chen, J.; Rafique, I.; Lu, Z. Star-shaped polycaprolactone bearing mussel-inspired catechol end-groups as a promising bio-adhesive. *European Polymer Journal* **2020**, *139*, 110025. DOI: https://doi.org/10.1016/j.eurpolymj.2020.110025.
(20) Raszewski, Z.; Nowakowska-Toporowska, A.; Nowakowska, D.; Więckiewicz, W. Update on Acrylic Resins Used in Dentistry. *Mini Rev Med Chem* **2021**, *21* (15), 2130-2137. DOI: 10.2174/1389557521666210226151214 From NLM.
(21) Abrisham, M.; Noroozi, M.; Panahi-Sarmad, M.; Arjmand, M.; Goodarzi, V.; Shakeri, Y.; Golbaten-Mofrad, H.; Dehghan, P.; Sahzabi, A. S.; Sadri, M.; et al. The role of polycaprolactone-triol (PCL-T) in biomedical applications: A state-of-the-art review. *European Polymer Journal* **2020**, *131*, 16, Review. DOI: 10.1016/j.eurpolymj.2020.109701.
(22) Jordan, A.; Whymark, K. D.; Sydenham, J.; Sneddon, H. F. A solvent-reagent selection guide for Steglich-type esterification of carboxylic acids. *Green Chemistry* **2021**, *23* (17), 6405-6413. DOI: 10.1039/d1gc02251b.
(23) Dikici, B. A.; Sherborne, C.; Reilly, G. C.; Claeyssens, F. Emulsion templated scaffolds manufactured from photocurable polycaprolactone. *Polymer* **2019**, *175*, 243-254. DOI: 10.1016/j.polymer.2019.05.023.
(24) Doganci, M. D. Effects of star-shaped PCL having different numbers of arms on the mechanical, morphological, and thermal properties of PLA/PCL blends. *Journal of Polymer Research* **2021**, *28* (1), 11. DOI: 10.1007/s10965-020-02380-2.
(25) (NIOSH), T. N. I. f. O. S. a. H. Methyl methacrylate. 2019.
(26) (NIOSH), T. N. I. f. O. S. a. H. Methyl acrylate. 2019.
(27) Moore, E. M.; West, J. L. Bioactive Poly(ethylene Glycol) Acrylate Hydrogels for Regenerative Engineering. *Regenerative Engineering and Translational Medicine* **2019**, *5* (2), 167-179. DOI: 10.1007/s40883-018-0074-y.
(28) Beamish, J. A.; Zhu, J.; Kottke-Marchant, K.; Marchant, R. E. The effects of monoacrylated poly(ethylene glycol) on the properties of poly(ethylene glycol) diacrylate hydrogels used for tissue engineering. *Journal of Biomedical Materials Research Part A* **2010**, *92A* (2), 441-450. DOI: https://doi.org/10.1002/jbm.a.32353 (acccessed 2024/03/05).
(29) Lavinia Cosmina, A.; Cristina Maria, B.; Angela Codruta, P.; Laura Cristina, R. Acrylates and Their Alternatives in Dental Applications. In *Acrylic Polymers in Healthcare*, Boreddy, S. R. R. Ed.; IntechOpen, 2017; p Ch. 1.
(30) Voller, L. M.; Warshaw, E. M. Acrylates: new sources and new allergens. *Clinical and Experimental Dermatology* **2020**, *45* (3), 277-283. DOI: https://doi.org/10.1111/ced.14093 (acccessed 2024/03/01).
(31) Zakeri, S.; Vippola, M.; Levanen, E. A comprehensive review of the photopolymerization of ceramic resins used in stereolithography. *Additive Manufacturing* **2020**, *35*. DOI: 10.1016/j.addma.2020.101177.
(32) Schwalm, R. Photoinitiators and Photopolymerization. In *Encyclopedia of Materials: Science and Technology*, Buschow, K. H. J., Cahn, R. W., Flemings, M. C., Ilschner, B., Kramer, E. J., Mahajan, S., Veyssière, P. Eds.; Elsevier, 2001; pp 6946-6951.
(33) Ligon, S. C.; Husár, B.; Wutzel, H.; Holman, R.; Liska, R. Strategies to Reduce Oxygen Inhibition in Photoinduced Polymerization. *Chemical Reviews* **2014**, *114* (1), 557-589. DOI: 10.1021/cr3005197.
(34) Panchal, A. C.; Asthana, G. Oxygen inhibition layer: A dilemma to be solved. *J Conserv Dent* **2020**, *23* (3), 254-258. DOI: 10.4103/jcd.jcd_325_19 From NLM.

(35) Husár, B.; Ligon, S. C.; Wutzel, H.; Hoffmann, H.; Liska, R. The formulator's guide to anti-oxygen inhibition additives. *Progress in Organic Coatings* **2014**, *77* (11), 1789-1798. DOI: https://doi.org/10.1016/j.porgcoat.2014.06.005.
(36) Zhou, J. Y.; Allonas, X.; Liu, X. X.; Wu, S. H. Facile modification on the oxygen-inhibited layer of photopolymerized acrylates via aza-Michael addition. *Polymer International* **2021**, *70* (6), 845-850. DOI: 10.1002/pi.6174.
(37) Rostami, N.; Graf, D.; Schranzhofer, L.; Hild, S.; Hanemann, T. Overcoming oxygen inhibition effect by TODA in acrylate-based ceramic-filled inks. *Progress in Organic Coatings* **2019**, *130*, 221-225. DOI: https://doi.org/10.1016/j.porgcoat.2019.01.048.
(38) Studer, K.; Decker, C.; Beck, E.; Schwalm, R. Overcoming oxygen inhibition in UV-curing of acrylate coatings by carbon dioxide inerting, Part I. *Progress in Organic Coatings* **2003**, *48* (1), 92-100. DOI: 10.1016/s0300-9440(03)00120-6.
(39) Tumbleston, J. R.; Shirvanyants, D.; Ermoshkin, N.; Janusziewicz, R.; Johnson, A. R.; Kelly, D.; Chen, K.; Pinschmidt, R.; Rolland, J. P.; Ermoshkin, A.; et al. Continuous liquid interface production of 3D objects. *Science* **2015**, *347* (6228), 1349-1352. DOI: 10.1126/science.aaa2397 (acccessed 2023/09/27).
(40) Johnson, D. W.; Langford, C. R.; Didsbury, M. P.; Lipp, B.; Przyborski, S. A.; Cameron, N. R. Fully biodegradable and biocompatible emulsion templated polymer scaffolds by thiol-acrylate polymerization of polycaprolactone macromonomers. *Polymer Chemistry* **2015**, *6* (41), 7256-7263, Article. DOI: 10.1039/c5py00721f.
(41) Hofer, M.; Moszner, N.; Liska, R. Oxygen Scavengers and Sensitizers for Reduced Oxygen Inhibition in Radical Photopolymerization. *Journal of Polymer Science Part a-Polymer Chemistry* **2008**, *46* (20), 6916-6927. DOI: 10.1002/pola.23001.
(42) Lowe, A. B. Thiol-ene “click” reactions and recent applications in polymer and materials synthesis. *Polymer Chemistry* **2010**, *1* (1), 17-36, 10.1039/B9PY00216B. DOI: 10.1039/B9PY00216B.
(43) Aldemir Dikici, B.; Malayeri, A.; Sherborne, C.; Dikici, S.; Paterson, T.; Dew, L.; Hatton, P.; Ortega Asencio, I.; MacNeil, S.; Langford, C.; et al. Thiolene- and Polycaprolactone Methacrylate-Based Polymerized High Internal Phase Emulsion (PolyHIPE) Scaffolds for Tissue Engineering. *Biomacromolecules* **2022**, *23* (3), 720-730. DOI: 10.1021/acs.biomac.1c01129.
(44) Huang, Y.; Liao, H.; Huang, R.; Huang, L.; Xie, G.; Hu, H.; Yang, J. Bis(trimethylsilyl)amino modified Type II photoinitiators can alleviate oxygen inhibition of near-UV LED photopolymerization due to moisture induced decomposition of initiators. *European Polymer Journal* **2022**, *172*, 111236. DOI: https://doi.org/10.1016/j.eurpolymj.2022.111236.
(45) Ovsianikov, A.; Viertl, J.; Chichkov, B.; Oubaha, M.; MacCraith, B.; Sakellari, I.; Giakoumaki, A.; Gray, D.; Vamvakaki, M.; Farsari, M.; et al. Ultra-Low Shrinkage Hybrid Photosensitive Material for Two-Photon Polymerization Microfabrication. *ACS Nano* **2008**, *2* (11), 2257-2262. DOI: 10.1021/nn800451w.
(46) Xing, J. F.; Chen, W. Q.; Gu, J.; Dong, X. Z.; Takeyasu, N.; Tanaka, T.; Duan, X. M.; Kawata, S. Design of high efficiency for two-photon polymerization initiator: combination of radical stabilization and large two-photon cross-section achieved by N-benzyl 3,6-bis(phenylethynyl)carbazole derivatives. *Journal of Materials Chemistry* **2007**, *17* (14), 1433-1438, Article. DOI: 10.1039/b616792f.
(47) Xing, J. F.; Zheng, M. L.; Duan, X. M. Two-photon polymerization microfabrication of hydrogels: an advanced 3D printing technology for tissue engineering and drug delivery. *Chemical Society Reviews* **2015**, *44* (15), 5031-5039, Review. DOI: 10.1039/c5cs00278h.
(48) Liu, Y.; Huang, X.; Han, K. C.; Dai, Y. H.; Zhang, X. Q.; Zhao, Y. X. High-Performance Lignin-Based Water-Soluble Macromolecular Photoinitiator for the Fabrication of Hybrid Hydrogel. *Acs Sustainable Chemistry & Engineering* **2019**, *7* (4), 4004-4011, Article. DOI: 10.1021/acssuschemeng.8b05357.
(49) Ovsianikov, A.; Mühleder, S.; Torgersen, J.; Li, Z.; Qin, X.-H.; Van Vlierberghe, S.; Dubruel, P.; Holnthoner, W.; Redl, H.; Liska, R.; et al. Laser Photofabrication of Cell-Containing Hydrogel Constructs. *Langmuir* **2014**, *30* (13), 3787-3794. DOI: 10.1021/la402346z.
(50) Tomal, W.; Ortyl, J. Water-Soluble Photoinitiators in Biomedical Applications. *Polymers* **2020**, *12* (5), ; Review. DOI: 10.3390/polym12051073.

(51) Nguyen, A. K.; Narayan, R. J. Two-photon polymerization for biological applications. *Materials Today* **2017**, *20* (6), 314-322, Article. DOI: 10.1016/j.mattod.2017.06.004.
(52) Nguyen, A. K.; Gittard, S. D.; Koroleva, A.; Schlie, S.; Gaidukeviciute, A.; Chichkov, B. N.; Narayan, R. J. Two-photon polymerization of polyethylene glycol diacrylate scaffolds with riboflavin and triethanolamine used as a water-soluble photoinitiator. *Regenerative Medicine* **2013**, *8* (6), 725-738. DOI: 10.2217/rme.13.60 (acccessed 2023/09/14).
(53) Brif, A.; Laity, P.; Claeyssens, F.; Holland, C. Dynamic Photo-cross-linking of Native Silk Enables Macroscale Patterning at a Microscale Resolution. *ACS Biomaterials Science & Engineering* **2020**, *6* (1), 705-714. DOI: 10.1021/acsbiomaterials.9b00993.
(54) Kim, S.-H.; Chu, C.-C. Fabrication of a biodegradable polysaccharide hydrogel with riboflavin, vitamin B2, as a photo-initiator and L-arginine as coinitiator upon UV irradiation. *Journal of Biomedical Materials Research Part B: Applied Biomaterials* **2009**, *91B* (1), 390-400. DOI: https://doi.org/10.1002/jbm.b.31414 (acccessed 2023/09/14).
(55) Thompson, J. R.; Worthington, K. S.; Green, B. J.; Mullin, N. K.; Jiao, C.; Kaalberg, E. E.; Wiley, L. A.; Han, I. C.; Russell, S. R.; Sohn, E. H.; et al. Two-photon polymerized poly(caprolactone) retinal cell delivery scaffolds and their systemic and retinal biocompatibility. *Acta Biomaterialia* **2019**, *94*, 204-218. DOI: https://doi.org/10.1016/j.actbio.2019.04.057.
(56) Reinhart, T. J. Overview of Composite Materials. In *Handbook of Composites*, Peters, S. T. Ed.; Springer US, 1998; pp 21-33.
(57) Campbell, F. C. Chapter 1 - Introduction to Composite Materials and Processes: Unique Materials that Require Unique Processes. In *Manufacturing Processes for Advanced Composites*, Campbell, F. C. Ed.; Elsevier Science, 2004; pp 1-37.
(58) Cabral, J. P.; Kafle, B.; Subhani, M.; Reiner, J.; Ashraf, M. Densification of timber: a review on the process, material properties, and application. *Journal of Wood Science* **2022**, *68* (1), 20. DOI: 10.1186/s10086-022-02028-3.
(59) Ahn, T.; Gidley, D. W.; Thornton, A. W.; Wong-Foy, A. G.; Orr, B. G.; Kozloff, K. M.; Banaszak Holl, M. M. Hierarchical Nature of Nanoscale Porosity in Bone Revealed by Positron Annihilation Lifetime Spectroscopy. *ACS Nano* **2021**, *15* (3), 4321-4334. DOI: 10.1021/acsnano.0c07478.
(60) Teo, W.-E.; Ramakrishna, S. Electrospun nanofibers as a platform for multifunctional, hierarchically organized nanocomposite. *Composites Science and Technology* **2009**, *69* (11), 1804-1817. DOI: https://doi.org/10.1016/j.compscitech.2009.04.015.
(61) Salernitano, E.; Migliaresi, C. Composite materials for biomedical applications: a review. *J Appl Biomater Biomech* **2003**, *1* (1), 3-18. From NLM.
(62) MartÍN-MartÍNez, J. M. Chapter 13 - Rubber base adhesives. In *Adhesion Science and Engineering*, Dillard, D. A., Pocius, A. V., Chaudhury, M. Eds.; Elsevier Science B.V., 2002; pp 573-675.
(63) Sharma, A.; He, Y.; Lowe, B.; Salam, A.; Altalhi, T. A.; Ye, Q. S.; Kumeria, T. Inorganic/organic combination: Inorganic particles/polymer composites for tissue engineering applications. *Bioactive Materials* **2023**, *24*, 535-550. DOI: 10.1016/j.bioactmat.2023.01.003.
(64) Wei, G. B.; Ma, P. X. Structure and properties of nano-hydroxyapatite/polymer composite scaffolds for bone tissue engineering. *Biomaterials* **2004**, *25* (19), 4749-4757, Article. DOI: 10.1016/j.biomaterials.2003.12.005.
(65) Huang, J.; Di Silvio, L.; Wang, M.; Tanner, K. E.; Bonfield, W. In vitro mechanical and biological assessment of hydroxyapatite-reinforced polyethylene composite. *J Mater Sci Mater Med* **1997**, *8* (12), 775-779. DOI: 10.1023/a:1018516813604 From NLM.
(66) Liu, F. H. Fabrication of Bioceramic Bone Scaffolds for Tissue Engineering. *Journal of Materials Engineering and Performance* **2014**, *23* (10), 3762-3769. DOI: 10.1007/s11665-014-1142-1.
(67) Bulina, N. V.; Titkov, A. I.; Baev, S. G.; Makarova, S. V.; Khusnutdinov, V. R.; Bessmeltsev, V. P.; Lyakhov, N. Z. Laser sintering of hydroxyapatite for potential fabrication of bioceramic scaffolds. *Materials Today-Proceedings* **2021**, *37*, 4022-4026. DOI: 10.1016/j.matpr.2020.06.199.

(68) Shuai, C. J.; Zhou, Y. Z.; Yang, Y. W.; Feng, P.; Liu, L.; He, C. X.; Zhao, M. C.; Yang, S.; Gao, C. D.; Wu, P. Biodegradation Resistance and Bioactivity of Hydroxyapatite Enhanced Mg-Zn Composites via Selective Laser Melting. *Materials* **2017**, *10* (3). DOI: 10.3390/ma10030307.
(69) Roeder, R. K.; Converse, G. L.; Kane, R. J.; Yue, W. Hydroxyapatite-reinforced polymer biocomposites for synthetic bone substitutes. *JOM* **2008**, *60* (3), 38-45. DOI: 10.1007/s11837-008-0030-2.
(70) Deligianni, D. D.; Katsala, N. D.; Koutsoukos, P. G.; Missirlis, Y. F. Effect of surface roughness of hydroxyapatite on human bone marrow cell adhesion, proliferation, differentiation and detachment strength. *Biomaterials* **2000**, *22* (1), 87-96. DOI: https://doi.org/10.1016/S0142-9612(00)00174-5.
(71) Chen, L.; McCrate, J. M.; Lee, J. C.; Li, H. The role of surface charge on the uptake and biocompatibility of hydroxyapatite nanoparticles with osteoblast cells. *Nanotechnology* **2011**, *22* (10), 105708. DOI: 10.1088/0957-4484/22/10/105708 From NLM.
(72) Gvaramia, M.; Mangiapia, G.; Pipich, V.; Appavou, M.-S.; Jaksch, S.; Holderer, O.; Rukhadze, M. D.; Frielinghaus, H. Tunable viscosity modification with diluted particles: when particles decrease the viscosity of complex fluids. *Colloid and Polymer Science* **2019**, *297* (11), 1507-1517. DOI: 10.1007/s00396-019-04567-6.
(73) Pfau, M. R.; McKinzey, K. G.; Roth, A.; Grunlan, M. A. PCL-Based Shape Memory Polymer Semi-IPNs: The Role of Miscibility in Tuning the Degradation Rate. *Biomacromolecules* **2020**, *21* (6), 2493-2501, Article. DOI: 10.1021/acs.biomac.0c00454.
(74) Zolghadr, M.; Shakeri, A.; Zohuriaan-Mehr, M. J.; Salimi, A. Self-healing semi-IPN materials from epoxy resin by solvent-free furan-maleimide Diels-Alder polymerization. *Journal of Applied Polymer Science* **2019**, *136* (40). DOI: 10.1002/app.48015.
(75) Altiparmak, S. C.; Yardley, V. A.; Shi, Z. S.; Lin, J. G. Extrusion-based additive manufacturing technologies: State of the art and future perspectives. *Journal of Manufacturing Processes* **2022**, *83*, 607-636. DOI: 10.1016/j.jmapro.2022.09.032.
(76) Liu, Q. Q.; Li, Q. T.; Xu, S.; Zheng, Q. J.; Cao, X. D. Preparation and Properties of 3D Printed Alginate-Chitosan Polyion Complex Hydrogels for Tissue Engineering. *Polymers* **2018**, *10* (6). DOI: 10.3390/polym10060664.
(77) Menshutina, N.; Abramov, A.; Tsygankov, P.; Lovskaya, D. Extrusion-Based 3D Printing for Highly Porous Alginate Materials Production. *Gels* **2021**, *7* (3). DOI: 10.3390/gels7030092.
(78) Zhang, X.; Jia, X.; Wang, X. Direct ink writing of polymers and their composites, and related applications. In *Structure and Properties of Additive Manufactured Polymer Components*, Friedrich, K., Walter, R., Soutis, C., Advani, S. G., Fiedler, I. H. B. Eds.; Woodhead Publishing, 2020; pp 391-408.
(79) Schwab, A.; Levato, R.; D'Este, M.; Piluso, S.; Eglin, D.; Malda, J. Printability and Shape Fidelity of Bioinks in 3D Bioprinting. *Chem Rev* **2020**, *120* (19), 11028-11055. DOI: 10.1021/acs.chemrev.0c00084 From NLM.
(80) Ramli, H.; Zainal, N. F. A.; Hess, M.; Chan, C. H. Basic principle and good practices of rheology for polymers for teachers and beginners. **2022**, *4* (4), 307-326. DOI: doi:10.1515/cti-2022-0010 (acccessed 2023-09-27).
(81) Alaee, P.; Kamkar, M.; Arjmand, M. Fumed Silica-Based Suspensions for Shear Thickening Applications: A Full-Scale Rheological Study. *Langmuir* **2022**, *38* (16), 5006-5019. DOI: 10.1021/acs.langmuir.2c00591.
(82) Catarino, S.; Lima, R.; Minas, G. 12 - Smart devices: Lab-on-a-chip. In *Bioinspired Materials for Medical Applications*, Rodrigues, L., Mota, M. Eds.; Woodhead Publishing, 2017; pp 331-369.
(83) Huang, J.; Qin, Q.; Wang, J. A Review of Stereolithography: Processes and Systems. In *Processes*, 2020; Vol. 8.
(84) Raguraman, M.; Rajan, M. Chapter 2 - Nanoengineering/technology for tissue engineering and organ printing. In *Emerging Nanotechnologies for Medical Applications*, Ahmad, N., Packirisamy, G. Eds.; Elsevier, 2023; pp 35-54.

(85) Kumar, A.; Kumar, P.; Mittal, R. K.; Singh, H. Chapter 6 - Printing file formats for additive manufacturing technologies. In *Advances in Additive Manufacturing*, Kumar, A., Mittal, R. K., Haleem, A. Eds.; Elsevier, 2023; pp 87-102.
(86) Dinh, D. H.; Chien, H. L.; Lee, Y. C. Maskless lithography based on digital micromirror device (DMD) and double sided microlens and spatial filter array. *Optics and Laser Technology* **2019**, *113*, 407-415. DOI: 10.1016/j.optlastec.2019.01.001.
(87) Carroll, G. T.; Turro, N. J.; Mammana, A.; Koberstein, J. T. Photochemical Immobilization of Polymers on a Surface: Controlling Film Thickness and Wettability. *Photochemistry and Photobiology* **2017**, *93* (5), 1165-1169. DOI: https://doi.org/10.1111/php.12751 (acccessed 2023/09/14).
(88) Toombs, J. T.; Luitz, M.; Cook, C. C.; Jenne, S.; Li, C. C.; Rapp, B. E.; Kotz-Helmer, F.; Taylor, H. K. Volumetric additive manufacturing of silica glass with microscale computed axial lithography. *Science* **2022**, *376* (6590), 308-312. DOI: 10.1126/science.abm6459 (acccessed 2023/09/27).
(89) Watson, G. P.; Aksyuk, V.; Simon, M. E.; Tennant, D. M.; Cirelli, R. A.; Mansfield, W. M.; Pardo, F.; Lopez, D. O.; Bolle, C. A.; Papazian, A. R.; et al. Spatial light modulator for maskless optical projection lithography. *Journal of Vacuum Science & Technology B: Microelectronics and Nanometer Structures Processing, Measurement, and Phenomena* **2006**, *24* (6), 2852-2856. DOI: 10.1116/1.2387156 (acccessed 9/14/2023).
(90) Choi, J. W.; Wicker, R. B.; Cho, S. H.; Ha, C. S.; Lee, S. H. Cure depth control for complex 3D microstructure fabrication in dynamic mask projection microstereolithography. *Rapid Prototyping Journal* **2009**, *15* (1), 59-70. DOI: 10.1108/13552540910925072 (acccessed 2023/09/27).
(91) Ozsoz, N. S.; Pashneh-Tala, S.; Claeyssens, F. Optimization of a High Internal Phase Emulsion-Based Resin for Use in Commercial Vat Photopolymerization Additive Manufacturing. *3d Printing and Additive Manufacturing* **2023**. DOI: 10.1089/3dp.2022.0235.
(92) Grigoryan, B.; Paulsen, S. J.; Corbett, D. C.; Sazer, D. W.; Fortin, C. L.; Zaita, A. J.; Greenfield, P. T.; Calafat, N. J.; Gounley, J. P.; Ta, A. H.; et al. Multivascular networks and functional intravascular topologies within biocompatible hydrogels. *Science* **2019**, *364* (6439), 458-464. DOI: 10.1126/science.aav9750 (acccessed 2023/09/27).
(93) Kaiser, W.; Garrett, C. G. B. 2-PHOTON EXCITATION IN CAF2 - EU2+. *Physical Review Letters* **1961**, *7* (6), 229-&. DOI: 10.1103/PhysRevLett.7.229.
(94) Göppert-Mayer, M. Über Elementarakte mit zwei Quantensprüngen. *Annalen der Physik* **1931**, *401* (3), 273-294. DOI: https://doi.org/10.1002/andp.19314010303 (acccessed 2023/09/14).
(95) Appendix C - Two photon absorption. In *Optical Spectroscopy*, Tkachenko, N. V. Ed.; Elsevier Science, 2006; pp 293-294.
(96) Pashneh-Tala, S.; Owen, R.; Bahmaee, H.; Rekstyte, S.; Malinauskas, M.; Claeyssens, F. Synthesis, Characterization and 3D Micro-Structuring via 2-Photon Polymerization of Poly(glycerol sebacate)-Methacrylate-An Elastomeric Degradable Polymer. *Frontiers in Physics* **2018**, *6*, 17, Article. DOI: 10.3389/fphy.2018.00041.
(97) Huang, Z. J.; Tsui, G. C. P.; Deng, Y.; Tang, C. Y. Two-photon polymerization nanolithography technology for fabrication of stimulus-responsive micro/nano-structures for biomedical applications. *Nanotechnology Reviews* **2020**, *9* (1), 1118-1136. DOI: 10.1515/ntrev-2020-0073.
(98) Arnoux, C.; Perez-Covarrubias, L. A.; Khaldi, A.; Carlier, Q.; Baldeck, P. L.; Heggarty, K.; Banyasz, A.; Monnereau, C. Understanding and overcoming proximity effects in multi-spot two-photon direct laser writing. *Additive Manufacturing* **2022**, *49*. DOI: 10.1016/j.addma.2021.102491.
(99) Moglia, R. S.; Holm, J. L.; Sears, N. A.; Wilson, C. J.; Harrison, D. M.; Cosgriff-Hernandez, E. Injectable polyHIPEs as high-porosity bone grafts. *Biomacromolecules* **2011**, *12* (10), 3621-3628. DOI: 10.1021/bm2008839 From NLM.
(100) Cameron, N. R.; Sherrington, D. C. High internal phase emulsions (HIPEs) - Structure, properties and use in polymer preparation. *Biopolymers Liquid Crystalline Polymers Phase Emulsion* **1996**, *126*, 163-214.

(101) Su, F.; Bray, C. L.; Tan, B.; Cooper, A. I. Rapid and Reversible Hydrogen Storage in Clathrate Hydrates Using Emulsion-Templated Polymers. *Advanced Materials* **2008**, *20* (14), 2663-2666. DOI: https://doi.org/10.1002/adma.200800550 (acccessed 2023/09/14).
(102) Pierre, S. J.; Thies, J. C.; Dureault, A.; Cameron, N. R.; van Hest, J. C. M.; Carette, N.; Michon, T.; Weberskirch, R. Covalent Enzyme Immobilization onto Photopolymerized Highly Porous Monoliths. *Advanced Materials* **2006**, *18* (14), 1822-1826. DOI: https://doi.org/10.1002/adma.200600293 (acccessed 2023/09/14).
(103) Yin, X.; Zhang, T.; Zhao, T.; Wang, K.; Xu, Z.; Zhao, Y. Cellulose-based, flexible polyurethane polyHIPEs with quasi-closed-cell structures and high stability for thermal insulation. *Carbohydrate Polymers* **2023**, *302*, 120385. DOI: https://doi.org/10.1016/j.carbpol.2022.120385.
(104) Young, G. A.; LaVon, G. D.; Taylor, G. W. High efficiency absorbent articles for incontinence management. Google Patents: 1992.
(105) Silverstein, M. S. PolyHIPEs: Recent advances in emulsion-templated porous polymers. *Progress in Polymer Science* **2014**, *39* (1), 199-234, Review. DOI: 10.1016/j.progpolymsci.2013.07.003.
(106) Aldemir Dikici, B.; Claeyssens, F. Basic Principles of Emulsion Templating and Its Use as an Emerging Manufacturing Method of Tissue Engineering Scaffolds. *Frontiers in Bioengineering and Biotechnology* **2020**, *8*, Review.
(107) Durgut, E.; Sherborne, C.; Aldemir Dikici, B.; Reilly, G. C.; Claeyssens, F. Preparation of Interconnected Pickering Polymerized High Internal Phase Emulsions by Arrested Coalescence. *Langmuir* **2022**, *38* (36), 10953-10962. DOI: 10.1021/acs.langmuir.2c01243.
(108) Zhang, T.; Liu, F.; Wu, J.; Ngai, T. Pickering emulsions stabilized by biocompatible particles: A review of preparation, bioapplication, and perspective. *Particuology* **2022**, *64*, 110-120. DOI: https://doi.org/10.1016/j.partic.2021.07.003.
(109) Furmidge, R.; Jackson, C. E.; Velázquez de la Paz, M. F.; Workman, V. L.; Green, N. H.; Reilly, G. C.; Hearnden, V.; Claeyssens, F. Surfactant-free gelatin-stabilised biodegradable polymerised high internal phase emulsions with macroporous structures. *Frontiers in Chemistry* **2023**, *11*, Original Research.
(110) Comer, J.; Tam, K. Lipophilicity Profiles: Theory and Measurement. In *Pharmacokinetic Optimization in Drug Research*, 2001; pp 275-304.
(111) Ohara, T.; Sato, T.; Shimizu, N.; Prescher, G.; Schwind, H.; Weiberg, O.; Marten, K. Acrylic Acid and Derivatives. In *Ullmann's Encyclopedia of Industrial Chemistry*, 2003.
(112) Ammer, J.; Baidya, M.; Kobayashi, S.; Mayr, H. Nucleophilic reactivities of tertiary alkylamines. *Journal of Physical Organic Chemistry* **2010**, *23* (11), 1029-1035. DOI: https://doi.org/10.1002/poc.1707 (acccessed 2023/09/13).
(113) Sorgi, K. L. Triethylamine. In *Encyclopedia of Reagents for Organic Synthesis (EROS)*, 2001.
(114) Cai, L.; Wang, S. F. Elucidating Colorization in the Functionalization of Hydroxyl-Containing Polymers Using Unsaturated Anhydrides/Acyl Chlorides in the Presence of Triethylamine. *Biomacromolecules* **2010**, *11* (1), 304-307, Article. DOI: 10.1021/bm901237t.
(115) Fujita, M.; Izato, Y.-i.; Iizuka, Y.; Miyake, A. Thermal hazard evaluation of runaway polymerization of acrylic acid. *Process Safety and Environmental Protection* **2019**, *129*, 339-347. DOI: https://doi.org/10.1016/j.psep.2019.08.003.
(116) Neises, B.; Steglich, W. Simple Method for the Esterification of Carboxylic Acids. *Angewandte Chemie International Edition in English* **1978**, *17* (7), 522-524. DOI: https://doi.org/10.1002/anie.197805221.
(117) Lutjen, A. B.; Quirk, M. A.; Kolonko, E. M. Synthesis of Esters Via a Greener Steglich Esterification in Acetonitrile. *Jove-Journal of Visualized Experiments* **2018**, (140). DOI: 10.3791/58803.
(118) Hassner, A.; Hart, A. P.; Pigza, J. A. 4-Dimethylaminopyridine. In *Encyclopedia of Reagents for Organic Synthesis (EROS)*, 2016; pp 1-6.
(119) Norouzi, S.; Mohseni, M.; Yahyaei, H. Preparation and characterization of an acrylic acid modified polyhedral oligomeric silsesquioxane and investigating its effect in a UV curable coating. *Progress in Organic Coatings* **2016**, *99*, 1-10, Article. DOI: 10.1016/j.porgcoat.2016.04.027.

(120) Wang, Y. D.; Ameer, G. A.; Sheppard, B. J.; Langer, R. A tough biodegradable elastomer. *Nature Biotechnology* **2002**, *20* (6), 602-606, Article. DOI: 10.1038/nbt0602-602.
(121) Liu, Q. Y.; Tian, M.; Shi, R.; Zhang, L. Q.; Chen, D. F.; Tian, W. Structure and properties of thermoplastic poly(glycerol sebacate) elastomers originating from prepolymers with different molecular weights. *Journal of Applied Polymer Science* **2007**, *104* (2), 1131-1137. DOI: 10.1002/app.25606.
(122) Bliley, J. M.; Marra, K. G. Chapter 11 - Polymeric Biomaterials as Tissue Scaffolds. In *Stem Cell Biology and Tissue Engineering in Dental Sciences*, Vishwakarma, A., Sharpe, P., Shi, S., Ramalingam, M. Eds.; Academic Press, 2015; pp 149-161.
(123) Arakawa, C. K.; DeForest, C. A. Chapter 19 - Polymer Design and Development. In *Biology and Engineering of Stem Cell Niches*, Vishwakarma, A., Karp, J. M. Eds.; Academic Press, 2017; pp 295-314.
(124) Doyle, S. E.; Henry, L.; McGennisken, E.; Onofrillo, C.; Bella, C. D.; Duchi, S.; O'Connell, C. D.; Pirogova, E. Characterization of Polycaprolactone Nanohydroxyapatite Composites with Tunable Degradability Suitable for Indirect Printing. *Polymers (Basel)* **2021**, *13* (2). DOI: 10.3390/polym13020295 From NLM.
(125) Christen, M. O.; Vercesi, F. Polycaprolactone: How a Well-Known and Futuristic Polymer Has Become an Innovative Collagen-Stimulator in Esthetics. *CLINICAL COSMETIC AND INVESTIGATIONAL DERMATOLOGY* **2020**, *13*, 31-48. DOI: 10.2147/CCID.S229054.
(126) Azimi, B.; Nourpanah, P.; Rabiee, M.; Arbab, S. Poly (epsilon-caprolactone) Fiber: An Overview. *JOURNAL OF ENGINEERED FIBERS AND FABRICS* **2014**, *9* (3), 74-90.
(127) Liu, J.; Zheng, H.; Poh, P. S. P.; Machens, H.-G.; Schilling, A. F. Hydrogels for Engineering of Perfusable Vascular Networks. In *International Journal of Molecular Sciences*, 2015; Vol. 16, pp 15997-16016.
(128) Elomaa, L.; Teixeira, S.; Hakala, R.; Korhonen, H.; Grijpma, D. W.; Seppälä, J. V. Preparation of poly(ε-caprolactone)-based tissue engineering scaffolds by stereolithography. *Acta Biomaterialia* **2011**, *7* (11), 3850-3856. DOI: https://doi.org/10.1016/j.actbio.2011.06.039.
(129) Samson, K. D. G.; Hidalgo-Alvarez, V.; Dargaville, T. R.; Melchels, F. P. W. Tough, Resorbable Polycaprolactone-Based Bimodal Networks for Vat Polymerization 3D Printing. *Advanced Functional Materials* **2023**, *33* (25), 2213797. DOI: https://doi.org/10.1002/adfm.202213797 (acccessed 2023/09/28).
(130) Woodard, L. N.; Page, V. M.; Kmetz, K. T.; Grunlan, M. A. PCL–PLLA Semi-IPN Shape Memory Polymers (SMPs): Degradation and Mechanical Properties. *Macromolecular Rapid Communications* **2016**, *37* (23), 1972-1977. DOI: https://doi.org/10.1002/marc.201600414 (acccessed 2023/09/27).
(131) Barral, V.; Dropsit, S.; Cayla, A.; Campagne, C.; Devaux, É. Study of the Influence of PCL on the In Vitro Degradation of Extruded PLA Monofilaments and Melt-Spun Filaments. In *Polymers*, 2021; Vol. 13.
(132) Fried, J. R. *Polymer Science and Technology*; Prentice Hall, 2014.
(133) Huang, J. R.; Fu, P.; Li, W. B.; Xiao, L. H.; Chen, J.; Nie, X. A. Influence of crosslinking density on the mechanical and thermal properties of plant oil-based epoxy resin. *RSC ADVANCES* **2022**, *12* (36), 23048-23056. DOI: 10.1039/d2ra04206a.
(134) Riley, A. 12 - Basics of polymer chemistry for packaging materials. In *Packaging Technology*, Emblem, A., Emblem, H. Eds.; Woodhead Publishing, 2012; pp 262-286.
(135) Kong, D.-C.; Yang, M.-H.; Zhang, X.-S.; Du, Z.-C.; Fu, Q.; Gao, X.-Q.; Gong, J.-W. Control of Polymer Properties by Entanglement: A Review. *Macromolecular Materials and Engineering* **2021**, *306* (12), 2100536. DOI: https://doi.org/10.1002/mame.202100536 (acccessed 2023/09/28).
(136) Przybysz, M.; Hejna, A.; Haponiuk, J.; Formela, K. Structural and Thermo-Mechanical Properties of Poly(ε-caprolactone) Modified by Various Peroxide Initiators. *Polymers (Basel)* **2019**, *11* (7). DOI: 10.3390/polym11071101 From NLM.
(137) Salaeh, S.; Nobnop, S.; Thongnuanchan, B.; Das, A.; Wießner, S. Thermo-responsive programmable shape memory polymer based on amidation cured natural rubber grafted with

poly(methyl methacrylate). *Polymer* **2022**, *262*, 125444. DOI: https://doi.org/10.1016/j.polymer.2022.125444.
(138) Van Damme, L.; Blondeel, P.; Van Vlierberghe, S. Injectable biomaterials as minimal invasive strategy towards soft tissue regeneration-an overview. *JOURNAL OF PHYSICS-MATERIALS* **2021**, *4* (2). DOI: 10.1088/2515-7639/abd4f3.
(139) Chen, H.; Gonnella, G.; Huang, J.; Di-Silvio, L. Fabrication of 3D Bioprinted Bi-Phasic Scaffold for Bone-Cartilage Interface Regeneration. *Biomimetics (Basel)* **2023**, *8* (1). DOI: 10.3390/biomimetics8010087 From NLM.
(140) Geoghegan, N.; O'Loughlin, M.; Delaney, C.; Rochfort, K. D.; Kennedy, M.; Kolagatla, S.; Podhorska, L.; Rodriguez, B. J.; Florea, L.; Kelleher, S. M. Controlled degradation of polycaprolactone-based micropillar arrays. *Biomater Sci* **2023**, *11* (9), 3077-3091. DOI: 10.1039/d3bm00165b From NLM.
(141) Lyu, S.; Untereker, D. Degradability of polymers for implantable biomedical devices. *Int J Mol Sci* **2009**, *10* (9), 4033-4065. DOI: 10.3390/ijms10094033 From NLM.
(142) James, E. N.; Hanna, C.; Nair, L. S. Chapter 16 - Nanobiomaterials for Tissue Engineering Applications. In *Stem Cell Biology and Tissue Engineering in Dental Sciences*, Vishwakarma, A., Sharpe, P., Shi, S., Ramalingam, M. Eds.; Academic Press, 2015; pp 221-234.
(143) Ragunathan, S.; Govindasamy, G.; Raghul, D. R.; Karuppaswamy, M.; VijayachandraTogo, R. K. Hydroxyapatite reinforced natural polymer scaffold for bone tissue regeneration. *Materials Today: Proceedings* **2020**, *23*, 111-118. DOI: https://doi.org/10.1016/j.matpr.2019.07.712.
(144) Šupová, M. Substituted hydroxyapatites for biomedical applications: A review. *Ceramics International* **2015**, *41* (8), 9203-9231. DOI: https://doi.org/10.1016/j.ceramint.2015.03.316.
(145) Ratnayake, J. T. B.; Mucalo, M.; Dias, G. J. Substituted hydroxyapatites for bone regeneration: A review of current trends. *J Biomed Mater Res B Appl Biomater* **2017**, *105* (5), 1285-1299. DOI: 10.1002/jbm.b.33651 From NLM.
(146) Kunjalukkal Padmanabhan, S.; Nitti, P.; Stanca, E.; Rochira, A.; Siculella, L.; Raucci, M. G.; Madaghiele, M.; Licciulli, A.; Demitri, C. Mechanical and Biological Properties of Magnesium- and Silicon-Substituted Hydroxyapatite Scaffolds. *Materials (Basel)* **2021**, *14* (22). DOI: 10.3390/ma14226942 From NLM.
(147) Yang, W.; Wu, Y.; Pei, X.; Zhou, F.; Xue, Q. Contribution of Surface Chemistry to the Shear Thickening of Silica Nanoparticle Suspensions. *Langmuir* **2017**, *33* (4), 1037-1042. DOI: 10.1021/acs.langmuir.6b04060.
(148) Huang, Y.; Li, P.; Zhao, R.; Zhao, L.; Liu, J.; Peng, S.; Fu, X.; Wang, X.; Luo, R.; Wang, R.; et al. Silica nanoparticles: Biomedical applications and toxicity. *Biomedicine & Pharmacotherapy* **2022**, *151*, 113053. DOI: https://doi.org/10.1016/j.biopha.2022.113053.
(149) Rezania, N.; Asadi-Eydivand, M.; Abolfathi, N.; Bonakdar, S.; Mehrjoo, M.; Solati-Hashjin, M. Three-dimensional printing of polycaprolactone/hydroxyapatite bone tissue engineering scaffolds mechanical properties and biological behavior. *J Mater Sci Mater Med* **2022**, *33* (3), 31. DOI: 10.1007/s10856-022-06653-8 From NLM.
(150) Zhou, S.; Zheng, X.; Yu, X.; Wang, J.; Weng, J.; Li, X.; Feng, B.; Yin, M. Hydrogen Bonding Interaction of Poly(d,l-Lactide)/hydroxyapatite Nanocomposites. *Chemistry of Materials* **2007**, *19* (2), 247-253. DOI: 10.1021/cm0619398.
(151) Zhang, X.; Li, Y.-B.; Zuo, Y.; Lv, G.-Y.; Mu, Y.-H.; Li, H. Morphology, hydrogen-bonding and crystallinity of nano-hydroxyapatite/polyamide 66 biocomposites. *Composites Part A: Applied Science and Manufacturing* **2007**, *38* (3), 843-848. DOI: https://doi.org/10.1016/j.compositesa.2006.08.002.
(152) James, S.; Fox, J.; Afsari, F.; Lee, J.; Clough, S.; Knight, C.; Ashmore, J.; Ashton, P.; Preham, O.; Hoogduijn, M.; et al. Multiparameter Analysis of Human Bone Marrow Stromal Cells Identifies Distinct Immunomodulatory and Differentiation-Competent Subtypes. *Stem Cell Reports* **2015**, *4* (6), 1004-1015. DOI: https://doi.org/10.1016/j.stemcr.2015.05.005.
(153) Kunzler, T. P.; Huwiler, C.; Drobek, T.; Vörös, J.; Spencer, N. D. Systematic study of osteoblast response to nanotopography by means of nanoparticle-density gradients. *Biomaterials* **2007**, *28* (33), 5000-5006. DOI: https://doi.org/10.1016/j.biomaterials.2007.08.009.

(154) Sugino, Y.; Kawaguchi, M. Fumed and Precipitated Hydrophilic Silica Suspension Gels in Mineral Oil: Stability and Rheological Properties. *Gels* **2017**, *3* (3). DOI: 10.3390/gels3030032 From NLM.
(155) Gashti, M. P.; Moradian, S.; Rashidi, A.; Yazdanshenas, M. E. Dispersibility of Hydrophilic and Hydrophobic Nano-silica Particles in Polyethylene Terephthalate Films: Evaluation of Morphology and Thermal Properties. *POLYMERS & POLYMER COMPOSITES* **2015**, *23* (5), 285-295. DOI: 10.1177/096739111502300502.
(156) Lin, W. C.; Mohd Razali, N. A. Temporary Wettability Tuning of PCL/PDMS Micro Pattern Using the Plasma Treatments. *Materials (Basel)* **2019**, *12* (4). DOI: 10.3390/ma12040644 From NLM.
(157) Gu, X.; Lin, W.; Li, D.; Guo, H.; Li, P.; Fan, Y. Degradation and biocompatibility of a series of strontium substituted hydroxyapatite coatings on magnesium alloys. *RSC Advances* **2019**, *9* (26), 15013-15021, 10.1039/C9RA02210D. DOI: 10.1039/C9RA02210D.
(158) Alabugin, I. V.; Gilmore, K. M.; Peterson, P. W. Hyperconjugation. *Wiley Interdisciplinary Reviews-Computational Molecular Science* **2011**, *1* (1), 109-141. DOI: 10.1002/wcms.6.
(159) Waheed, S.; Cabot, J. M.; Macdonald, N. P.; Lewis, T.; Guijt, R. M.; Paull, B.; Breadmore, M. C. 3D printed microfluidic devices: enablers and barriers. *Lab on a Chip* **2016**, *16* (11), 1993-2013. DOI: 10.1039/c6lc00284f.
(160) Sala, F.; Ficorella, C.; Vazquez, R. M.; Eichholz, H. M.; Kas, J. A.; Osellame, R. Rapid Prototyping of 3D Biochips for Cell Motility Studies Using Two-Photon Polymerization. *Frontiers in Bioengineering and Biotechnology* **2021**, *9*. DOI: 10.3389/fbioe.2021.664094.
(161) Sima, F.; Xu, J.; Wu, D.; Sugioka, K. Ultrafast Laser Fabrication of Functional Biochips: New Avenues for Exploring 3D Micro- and Nano-Environments. *Micromachines* **2017**, *8* (2). DOI: 10.3390/mi8020040.
(162) Tsakos, M.; Schaffert, E. S.; Clement, L. L.; Villadsen, N. L.; Poulsen, T. B. Ester coupling reactions - an enduring challenge in the chemical synthesis of bioactive natural products. *Natural Product Reports* **2015**, *32* (4), 605-632. DOI: 10.1039/c4np00106k.
(163) Sheehan, J. C.; Boshart, G. L.; Cruickshank, P. A. CONVENIENT SYNTHESIS OF WATER-SOLUBLE CARBODIIMIDES. *Journal of Organic Chemistry* **1961**, *26* (7), 2525-&. DOI: 10.1021/jo01351a600.
(164) Hassner, A.; Hart, A. P.; Pigza, J. A. 4-Dimethylaminopyridine. In *Encyclopedia of Reagents for Organic Synthesis (EROS)*, pp 1-6.
(165) Yagci, Y.; Jockusch, S.; Turro, N. J. Photoinitiated Polymerization: Advances, Challenges, and Opportunities. *Macromolecules* **2010**, *43* (15), 6245-6260. DOI: 10.1021/ma1007545.
(166) Skliutas, E.; Lebedevaite, M.; Kabouraki, E.; Baldacchini, T.; Ostrauskaite, J.; Vamvakaki, M.; Farsari, M.; Juodkazis, S.; Malinauskas, M. Polymerization mechanisms initiated by spatio-temporally confined light. *NANOPHOTONICS* **2021**, *10* (4), 1211-1242. DOI: 10.1515/nanoph-2020-0551.
(167) Kerns, J.; Piponov, H.; Helder, C.; Amirouche, F.; Solitro, G.; Gonzalez, M. Mechanical Properties of the Human Tibial and Peroneal Nerves Following Stretch With Histological Correlations. *Anatomical Record-Advances in Integrative Anatomy and Evolutionary Biology* **2019**, *302* (11), 2030-2039. DOI: 10.1002/ar.24250.
(168) Gou, L. J.; Coretsopoulos, C. N.; Scranton, A. B. Measurement of the dissolved oxygen concentration in acrylate monomers with a novel photochemical method. *JOURNAL OF POLYMER SCIENCE PART A-POLYMER CHEMISTRY* **2004**, *42* (5), 1285-1292. DOI: 10.1002/pola.11083.
(169) Kloosterboer, J. G.; Lijten, G.; Zegers, C. P. G. FORMATION OF DENSELY CROSSLINKED POLYMER GLASSES BY PHOTOPOLYMERIZATION. *ABSTRACTS OF PAPERS OF THE AMERICAN CHEMICAL SOCIETY* **1989**, *197*, 28-PMSE.
(170) Lee, T. Y.; Guymon, C. A.; Jönsson, E. S.; Hoyle, C. E. The effect of monomer structure on oxygen inhibition of (meth)acrylates photopolymerization. *Polymer* **2004**, *45* (18), 6155-6162. DOI: https://doi.org/10.1016/j.polymer.2004.06.060.
(171) Luo, Y.; Wang, Y.; Niu, X.; Shang, J. Evaluation of the cytocompatibility of butanediamine- and RGDS-grafted poly(dl-lactic acid). *European Polymer Journal* **2008**, *44* (5), 1390-1402. DOI: https://doi.org/10.1016/j.eurpolymj.2008.01.043.

(172) Niu, X.; Luo, Y.; Li, Y.; Fu, C.; Chen, J.; Wang, Y. Design of bioinspired polymeric materials based on poly(D,L-lactic acid) modifications towards improving its cytocompatibility. *Journal of Biomedical Materials Research Part A* **2008**, *84A* (4), 908-916. DOI: https://doi.org/10.1002/jbm.a.31360 (acccessed 2023/09/28).
(173) Fouassier, J. P.; Morlet-Savary, F.; Lalevée, J.; Allonas, X.; Ley, C. Dyes as Photoinitiators or Photosensitizers of Polymerization Reactions. *Materials (Basel)* **2010**, *3* (12), 5130-5142. DOI: 10.3390/ma3125130 From NLM.
(174) Lobo, V.; Patil, A.; Phatak, A.; Chandra, N. Free radicals, antioxidants and functional foods: Impact on human health. *Pharmacogn Rev* **2010**, *4* (8), 118-126. DOI: 10.4103/0973-7847.70902 From NLM.
(175) Taylor, C. S.; Chen, R.; D' Sa, R.; Hunt, J. A.; Curran, J. M.; Haycock, J. W. Cost effective optimised synthetic surface modification strategies for enhanced control of neuronal cell differentiation and supporting neuronal and Schwann cell viability. *Journal of Biomedical Materials Research Part B: Applied Biomaterials* **2021**, *109* (11), 1713-1723. DOI: https://doi.org/10.1002/jbm.b.34829 (acccessed 2023/09/24).
(176) Venkataramani, D.; Tsulaia, A.; Amin, S. Fundamentals and applications of particle stabilized emulsions in cosmetic formulations. *Advances in Colloid and Interface Science* **2020**, *283*, 102234. DOI: https://doi.org/10.1016/j.cis.2020.102234.
(177) Lam, C. X. F.; Teoh, S. H.; Hutmacher, D. W. Comparison of the degradation of polycaprolactone and polycaprolactone-(beta-tricalcium phosphate) scaffolds in alkaline medium. *Polymer International* **2007**, *56* (6), 718-728. DOI: 10.1002/pi.2195.
(178) Bartnikowski, M.; Dargaville, T. R.; Ivanovski, S.; Hutmacher, D. W. Degradation mechanisms of polycaprolactone in the context of chemistry, geometry and environment. *Progress in Polymer Science* **2019**, *96*, 1-20. DOI: 10.1016/j.progpolymsci.2019.05.004.
(179) Burkersroda, F. v.; Schedl, L.; Göpferich, A. Why degradable polymers undergo surface erosion or bulk erosion. *Biomaterials* **2002**, *23* (21), 4221-4231. DOI: https://doi.org/10.1016/S0142-9612(02)00170-9.
(180) Aleemardani, M.; Trikić, M. Z.; Green, N. H.; Claeyssens, F. Elastomeric, bioadhesive and pH-responsive amphiphilic copolymers based on direct crosslinking of poly(glycerol sebacate)-co-polyethylene glycol. *Biomater Sci* **2022**, *10* (24), 7015-7031. DOI: 10.1039/d2bm01335e From NLM.
(181) He, Y.; Jiang, M.; Hu, W.; Ahmad, I.; Gan, L.; Pang, A.; Huang, J. Structure and mechanical properties of Poly(styrene-co-acrylate)/cellulose nanocrystals co-continuous composites via one-pot pickering emulsion polymerization. *Journal of Polymer Research* **2022**, *29* (9), 399. DOI: 10.1007/s10965-022-03062-x.